STRUCTURAL INSIGHTS INTO THE SHROOM-ROCK INTERACTION AND THE REGULATION OF THE ACTOMYOSIN CYTOSKELETON.

by

Swarna Mohan

Bachelor of Science, University of Pittsburgh, 2006

Submitted to the Graduate Faculty of the Kenneth P.

Dietrich School of Arts and Sciences in partial fulfillment

of the requirements for the degree of

Doctor of Philosophy

University of Pittsburgh

2012

UNIVERSITY OF PITTSBURGH

KENNETH P. DIETRICH SCHOOL OF ARTS AND SCIENCES

This dissertation was presented

by

Swarna Mohan

It was defended on

July 17th, 2012

and approved by

Karen Arndt, PhD., Professor, Biological Sciences

Jeff Brodsky, PhD., Professor, Biological Sciences

Michael Grabe, PhD., Assistant Professor, Biological Sciences

Mark Macbeth, PhD., Assistant Professor, Biological Sciences (Carnegie Mellon University)

Dissertation Advisor: Andrew P. VanDemark, PhD., Assistant Professor, Biological Sciences

STRUCTURAL INSIGHTS INTO THE SHROOM-ROCK INTERACTION AND THE REGULATION OF THE ACTOMYOSIN CYTOSKELETON.

Swarna Mohan, PhD

University of Pittsburgh, 2012

During development, tissues undergo precise and controlled changes in shape and size. Various signaling pathways regulate these changes, temporally and spatially, by altering cytoskeleton dynamics to alter cell shape. One such pathway involves the Shroom and Rock proteins that reorganize the actomyosin cytoskeleton in epithelial cells to alter tissue morphology. The Shroom family of proteins are multi-domain, actin-binding proteins required for many developmental processes such as neural tube formation, and retinal morphogenesis. Shroom proteins interact with Rho-kinase (Rock), another conserved cytoskeleton regulator, to activate non-muscle Myosin II and assemble a contractile actomyosin network. All Shroom proteins contain a highly conserved C-terminal domain called Shroom Domain 2 (SD2) that interacts with the Rock Shroom binding domain (SBD) and is required for Shroom-mediated apical constriction. In the Shroom-Rock system it is unclear how this interaction activates the kinase activity of Rock. The goal of this dissertation is to understand the mechanistic details of the Shroom-Rock interaction. Using structural studies I have started to dissect the SD2-SBD interaction. I first determined the crystal structure of the Drosophila Shroom SD2 domain at 2.7 Å resolution to be a novel fold composed of a three-segmented, anti-parallel, coiled-coil dimer. Using mutational analysis and a combination of *in vivo* and *in vitro* assays we identified surfaces within the central coiled-coil segment of the SD2 domain that mediate Rock binding. The anti-parallel nature of the SD2 domain introduces internal symmetry into the SD2 domain such that

there are two identical binding sites for Rock on opposite sides of the molecules suggesting interesting implications for the Shroom-Rock interaction. We also determined the crystal structure of the Rock SBD to 2.5 Å resolution and saw that it is a parallel coiled-coil dimer. Using mutational analysis combined with biochemical assays I have identified two conserved patches on opposite ends of Rock SBD that are required for Shroom interaction. These patches, unlike the patches on the SD2 domain, are not identical. Biochemical characterization of the SD2-SBD complex suggests that molar ratio of this complex is 1:1. Based on these results we can start to suggest models for how Shroom and Rock interact.

TABLE OF CONTENTS

LIST OF TABLES

LIST OF FIGURES

PREFACE

I would like to start by thanking my advisor Andy VanDemark. For the past five years Andy has been incredibly patient and supportive. When I joined the lab I knew almost nothing about x-ray crystallography and expressed my concerns to Andy about whether or not I would be able to learn and understand crystallography. Andy assured me that I would have no problem learning crystallography and promised me that he would make sure I would understand and enjoy crystallography. And lo and behold, he delivered on his promise! While there are aspects of crystallography I am not particularly fond of, such as my crystals always forming the cold room, building my structures has been exceptionally fun. When I started learning the principles of crystallography Andy patiently answered every single question I had. He helped me learn how to manipulate and loop crystals and only lost his cool once, when I almost dipped my hand in liquid nitrogen. Without Andy's guidance and support I could not have overcome all the challenges I encountered while completing my project.

I would like to thank all of my past and present lab members who have made the lab a fun and fantastic place to work in. I cannot imagine what the past four years would've been like without Aubrey. She is not just our wonderful lab manager without whom our lab would just come to a screeching halt, but also one of my closest and best friends. Thank you Aubrey for helping me keep my sanity throughout all these years and for patiently listening to me complain about all of my problems big or small. To the current graduate students in our lab Adam and

Chris: thank you for making the lab such a great environment. You both have helped me so much over the years with experiments, writing proposals, and making presentations and posters. You are not just great lab mates but also great friends. I am going to sorely miss our daily lunches. To the past and current undergraduate members of the lab, it has been really great pleasure working with you and teaching you different lab techniques. I would like to thank one particular undergraduate student Racheli Schoenburg, who was instrumental in obtaining diffraction quality hRock SBD crystals. She also worked with me to optimize the mShroom2 SD2 crystals and the SD2-SBD complex crystals. Mentoring Racheli was wonderful experience not only because she was such a talented student but also because she was a great person to be around.

I would like thank our great collaborator Jeff Hildebrand who has been key to my success in this project and the members of his lab specifically Debamitra Das and Ryan Rizaldy. I have had the pleasure working closely with D who is a current graduate student and Ryan who was the former lab technician in the Hildebrand lab. Ryan was instrumental in the designing, cloning and purification of the initial SD2 and SBD constructs for crystallography. Both Ryan and D performed all of the cell-based assays presented in this work. I would also like to thank both Ryan and D for their contribution to the biochemical assays presented in this work. Jeff was always available whenever I had questions about experiments and always gave me great advice to improve my presentations. It has been absolutely fantastic working with the Hildebrand on this project and I couldn't ask for better collaborators.

I would also like to thank my committee members Karen Arndt, Jeff Brodsky, Michael Grabe, and Mark Macbeth who have provided me with indispensible suggestions, criticisms, and guidance throughout my graduate career.

I would like to acknowledge the labs and facilities that provided me with help, reagents and equipment for this work. I used the x-ray facilities here at the University Of Pittsburgh and at the National Synchrotron Light Source (NSLS) in Brookhaven for all of my data collection. Ivan Vorontsov and Laurie Betts were the facilities managers at the x-ray facilities here at Pitt and were extremely helpful with any problems I experienced during data collection and data processing. Annie Heroux collected and processed all of the data collected at the NSLS. I would also like to thank our collaborators in the Trakselis lab specifically Micheal Traselis and Robert Bauer for their work on the fluorescent experiments done to characterize the Shroom-Rock complex. I would like the thank Tom Harper for taking beautiful pictures of my crystals and Eric Polinko for helping me with all of my problems with running crystallographic programs. Lastly, I would like to thank our neighbors the Arndt, Martens, Brodsky, and Hendrix labs for reagents, equipment and advise.

I have a taught two classes and guest lectured a few times for computational biology in the past four years. I would like to thank Craig Peebles and Nancy Kaufman for being great teaching mentors for the courses that I taught. Also, I would like to thank Eric Polinko for giving me the opportunity to give guest lectures in his Computational Biology class. I was very surprised and grateful that he invited me back every semester after my first attempt to teach his class about proteins where I talked so fast that I was done with a 50 minute lecture in 15 minutes. All of my teaching experiences have been very rewarding and have helped me improve my public speaking abilities.

1.0 INTRODUCTION

During development tissues undergo controlled changes in shape and structure culminating in a highly organized embryo. In most animals, common types of morphogenetic events such as tissue folding or tissue elongation bring about changes in embryonic tissue. Bending of epithelial sheets is a central morphogenetic process that is required for the formation of the gut, the eye, and the neural tube (Fig. 1). This bending is facilitated by a combination of apical constriction and cortical tension along the apicobasal axis. Further, at the cellular level intrinsic and extrinsic elements, such as the extracellular matrix and the cytoskeleton, provide the forces required to alter cell shape to drive bending of epithelial sheets. The forces that shape epithelial tissues are regulated spatially and temporally by a variety of proteins that regulate the cytoskeletal dynamics. Forces generated locally on a single cell need to be coordinated throughout the epithelial sheet for proper bending to occur. The cytoskeleton also plays a role in integrating these local signals and forces to produce coordinated movements in sheets of epithelial cells. Thus, tight regulation of the cytoskeleton is key to proper embryonic development.

The major cytoskeletal proteins that alter epithelial cell shape are myosin II and actin filaments. Myosin II binds actin filaments to generate the force required for epithelial morphogenesis. Together these proteins form the basic molecular force that drives tissue morphogenesis, and not surprisingly require precise regulation of their subcellular localization and activation. In epithelial cells, the activity of myosin II is primarily regulated by Rho-kinase.

Rho-kinase phosphorylates and activates the actin associated ATPase activity of myosin II [1]. Epithelial cells can regulate the activity of the actin-myosin (actomyosin) network by regulating the subcellular localization of Rho-kinase. In a number of epithelial cells, the actin binding protein Shroom interacts with Rho-kinase (Rock) and recruits it to apical surfaces [2]. Apart from altering Rock subcellular localization Shroom proteins also reorganize and alter the subcellular localization of actin filaments [3, 4]. Via the Shroom-Rock interaction non-muscle myosin II is activated at apical surfaces resulting in the formation of a contractile actomyosin cytoskeleton. This reorganization of the actomysoin cytoskeleton by the Shroom and Rock proteins is required for various developmental processes such as neural tube closure, retinal morphogenesis, and the development of vasculature [3, 5-7]. There are several aspects of the Shroom-Rock pathway that are still unclear. The biggest unanswered question in this pathway is how Rock is activated upon binding Shroom. This dissertation will focus on understanding the Shroom-Rock interaction to gain insight into the regulation of actomyosin dynamics during embryonic development.

1.1 EPITHELIAL MORPHOGENESIS

Epithelial cells undergo highly coordinated cell shape changes during embryogenesis. There are several general morphogenetic processes such as, intercalation, invagination, sheet extension, and tube formation, elongation and constriction that bring about changes in epithelial sheets. At the cellular level a mixture of apical constriction and asymmetric cortical tension drives these processes. Myosin II is the primary cytoskeletal motor that drives shape change in epithelial cells. In epithelial cells, activated myosin II walking along actin filaments generates the

contractile force required to shrink the apical surfaces (reviewed in [8]). Understanding the regulation of epithelial morphogenesis will provide insight into how organisms orchestrate complex changes in tissue architecture during development.

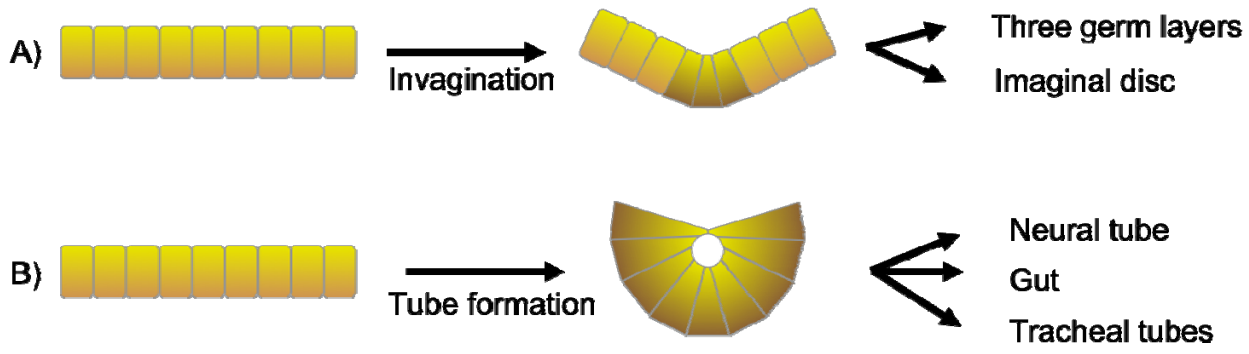

Figure 1: Common tissue morphogenetic events.

(A) Invagination is a process during which a few cells apically constrict to facilitate the inward folding of a sheet of cells.

(B) During tube formation epithelial cells apically constrict and elongate to convert a sheet of cells into a tube.

1.1.1 Apical Constriction

Apical constriction is a process where the actomyosin network, localized to the apical surface of cells, contracts resulting in shrinking of cellular apices. During development, apical constriction is important for various morphogenetic processes such as tissue bending, tube formation, invagination, and internalization of small numbers of cells. In many organisms apical constriction commonly occurs during gastrulation when the three germ layers are established. In *X. laevis* and sea urchins apical constriction drives the primary invagination of cells during the formation of the archenteron or the primitive gut [9-11]. Apical constriction also drives the ingression of cells during gastrulaion in *C. elegans* [12]. In fruit files apical constriction regulates ventral furrow formation, internalization of the mesoderm, dorsal closure, eye development, and the formation of the salivary glands and tracheal tubes [13-17]. Apical constriction also plays a role in shaping tissue during neurulation in vertebrates [18]. During development of the central nervous system, a flat epithelial sheet called the neural plate bends, extends, and folds into the neural tube. Neural tube closure is driven by apical constriction of cells in the neural plate [19, 20]. Thus, apical constriction is a conserved process used by most animals to bring about changes in tissue shape during embryogenesis.

Numerous signaling pathways regulate apical constriction by controlling the actomyosin cytoskeleton dynamics. In several of these processes, Rho GTPases and Rho-kinase activate myosin II and trigger the formation of a contractile actomyosin network [2, 4, 21-28]. During neural tube closure circular bands of actin filaments accumulate at the apical junction and non-muscle myosin II binds to these actin filaments [29]. The actin binding protein Shroom3 is one

of the most important cytoskeletal regulators required for neural tube closure [2, 3, 30]. Shroom3 recruits the actin binding proteins Ena/VASP and cell adhesion proteins nectin-2 and N-cadherin to the apical side of neuroepithelial cells [5, 31-35]. Shroom3 also binds to Rho-kinase and recruits it to the apical side of neuroepithelial cells where it phosphorylates and activates non-muscle myosin II [2, 4]. Accumulation of F-actin and activated myosin at the apical surfaces of cells always precedes apical constriction [9]. While the upstream regulators of all these developmental processes vary greatly the central effectors that cause apical constriction and alter cell morphology are actin filaments and myosin II motors.

1.1.2 Actomyosin Cytoskeleton

Myosin II and actin filaments are the major cytoskeletal proteins that bring about changes cell shape. Non-muscle myosin II is an actin-based motor that is composed of two heavy chains, two essential light chains and two regulatory light chains. Each heavy chain is composed of an N-terminal globular head domain that has the actin-binding and ATP-binding sites. Following the head domain is an alpha helical neck region that is thought to act as a lever arm [36]. The C-terminal portion mediates dimerization and filament formation. The light chains are small proteins interact with the neck and head regions of the heavy chains. Myosin motors attach and detach from actin filaments in a cyclical manner. When bound to ATP, myosin II can bind to actin filaments. Upon binding actin filaments myosin undergoes a conformational change that is coupled to ATP hydrolysis. This ATP hydrolysis moves the myosin motor along the filament resulting in displacement of the filament [37]. This myosin II stroke activity can reduce the overall length of junctional membrane between cells and accumulation of myosin II at apical

surfaces can cause the apical plasma membrane to shrink. The contractile forces generated by myosin II motors walking along actin filaments drive epithelial cell shape change.

Tissue morphogenesis requires a balance between stiffness and contractility, both of which depend on the actomyosin network [38]. Actomyosin contractility in epithelial cells undergoing morphogenesis is not completely understood. Epithelial cells undergoing apical constriction contain activated myosin II that colocalizes and binds to circular bands of actin filaments accumulated at apical surfaces. Contracting epithelial cells display dynamic actomyosin activity where actin and myosin transiently accumulate at the cell cortex and condense to form foci. This accumulation of condensed actomyosin foci is correlated with pulses of cell contraction [39, 40]. These pulses of cellular contraction need to be stabilized for productive tissue contraction. Models describing changes in tissue shape suggest that the junctional actomyosin network acts as a ratchet that maintains the contraction generated by the medial network. Alternatively, high frequency of foci formation can result in rapid contraction and surpass the need of the junctional ratchet [39]. Here, transition to a supracellular actomyosin network stabilizes the fluctuations in cellular contractility and increases tissue stiffness [41, 42]. Actomyosin dynamics is required for various aspects of tissue morphogenesis during development.

The spatial and temporal regulation of actomyosin activity is key to coordinating the morphogenetic events that control epithelial morphogenesis. Myosin II motor activity is regulated by phophosrylation of the regulatory myosin light chain, which increases the ATPase activity of myosin II allowing it move along actin filaments [43]. In epithelial cells, Rock is the primary kinase that phosphorylates the regulatory myosin light chain and activates non-muscle myosin II [1]. The regulation of actomyosin dynamics can be controlled by spatially and

temporally regulating the activation of Rock. Thus, understanding the mechanisms that activate Rock provide insight into how cytoskeleton dynamics is regulated to bring about changes in cell shape during development.

1.2 RHO-KINASE

Rock is a major cytoskeleton regulator that causes cytoskeletal rearrangements by activating myosin II. It is important for various processes such as smooth muscle contraction, formation of stress fibers and focal adhesion complexes, intermediate filament disassembly, neurite rectraction, microvilli formation, cytokinesis and cell migration [44-53]. The actin-induced ATPase activity of myosin II is activated upon phosphorylation of Ser-19 of the regulatory myosin light chain (MLC). MLC phosphatase inactivates myosin II by removing the phosphorylation mark at Ser-19 on MLC [54-56]. Rock directly activates myosin II by phosphorylating MLC at Ser-19 allowing myosin II to associate with actin. Additionally, Rock phosphorylates MLC phosphatase at Thr-697 and Ser-854, inhibiting the phosphatase activity of MLC phophatase and increasing the active population of myosin II [1, 57-60]. In addition to MLC and myosin phosphatase, Rock targets several other proteins that are involved in cytoskeleton dynamics. Rock phosphorylates Ezrin/Radixin/Moesin family of proteins that play a role in linking actin filaments with the plasma membrane [61-63]. Another actin binding protein, adducin, is phosphorylated by Rock and this mark is required for membrane ruffling and cell motility [53, 64]. Rock also plays a role in stabilizing actin filaments by phosphorylating LIM-kinases [65]. This phosphorylation mark enhances the kinase activity of LIM-kinases to phosphorylate and inactivate the actin-depolymerizing protein cofilin [66]. Lastly, Rock also

phosphorylates and induces depolymerization of intermediate filaments during cytokinesis [45, 50, 67]. Thus, Rock is a central cytoskeleton regulator that plays a key role in controlling cytoskeleton dynamics.

Rho-kinase (Rock) is a Ser/Thr protein kinase identified in various biochemical assays performed to find binding partners for the GTPase Rho [68-70]. There are two Rock isoforms, Rock I and Rock II, that share 64% overall identity [47, 70-72]. Rock I and Rock II are both expressed in most tissues; however, there are a few differences in the expression pattern of the two isoforms and in their roles in regulating cytoskeleton dynamics [71, 72]. Both Rock I and II have a N-terminal kinase domain, a central region predicted to have an alpha helical coiled coil motif and a Rho binding domain located at the end of this coiled coil region (Fig. 1A) [47, 69, 73]. The very C-terminal portion of Rock contains a pleckstrin homology domain split by a cysteine rich region (Fig. 1A) [69, 70]. Both Rock isoforms bind GTP-RhoA and have the highly conserved N-terminal kinase domain that shares 44% sequence identity to myotonic dystrophy kinase [68, 69, 71].

1.2.1 The kinase domain of Rock

The Rock kinase domain is the most conserved region of the protein and is 95% identical in Rock I and Rock II [47, 72]. The crystal structure of the kinase domain from Rock I reveals that this domain has a typical Ser/Thr kinase fold consisting of two lobes linked by a hinge [74]. The structure also revealed that the kinase domains dimerize in a head to head manner using an N-terminal α-helical dimerization domain and the kinase tail [74]. The dimer interactions orient the two monomers such that active sites of the kinase domains appear on a single face. This was the first structure of a kinase domain from the mytonic dystrophy kinase family. Structural

alignments with other kinase domains revealed that the PKA kinase domain and Rock kinase domain align with a root mean square deviation of 1.3 Å [74]. Structural comparisons revealed that the Rock kinase domain resembled the catalytically active conformation of the PKA kinase domain. The residues in the Rock kinase active site arranged in a manner similar to the residues in the active site of the activated PKA kinase domain and the Rock activation loop resembles an active conformation [74, 75]. In many kinases the catalytically competent conformation is stabilized by phosphorylation of a serine or threonine on the activation loop. No such phosphorylation mark was seen in the crystal structure of the Rock kinase domain suggesting that phosphorylation of the activation loop might not be essential for Rock activation [74]. These results indicate that the Rock has a canonical Ser/Thr kinase domain that is activated in a phosphorylation independent manner.

1.2.2 Regulation of Rock activity

Similar to myotonic dystrophy kinase Rock proteins have an autoinhibitory C-terminal region [76, 77]. The C-terminal region, consisting of the Shroom-binding domain, Rho-binding domain, and the split pleckstrin homology (PH) domain, can interact with the N-terminal kinase domain and inhibit the kinase activity of Rock [76, 78]. Additionally, deleting the C-terminal region results in constitutively active Rock [47, 48]. Autoinhibtion of Rock can be relieved by numerous mechanisms the most common of which is by association with activated GTP-Rho [1, 57, 68-70]. Rock acts downstream of Rho in numerous processes including the formation of stress fibers and focal adhesions, smooth muscle contraction, and several others [46, 48, 49]. Interaction with activated GTP-RhoA can recruit Rock to the plasma membrane and is thought to relieve the autoinhibition of the N-terminal kinase domain of Rock [70]. Other activation

mechanisms include binding to lipids, cleavage of the C-terminus of Rock by Caspase-3 or oligomerization [78-81]. These observations suggest that Rock kinase activity is dependent on the Rock C-terminal region and the effector proteins that interact with this region.

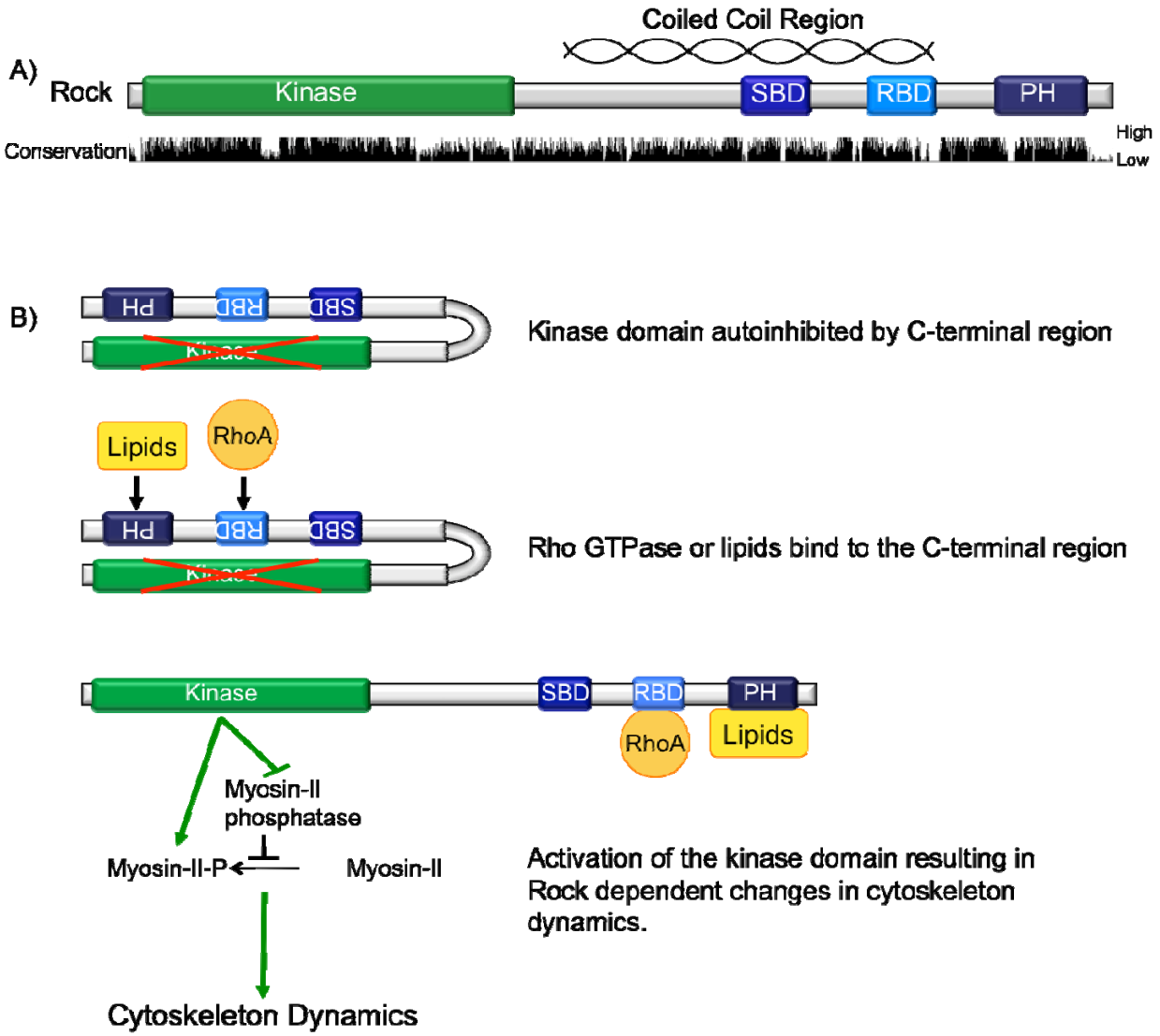

Figure 2: Domain profile and Activation Schematic of Rock.

(A) Domain architecture of Rock. The kinase domain is shown in green and the binding regions for Rock binding partners are shown in blue. The conservation of each domain shown as black bars underneath. The conservation was obtained from a multiple sequence alignment of 16 Rock I and Rock II proteins in ClustalW. The image was created in JalView.

(B) Regulation of the kinase domain by the C-terminal region of Rock and Rock effectors. The autoinhibition by the C-terminal region of Rock relieved by interaction with Rhoa or lipids.

1.2.3 Rho-binding domain of Rock

The Rho binding domain of Rock belongs to the class II group of Rho binding motifs that includes mostly coiled coil proteins [73, 82]. This domain in Rock corresponds to approximately 80 amino acids at the end of the central coiled coil region (934-1015 in human Rock). There are two patches within these 80 amino acids that are required for Rho binding, 934-945 and 1005-1015 [73]. The structures of the Rho binding domains (RBD) from Rock I and Rock II have been determined to be parallel coiled coil dimers [83, 84]. The structure of Rock I RBD was solved in complex with GTP-RhoA while the structure of Rock II RBD was solved in its unbound form. Structural comparison of both the RBDs indicates that while there are differences in the N-terminal and central portions of the coiled coil RBD dimer, the C-terminal portions are very similar [84]. Mutational analysis identified residues that are important for the Rho-Rock interaction and these residues localize to the C-terminal portion of the RBD crystal structures [47, 73, 83, 84]. The structure of the Rock-RhoA complex revealed that both the helices in the coiled coil interact with the switch regions of RhoA. The Rock-RhoA interaction is primarily mediated by hydrophobic interactions with a few electrostatic interactions at the edges of the binding interface [84]. The hydrophobic interactions at the RhoA-Rock interface resemble the hydrophobic interactions at the Cdc42-PAK1 interface [85]. Cdc42 activates autoinhibited PAK1 kinase domain by causing a conformational change upon binding to the kinase [85, 86]. Since RhoA and Rock interact in a manner similar to Cdc42 and PAK1 it is possible that GTP-RhoA could cause a conformational change upon binding to the Rock RBD resulting in dissociating the C-terminal region from the kinase domain (Fig. 1B). The structures of the Rock RBDs revealed that RhoA interacts with a small patch of residues in the RBD of Rock and via this interaction RhoA could induce a conformational change that activates the kinase activity of Rock.

1.2.4 PH domain of Rock

Rock can also be activated by binding to lipids such as arachidonic acid or PI(3,4,5,)P_3 using its PH domain [72, 87]. The structure of the split PH domain from Rock II has been determined using NMR [88]. This domain in Rock has a canonical PH fold consisting of 7 β-strands and a C-terminal α-helix. In Rock the PH domain is split between β6 and β7 by a cysteine rich region that folds into a C1 domain [88]. C1 domains from other proteins have been known to bind phorbol esters and DAG. The Rock C1 domain, however, lacks the phorbol ester/DAG binding motif and most likely does not interact with these molecules. Additionally, the Rock II spilt PH domain lacks the canonical phosphoinsositol lipid binding motif instead, it has a flat positively charged surface at the C-terminal end that mediates interactions with lipid membranes with PI(3,4,5)P_3, PI(3,4)P_2 or PI(4,5)P_2 embedded in them [88]. It is possible that via its interactions with the lipids Rock could be activated and recruited to the plasma membrane.

1.2.5 Shroom-binding domain of Rock

During development, Rock can activate non-muscle myosin II and induce apical constriction causing epithelial cells to invaginate. During mesoderm invagination in fruit flies RhoGEF2 is activated and anchored to the plasma membrane [22, 25]. This in turn results in activation of Rho1 and Rock resulting in apical constriction. Rock is also required for Shroom mediated apical constriction especially during neural tube closure in vertebrates and dorsal closure in fruit flies [2, 4, 89]. In epithelial cell lines as well as neuroepithelial cells Shroom proteins recruit Rock to the apical junctions or apical surfaces. In these cells phosphorylated MLC also colocalizes with Shroom and Rock at the apical junctions [2]. In Shroom the highly conserved C-terminal SD2

domain mediates this interaction and both Rock I and Rock II bind equally well to the Shroom SD2 domain [2]. Via this interaction, Shroom recruits Rock to the apical junction during development to activate non-muscle myosin II and induce apical constriction.

The Shroom-Rock interaction was identified in a pull-down assay screening for molecules that interact with the Shroom SD2 domain [2]. The Shroom binding domain in Rock is located in the central coiled coil region and is distinct from the Rho binding domain (Fig. 1A) [2] [unpublished data from VanDemark and Hildebrand labs]. Activation of Rock in the Shroom-Rock pathway occurs independent of Rho or lipids. RhoA and Shroom bind Rock independently and RhoA is not required for Shroom mediated apical constriction [5, 90]. Activation of Rock during Shroom mediated apical constriction most likely occurs via a unique mechanism different from the ones described above. Understanding the Shroom-Rock interaction will allow us to further understand Rock activation and its role in cytoskeleton dynamics.

1.3 SHROOM FAMILY OF PROTEINS

Shroom proteins are conserved actin binding cytoskeleton regulators that play an important role in a wide variety of developmental processes. There are four Shroom family members, Shroom 1-4, and they are mainly expressed in epithelial cells [91]. Most Shroom proteins have an N-terminal PDZ domain and two conserved domains only found within the Shroom family of proteins. These two domains are called Shroom Domain 1 (SD1) for the centrally located domain and Shroom Domain 2 (SD2) for the C-terminally located domain [3] (Fig. 2). The C-terminal SD2 domain is the most conserved domain, is found in all Shroom proteins and is essential for Shroom function [3, 92, 93]. Shroom3 is the best-characterized member of this

family of proteins. It has been shown to bind to F-actin and mediate epithelial morphogenesis by inducing apical constriction. The other members of the Shroom family also have roles in regulating cell morphogenensis; however, they differ from Shroom3 in their actin binding properties and subcellular localization [93]. Shroom proteins from invertebrates and Shroom2 bind to cortical actin while Shroom4 binds to punctate actin fibers in the cytoplasm [93, 94]. All Shroom proteins can reorganize the actomyosin network via a conserved interaction with the cytoskeleton regulator Rock [2, 89].

However, expression of Shroom2, Shroom4 or *Drosophila* Shroom (dShroom) in MDCK cells does not cause apical constriction [93]. Therefore, while there are various conserved aspects in the function of the different Shroom proteins, specifically with regards to the SD2 domain, they play distinct roles in cellular morphogenesis.

1.3.1 Shroom3

Shroom3 was identified in a gene trap assay in mice where mutations in the gene resulted in severe neural tube defects [3]. Mice embryos with mutations in this gene have defects in neural tube closure that result in exencephaly, acrania and facial clefting [3]. Inhibiting Shroom3 activity in *Xenopus* embryos using a dominant negative construct or a morpholino also causes neural tube defects [30]. In these mutant embryos the anterior folds fail to move towards midline thus inhibiting neural tube closure. In both mice and frog embryos Shroom3 mutations caused prominent anterior neural tube defects [3, 30]. During neural tube formation apical constriction is most pronounced at the hingepoint regions in the neural plate which form distinct lines of bending and facilitate movement of the neural folds [20]. Knock out analysis of Shroom3 in *Xenopus* revealed that inhibiting Shroom3 activity inhibits the formations of hingepoints which

in turn prevents normal bending of the neural epithelium [30]. These defects caused by Shroom3 mutations are not due to alterations in tissue patterning, cell proliferation or cell survival [3]. These observations indicate that Shroom3 is required for proper neural tube formation in vertebrates.

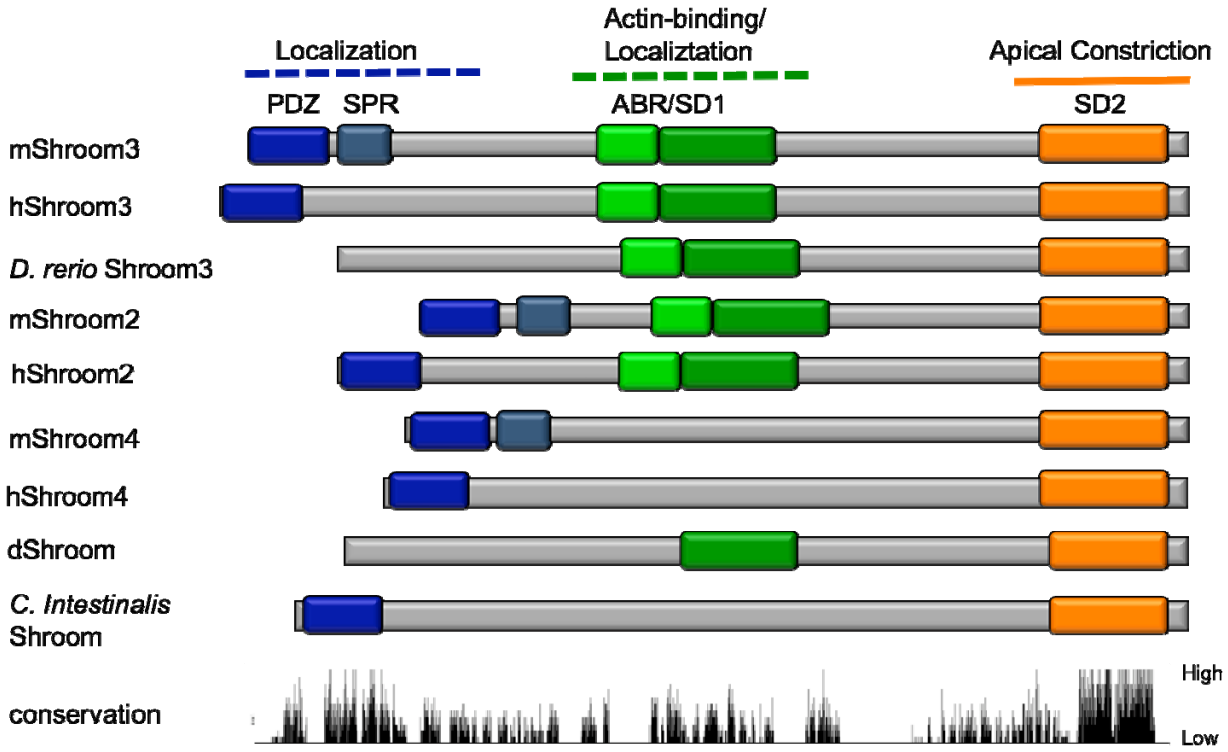

Figure 3: Domain architecture of Shroom proteins.

Domain architecture of all four Shroom family members. The PDZ domain is shown in blue, the SD1 and acting binding regions are shown green and the highly conserved SD2 domain is shown in orange. The conservation of each domain is shown below as black bars. The conservation was obtained from a multiple sequence alignment of 12 Shroom proteins in ClustalW. The image was created in JalView.

Shroom3 is expressed in the neuroepithelium, heart, skeletal muscle, and gut and localizes primarily with F-actin at apical junctions [3]. It has been shown to co-localize with F-actin and adherens junction proteins at apical surfaces of neuroepithelium in ring like structures [3, 4]. Ectopically expressed Shroom3 in epithelial cells or in *Xenopus* blastula is also concentrated at the apical surface [30]. When ectopically expressed in MDCK cells Shroom3 is restricted to the apical junctional complex (AJC) and causes cells to undergo apical constriction [4]. However, not all of the cells expressing Shroom3 in a monolayer go through apical constriction. Cells neighboring constricted cells have expanded apical surfaces and altered tight junction architecture. In these cells the tight junctions appear straight and rigid instead of wavy as if under tension [4]. These cells most likely expand their apical surfaces to keep the monolayer intact. In mixed population of cells, the Shroom3 expressing cells apically constrict and take on a wedge shape [4]. These cells arrange themselves into tightly packed clusters at the apical surfaces similar to the way cells arrange themselves in the ommatidia of the *Drosophila* eye [95]. Cells in the *Xenopus* blastula that express exogenous Shroom3 also apically constrict and take on a wedge shape. This phenomenon only occurs in cells that have already established apical and basal polarity [30]. Shroom3 not only binds to actin filaments but also regulates the subcellular localization of F-actin [3, 4, 30]. In the *Xenopus* blastula ectopically expressing Shroom3, actin filaments are accumulated at the apical surfaces [30]. In cells undergoing apical constriction the actin fibers appear to be more condensed at the apical surface and closely associated with the adherens junction marker ZO-1. In the neighboring cells with expanded apical surfaces the stress fibers traverse the apical surfaces perpendicular to the apical-basal axis [4]. These experiments revealed that Shroom3 alters cell morphology by reorganizing the actin

cytoskeleton at apical surfaces to trigger apical constriction; however, it does not alter cellular polarity [4].

The Shroom SD1 and SD2 domains are required in *cis* for Shroom induced apical constriction [30, 93]. The Shroom3 SD1 domain mediates the interaction with F-actin and determines the subcellular localization of Shroom and the SD2 domain triggers apical constriction. The SD2 domain expressed by itself in MDCK cells remains diffuse in the cytoplasm and dose not cause apical constriction. However, tagging the SD2 domain with Endolyn and targeting it to the apical plasma membrane causes apical constriction in cells [4]. Alternatively, expressing a truncated form of Endolyn tagged Shroom that lacks the SD2 domain does not induce apical constriction. Cortical actin in cells ectopically expressing Shroom3 or Endolyn-SD2 is reorganized into stress fibers [4]. These results suggest that as along as the SD2 domain is targeted to the apical membrane it is sufficient to induce apical constriction [4].

In addition to F-actin reorganization, Shroom3 mediated apical constriction also requires non-muscle myosin II and Rho-kinase (Rock) activity at the apical junctions [4]. The Shroom SD2 domain mediates this interaction with Rock and recruits Rock to apical junctions [2, 4]. Rap1 GTPase activity has also been shown to be required for Shroom3 mediated apical constriction [30]. Ectopic expression of Shroom3 or Endolyn-SD2 causes redistribution of activated non-muscle myosin II to the apical junctional complexes [4]. This Shroom3 dependent recruitment of F-actin and myosin II to the apical junctional complexes is also seen in developing embryos [4]. In neural tubes of embryos with mutations in Shroom3, F-actin is poorly localized to the apical surface [3]. The recruitment of actin filaments and activated myosin II to the apical surfaces facilitates the formation of a contractile actomyosin network that

can cause changes in cell shape. These results indicate that Shroom3 regulates apical constriction via reorganizing and redistributing the actomyosin cytoskeleton.

During embryogenesis apical constriction is tightly coupled to apicobasal elongation. Microtubules are the cytoskeletal components that mediate cell elongation during neurulation and their assembly is primarily regulated by γ-tubulin [29, 96]. Shroom3 redistributes γ-tubulin resulting in the assembly of parallel microtubles that drive apicobasal elongation [97]. Shroom3 regulates neuroepithelial morphogenesis not just by triggering apical constriction but also by regulating apicobasal elongation.

Apart from regulating neural tube closure Shroom3 mediates changes in cell morphology in numerous other developmental processes. Shroom3 can associate with Plenty of SH_3 (POSH) and negatively regulate axon outgrowth in primary cortical neurons [98]. POSH is a multi-domain scaffold protein that has roles in regulating changes in cell shape [99]. Shroom3 binds to the third SH domain in POSH and knockdown of either protein causes in an increase of myosin II in primary cortical neurons resulting in axon outgrowth [98]. Shroom3 is also required for proper lens development in mice [5]. In the lens Shroom3 expression is dependent on Pax6 a crucial transcription regulator in eye development [5, 100]. During lens development Shroom3 binds to the actin binding protein Vasp via its EVH1 binding domain and recruits Vasp to the apical surface [5]. This recruitment is required for proper apical constriction in the lens pit and proper development of the lens. Shroom3 mediated apical constriction in the lens pit is also dependent on Rock activity and myosin II [5]. In *Xenopus* and mice Shroom3 is required for proper gut morphogenesis [31, 101]. In mice Shroom3 acts in conjuction with N-cadherin to regulate apical constriction during gut morphogenesis [31]. Ptix, a major transcription

factor involved in gut development, drives Shroom3 expression in the developing gut [31, 101]. Shroom3 mediated apical constriction is required throughout embryogenesis for the development of various organs.

1.3.2 Shroom2

Shroom2 is also expressed primarily in epithelial cells and is implicated in regulating cell morphogenesis during development of vasculature, retinal pigment epithelium, and the neural tube [6, 7, 91, 93]. In the vascular endothelium, Shroom2 binds to cortical actin and is localized at cell-cell junctions [93]. During vascular morphogenesis Rock and myosin II are required to induce cortical tension to inhibit membrane protrusion and cell migration [102]. Shroom2 also plays a role in this process as deletion of Shroom2 in vascular epithelia decreases Rock and myosin II activity and increases angiogenesis [7]. Pigmentation in the retinal pigment epithelium (RPE) is the result of apical accumulation of mature melanosomes [103-105]. Mature melanosomes are targeted to apical surface via microtubules and actin cytoskeleton [104]. Shroom2 facilitates apical pigment accumulation in a Rab27a dependent manner and is required for proper melanosome maturation [6]. These studies suggest that Shroom2 is a central regulator of RPE pigmentation in *Xenopus* [6]. Similar to Shroom3, Shroom2 also mediates the assembly of microtubules in the neural plate to induce apicobasal cell elongation [91]. The majority of the processes regulated by Shroom proteins require myosin II activity. Additionally, Shroom2 has also been shown to bind to unconventional myosin VIIa in embryonic and adult epithelia [106]. Both Shroom2 and Myosin VIIa localize to tight junctions in a wide variety of epithelial cells and possibly play a role in maintaining and strengthening tight junctions. These studies suggest

that Shroom2 also plays a key role in regulating shape change in various types of tissues during embryonic development.

1.3.3 Shroom1 and Shroom4

Shroom1 and Shroom4 are not as well characterized as Shroom3 or Shroom2. Shroom1 is exclusive to *Xenopus* and is found in the apical surface of epithelial cells and is associated with epithelial sodium channel [107, 108]. Shroom4 lacks the SD1 domain and is expressed primarily in mesodermal tissue [91, 94]. Similar to Shroom2 and Shroom3, Shroom4 can also regulate microtubule assembly by altering γ-tubulin distribution [91]. Shroom4 is expressed in most tissues and can interact with populations of F-actin that are distinct from stress fibers or cortical actin [94]. Shroom4 is associated with human X-linked mental retardation and ocular alibinism type 1; however, its exact developmental role is unclear [92, 109]. The roles of these Shroom family members in development need to be further characterized.

1.3.4 Invertebrate Shroom proteins

Shroom proteins were identified in several invertebrate organisms such as fruit flies, sea urchins and sea squirts by searching for open reading frames encoding SD2 domain [93]. Among the Shroom proteins identified in invertebrates *Drosophila* Shroom is the best-characterized protein. dShroom lacks the N-terminal PDZ domain but has a loosely conserved SD1 region and the highly conserved SD2 domain [89, 93]. There are two Shroom isoforms in *Drosophila*, dShroomA and dShroomB that differ in their subcellular distribution [89]. dShroomA, the longest isoform, is the most abundant isoform expressed in the developing embryo [89]. The two

isoforms vary at the N-terminus and use different mechanisms for localization. F-actin is required to localize dShroomA to the adherens junctions. dShroomA binds actin filaments using a region that has moderate (26%) homology to vertebrate SD1 domain [89]. The shorter dShroomB isoform is not found at the adherens junctions; instead, it localizes to the apical plasma membrane of the ectoderm. While dShroomA cannot cause apical constriction in MDCK cells, dShroomB localizes to the apical membrane and moderately decreases the apical area [89]. Overexpression of either isoform in the developing *Drosophila* embryo causes defects in dorsal closure. At the cellular level these defects seem to be due to aberrant apical constriction occurring in cells overexpressing dShroom [89]. In these cells there is an increase in accumulation of F-actin and activated myosin II at the adherens junctions. The C-terminal regions, which contain the SD2 domain of these two isoforms, are identical. *In vitro* experiments indicated that *Drosophila* Rock binds to dShroom SD2 domain and Rock is required for dShroom mediated cytoskeletal reorganization *in vivo* [89]. These results suggest that the Shroom-Rock pathway has been conserved over animal evolution.

1.3.5 Conserved domains in Shroom proteins

Not all the Shroom family members have the N-terminal PDZ domain or the centrally located SD1 domain (Fig. 2). However, all Shroom proteins have the C-terminal SD2 domain and regulate myosin II activity via this domain. The SD2 domains from all Shroom proteins can cause actomyosin based apical constriction if targeted to the apical surface [93]. Only expression of full length Shroom3 can cause apical constriction in epithelial cells. However, expression of chimeric Shroom proteins that have the N-terminal portion from Shroom3 and the C-terminal SD2 domain from Shroom2, invertebrate Shroom, or Shroom4 in MDCK cells can cause apical

constriction [93]. Shroom directly interacts with Rock via the SD2 domain and this interaction is required for the recruitment of Rock and myosin II to the apical junctions [2]. It is unclear how the interaction between Shroom and Rock activates the kinase activity of Rock. The most common mechanism by which Rock is activated is by binding GTP-Rho. Binding to Rho, however, is not required for Shroom mediated apical constriction. Shroom3 might cooperate with Rho to promote apical constriction; however, it is not dependent on Rho to induce apical constriction [90]. Both Shroom3 and RhoA can bind Rock simultaneously *in vitro* indicating that these two proteins do not compete to interact with Rock [5]. While the N-terminal and central portions of Shroom bring specificity to Shroom proteins, the basic function of all Shroom proteins is carried out by the SD2 domain. Understanding how the SD2 domain interacts with Rock and recruits it to the apical junctions is key to understanding the mechanistic details of Shroom function.

1.4 DISSERTATION AIMS

The Shroom-Rock pathway is a conserved pathway found in vertebrates and invertebrates [93]. It is important for numerous developmental pathways including neural tube closure, dorsal closure in fruit files, retinal morphogenesis and several others [3, 6, 89]. Shroom is an actin binding protein that can localize to actin filaments and bring about changes in cell shape by reorganizing the actin cytoskeleton. There are four Shroom family members that differ primarily in their actin binding activities and subcellular localization. Shroom proteins can have a N-terminal PDZ domain and a centrally located SD1 domain. These domains mediate localization and the actin binding activity of Shroom. All Shroom proteins identified so far have a highly conserved C-

terminal SD2 domain. This domain mediates the interaction with Rock and is required for the basic function of Shroom. SD2 domains from any Shroom proteins can cause apical constriction as long as they are localized to the apical surface [2, 93]. The SD2 domain interacts with a conserved centrally located Shroom binding domain (SBD) in Rock [2].

Rock proteins are highly conserved cytoskeleton regulators that phosphorylate and activate myosin II. In the Shroom-Rock pathway, Rock is recruited to the apical surface by its interaction with Shroom where it can then activate myosin II and induce a contractile actomyosin network. The kinase domain of Rock is autoinhibited by its C-terminal region. There are several known mechanisms for how the kinase domain is activated however; none of these mechanisms describe Rock activation during Shroom mediated apical constriction. It is possible that Rock is activated upon binding to Shroom or an active form of Rock binds to Shroom.

I used structural studies to understand the mechanistic details of the Shroom-Rock interaction. The SD2 domain and the SBD do not have sequence homologs outside of Shroom or Rock. Therefore, before making predictions about the SD2-SBD complex it is necessary to first determine the structures of these two domains. Using x-ray crystallography I will determine the structures of the SD2 and SBD domains individually. Upon determining the structures of the individual domains I will attempt to crystallize and determine the structure of the SD2-SBD complex.

2.0 STRUCTURE OF THE SHROOM SD2 DOMAIN

2.1 INTRODUCTION

Shroom proteins play important roles in inducing changes in tissue shape during development. Mutations in Shroom result in birth defects such as excenphaly and spina bifida [3]. The SD2 domain is the most conserved domain in Shroom. It is found in all known Shroom family members and is required for Shroom function. The Shroom SD2 mediates the interaction with the highly conserved cytoskeleton regulator Rock. Via this interaction Rock is recruited to the apical junction to phosphorylate and activate non-muscle myosin II. Upon activation myosin II can bind actin and form a contractile actomyosin network that generates the force required for apical constriction. To understand the Shroom-Rock interaction I chose to first structurally characterize the Shroom SD2 domain.

In collaboration with the Hildebrand lab we designed multiple SD2 constructs from mouse Shroom3 (mShroom3), mouse Shroom2 (mShroom2) and *Drosophila* Shroom (dShroom). The boundaries of these constructs were chosen based on conservation and secondary structure predictions (Fig. 3). The stability of each construct upon purification was assayed by limited proteolysis. These assays indicated that the shortest constructs from each Shroom homolog were proteolytically stable. We termed these the core SD2 domains. The Hildebrand lab showed that these core SD2 domains are capable of inducing apical constriction

in MDCK cells. These SD2 domain constructs expressed well and were easily purified to large quantities. We set up crystallization trials with the core SD2 domains from mShroom3, mShroom2 and dShroom. While the mShroom3 and mShroom2 SD2 domains did not crystallize the dShroom SD2 domain formed crystals in several conditions. I was able to optimize these crystals and collect a high quality dataset to use for structure determination.

Using single-wavelength anomalous dispersion I determined the crystal structure of the *Drosophila* Shroom SD2 domain spanning residues 1393-1576. The structure revealed that the SD2 domain has a novel fold composed of an anti-parallel, three-segmented, coiled coil dimer. Using biochemical and cell based assays, in collaboration with the Hildebrand lab, I have shown that dimerization is important for Rock interaction and Shroom function. Additionally using mutational analysis I have identified two binding conserved patches in the SD2 domain that mediates interaction with Rock. These results suggest that the SD2 domain interacts with Rock as a dimer using its central coiled coil segment.

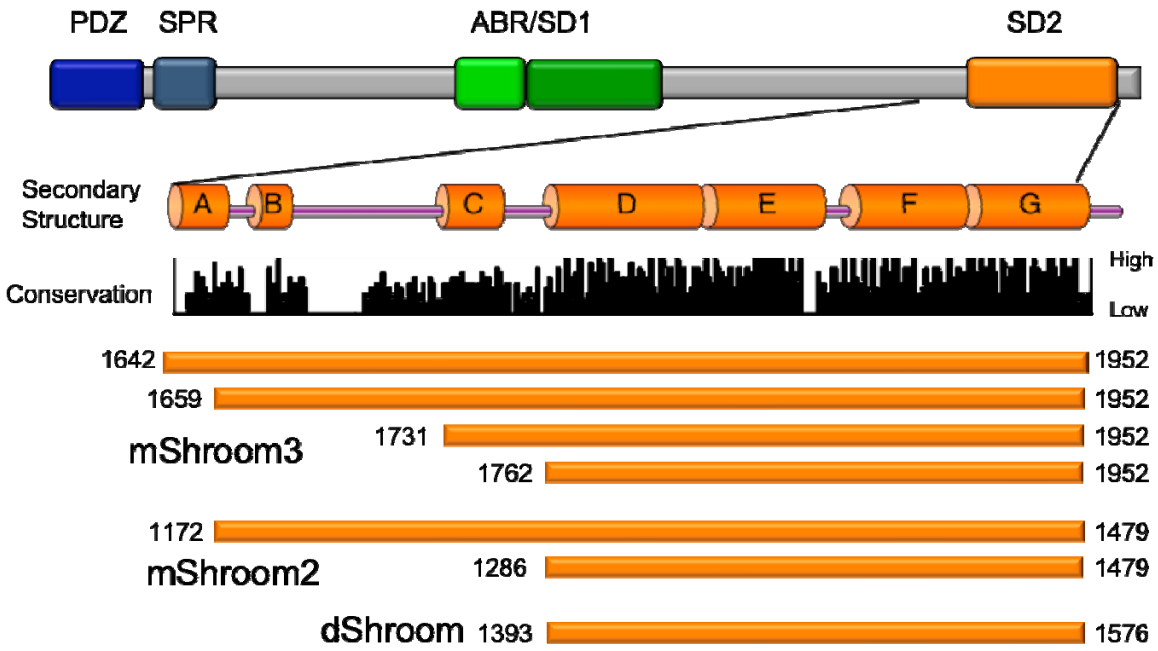

Figure 4: SD2 constructs.

mShroom3, mShroom2 and dShroom SD2 constructs designed for crystallographic screens. The boundaries of the constructs were based on conservation and secondary structure predictions. Conservation is represented as black bars. The secondary structure prediction is represented as orange cylinders denoting alpha helices A-G. The SD2 domain is predicted to be composed entirely of alpha helices. The conservation was obtained from a multiple sequence alignment of 12 SD2 sequences using ClaustalW and JalView. The secondary structure was predicted using PSIPRED [110].

2.2 RESULTS

2.2.1 Crystallizing the Drosophila Shroom SD2 domain

The core SD2 domain from Drosophila Shroom (1393-1576) was cloned into the pET-151/D-TOPO expression vector and transformed into BL21-CodonPlus *E. coli* cells. Protein expression was induced using the autoinduction method and dShroom SD2 expressed to a high degree (with a yield of ~100mg/L of culture) [111]. The dShroom SD2 domain was easily purified using nickel affinity chromatography and size exclusion chromatography. Crystal screens were set up with the pure homogenous dShroom SD2 (≈ 98% purity) at a concentration of 10mg/ml in buffer containing 8% glycerol, 500mM NaCl, 20mM Tris PH 8.0 and 5mM β-mercaptoethanol. Crystals formed in several conditions the most promising of which were in crystallization buffer containing 30% PEG-400 and CHES pH 9.5. Crystals in this buffer were small cubes and after several attempts at optimization these crystals only diffracted to 4 Å. For the purpose of structural studies proposed here I require data from crystals that diffract to a resolution of 3 Å or higher. I therefore chose to pursue crystals from other conditions.

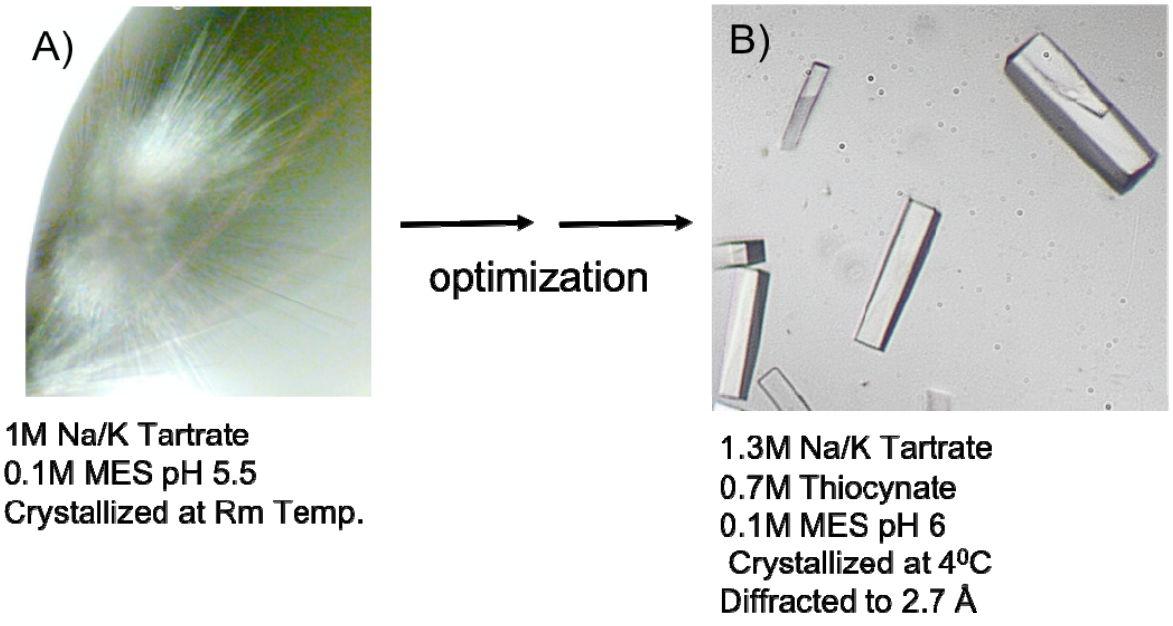

Figure 5: Optimizing dShroom SD2 crystals.

(A) Initial needle cluster dShroom SD2 crystals.

(B) Optimized diffraction quality rod shaped dShroom SD2 crystals. The needle cluster crystals were transformed into the rod shaped crystals by changing the crystallization buffer and temperature.

I next chose to optimize crystals in buffer containing 1.0M Na/K Tartrate and 0.1M MES pH 5.5 and 4mM DTT. These crystals were clusters of needles when crystallized at room temperature (Fig. 4A). A variety of conditions were used to optimize these needle shaped crystals. Changing the buffer condition to 1.3-1.4M Na/K Tartrate, 0.1M MES pH 6.0, 11% glycerol, 0.6-1.0M Na Thiocynate and 4mM DTT and the crystallization temperature to 4°C transformed the crystals from thin needles to thicker rod shaped crystals (Fig. 4B). Before freezing the optimized crystals I transferred them into buffer containing 1.4M Na/K tartrate,

0.1M MES acid pH 6.0, 0.9M Na thiocynate, 15% glycerol and 4mM DTT. Optimization of these conditions resulted in significantly improved crystals that diffracted to a much higher resolution (2.7 Å) than the previous condition. Using these crystals I collected a diffraction dataset to determine the structure of the SD2 domain.

2.2.2 Determining the structure of the dShroom SD2 domain

When crystals are shot with an x-ray beam the x-rays will diffract off the electrons in the crystal in all directions. These diffracted x-rays can be measured by a detector placed in front of the crystals and can be visualized as a spots or reflections. To determine the structure of a molecule using x-ray crystallography we need to calculate the indices, the intensity, and phase angle for each reflection measured in a diffraction pattern. The indices and the intensities can be measured experimentally, however, there is no way to measure the phase angles. Instead, there are a few techniques that can be used to estimate phases. One of these techniques, called single wavelength anomalous dispersion, uses the anomalous scattering of selenium atoms to calculate phases.

To solve the phase problem I purified selenomethionine substituted dShroom SD2 and obtained crystals in conditions similar to the native protein. These crystals were cryoprotected and frozen in a manner similar to the native protein and used to collect anomalous diffraction data. The majority of the dShroom SD2 crystals I screened were not ideal for data collection because they displayed several defects such as a high degree of mosaicity, ice rings and poor diffraction. After screening a variety of crystals I was able to collect data from a few that did not have these defects. The anomalous and native data sets were collected using the X25 beamline at the National Synchrotron Light Source, Brookhaven National Laboratory. Several of the datasets collected were of poor quality and made model refinement difficult. Using programs in the CCP4

suite and in Phenix I was able to analyze the processed datasets and rule out problems such as merohedral twinning and pseudo-translation symmetry [112]. Ultimately I was able to collect anomalous and native datasets that were of reasonable quality and used them to calculate phases, obtain a map and build a model.

The selenomethionine substituted crystal diffracted to 2.4 Å while the native crystal diffracted to 2.7 Å. Both datasets were processed using HKL2000, a suite of programs that allow you analyze and process diffraction data [113]. Both the native and selenomethionine crystals form in space group $P2_12_12$ with unit cell dimensions a = 72 Å, b = 85 Å, and c = 93 Å. The structure of dShroom SD2 domain was determined by single-wavelength anomalous dispersion. Phases were calculated at 3.5 Å from the anomalous data using the program SHELX C/D/E and a preliminary model was built into the resulting electron density map, using the macromolecular model building program COOT [114, 115]. The structure was refined against the 2.7 Å native data using positional, B-factor and TLS refinement with the Phenix.refine program within the Phenix software suite [116]. The final R-factors for the structure are 22.78 for R-work and 28.38 for R-free. The asymmetric unit of the crystal contains two molecules of the dShroom SD2 domain. The final model contains resides 1396-1571 in molecule A and 1397-1571 in molecule B (Fig. 5). Analysis of the structure with the structure validation program, Molprobity, indicates that all of the residues in both chains lie in the favored regions of the Ramachandran plot [117]. The average B-factor for both molecules is 75.9 $Å^2$ (Table 1).

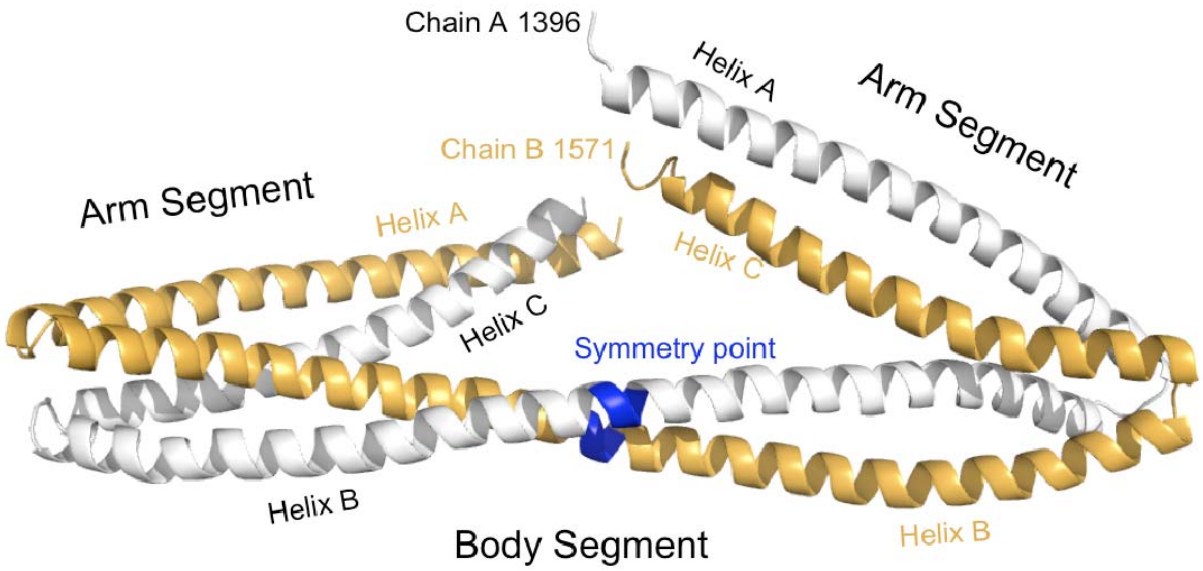

Figure 6: Structure of dShroom SD2 domain.

Ribbon diagram of the dShroom SD2 dimer. The two SD2 molecules are shown in white (Chain A) and gold (Chain B). The arm and body coiled coil segments are labeled and the symmetry point is highlighted in blue.

Table 1: Data collection and refinement statistics for dShroom SD2.

Data collection and refinement statistics for dShrm SD2		
	SeMet (SAD)	Native
Data Collection		
Space Group	$P2_12_12$	$P2_12_12$
Cell Dimensions		
a (Å)	72.2	72.8
b (Å)	84.9	85.6
c (Å)	93.0	93.0
Resolution (Å)	30.0-3.5 (3.56-3.50)	50.0-2.7 (2.75-2.70)
Unique Reflections	7573	16446
R_{merge}	8.5 (8.2)	6.9 (46.3)
$I/\sigma I$	42.1 (34.1)	34.2 (3.5)
Completeness (%)	99.3 (100)	99.9 (99.9)
Redundancy	10.0 (10.7)	8.5 (8.1)
Refinement		
Resolution (Å)		47.0-2.7
R_{work} / R_{free}		22.78/28.38
No. atoms		
Protein		2749
R.m.s. deviations		
Bond lengths (Å)		0.10
Bond angles (°)		0.600
Average isotropic B values (Å^2)		75.9
Ramachandran statistics		
Outliers		0
Allowed		0
Favored		100

Values in parentheses correspond to those in the outer resolution shell.

R_{merge} = $(|(\Sigma I - \langle I \rangle)|)/(\Sigma I)$, where $\langle I \rangle$ is the average intensity of multiple measurements.

$R_{work} = \Sigma_{hkl}||F_{obs}(hkl)|| - F_{calc}(hkl)||/\Sigma_{hkl}|F_{obs}(hkl)|$.

R_{free} = crossvalidation R factor for 7.3% of the reflections against which the model was not refined.

2.2.3 dShroom SD2 domain is an anti-parallel coiled-coil dimer

The crystal structure reveals that the dShroom SD2 domain is a dimer and the asymmetric unit of the crystal contains a single dimer. Each monomer is made up of three helices, denoted A, B and C, with the helix B being twice the length of helices A and C. In the dimer the B helices wrap around each other to form the "body" coiled-coil segment and the A and C helices wrap around each other to form the flanking "arm" segments (Fig. 5). There are a number of hydrophobic residues at the junction between the arm segments and the body segment that most likely play an important role in holding the arm segments in the observed conformation (Fig. 6A). I performed a structural homology search using DALI to identify structures with a fold similar to dShroom SD2 [118]. The structural homology search did not yield any structures that had similarity that extended beyond a single coiled-coil segment. Thus, dShroom SD2 domain has a novel fold consisting of three anti-parallel coiled-coil segments (Fig.5).

The three segments have canonical knobs-into-holes coiled coil packing interactions (Fig. 6B). Due to the extended nature of the structure, the dShroom SD2 domain lacks a traditional hydrophobic core. However, the coiled-coil interactions make up an extensive dimerization interface with a buried surface area of 4577 $Å^2$. There are several conserved leucines and isoleucines at the dimerization interface that interact in a manner similar to leucine zippers (Fig. 6B). In contrast to the SD2 domain, leucine zippers are almost always parallel coiled-coil proteins thus making the structure of the SD2 domain unique. The dShroom SD2 structure displays symmetry and asymmetry. There is a twist in the central coiled-coil segment such that the arm segments are rotated away from each other by $\sim 60°$ (Fig. 7A). The dShroom SD2 domain also has intrinsic symmetry such that one half dimer contains all of the amino acids

present in the monomer. The half dimers are also structurally identical such that when aligned they have a root mean square deviation of 0.6 Å (Fig. 7B). This internal symmetry has interesting biological implications since there are two potential binding sites for Rock present on opposite faces of the molecule. The extensive coiled coil interactions and the unique symmetry suggest that the dimerization of the SD2 domain could be important for function.

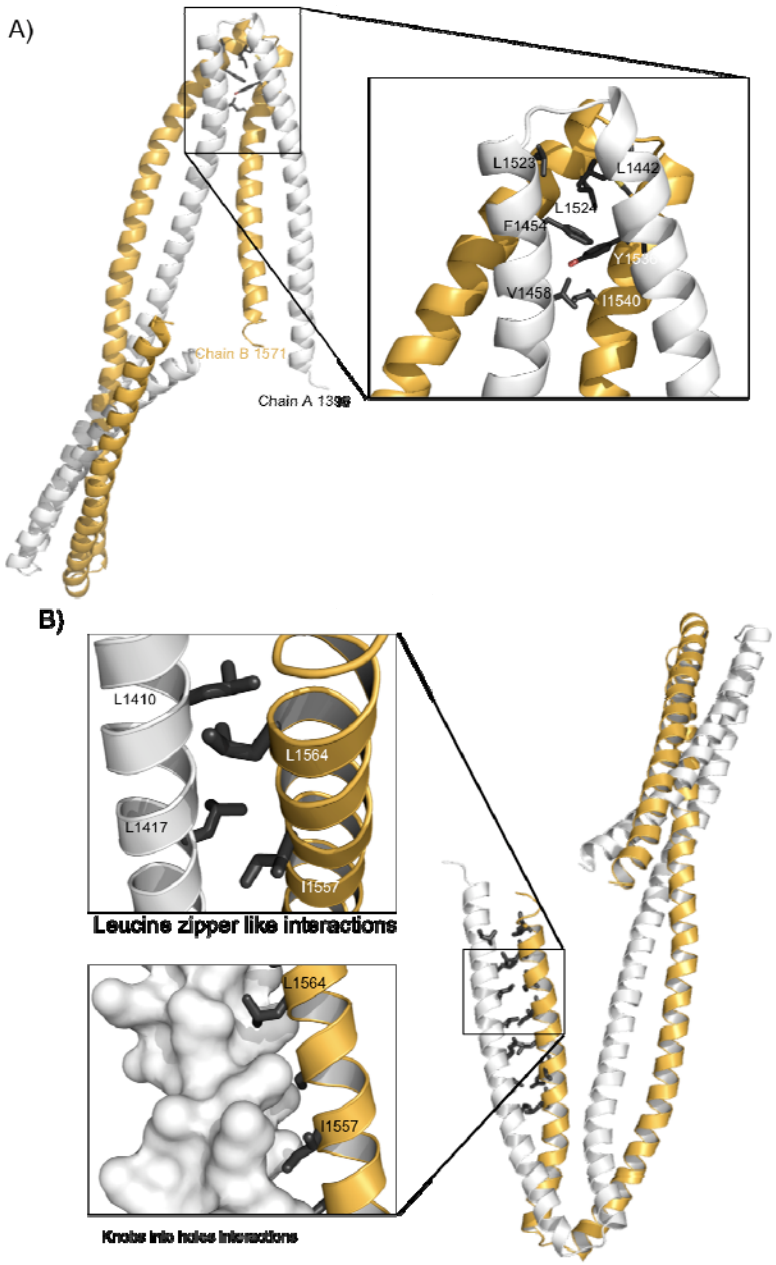

Figure 7: Structural features of the Shroom SD2 domain.

(A) Ribbon diagram of the SD2 domain shown in gold and white with the hydrophobic residues at the junction between the arm segment and the body segment are shown as stick diagrams in black. The hydrophobic residues are labeled in the inset.

(B) Canonical coiled coil interactions in one of the arm segments are represented as black stick diagrams. The top inset shows a zoomed in view of the leucine zipper like interactions. The bottom inset shows a zoomed in view of knobs into holes packing interactions with a surface view of one chain and a ribbon diagram of the other.

2.2.4 Dimerization of the SD2 domain is important for Shroom Function

To determine if the dShroom SD2 domain is a dimer in solution, I treated purified SD2 with small amounts of the chemical crosslinker glutaraldehyde. The crosslinked species were resolved on an SDS-PAGE and visualized using coomassie blue staining. The dShroom SD2 dimerized readily within seconds of being treated with glutaraldehye and longer exposure to the crosslinker resulted in the formation of higher order tetrameric forms (Fig. 8A). Since the crosslinking experiment is not quantitative I used gel-filtration to determine the ratio of monomer to dimer in solution. The dShroom SD2 domain elutes off the gel filtration column in two distinct peaks (Fig. 8B). The larger peak, which corresponds to the dimer and was used for crystallization, makes up about 89% of the peak area. These results indicate the dShroom SD2 domain is predominantly a dimer in solution.

To determine if SD2 dimerization is important for Shroom mediated apical constriction, I designed two mutations that cause local disruptions in the dimerization interface. Both mutations targeted conserved leucine and isoleucine residues that make canonical knobs-into holes packing interactions. I termed the mutations homodimerization (HD) mutations. The first mutation, HD1

(^{1468}LLSL^{1471} to AASA), targets residues in the body segment while the second mutation, HD2 (^{1546}LIADARDL^{1553} to AAADARDA) targets residues in the arm segments (Fig. 9A). Both mutations were made using site-directed mutagenesis.

First, I determined if these mutations altered the monomer-dimer equilibrium. I analyzed the gel filtration elution profiles of both HD mutants to measure the monomer to dimer ratio for each mutant. Neither mutant shifted the equilibrium towards the monomer species. Instead, both mutants had elution profiles very distinct from the wild-type protein. HD1 eluted off the gel filtration column in a single-wide peak that did not coincide with the wild-type monomer or dimer peak (Fig. 9B). For HD2, the majority of the protein eluted off the gel filtration column in a peak larger than the wild-type dimer peak (Fig. 9B). I pooled the fractions corresponding to the major peak for HD1 and the dimer peak for HD2 for the following biochemical assays. Limited proteolysis experiments indicated that these mutations also severely destabilized the proteins (Fig. 9C). Chemical crosslinking assays showed that the ability of these mutations to dimerize was also diminished (Fig. 9D). Native gel electrophoresis was used to test whether these mutants were capable of binding Rock (Fig. 10). These experiments were performed in collaboration with the Hildebrand lab. Gel shift assays show that both HD mutants were deficient in binding to Drosophila Rock SBD. These results indicate that even local perturbations to the dimerization interface severely destabilize the dShroom SD2 domain. Additionally, the Rock-binding site is made up of residues from both chains as disrupting the dimerization interface disrupts interactions with Rock SBD.

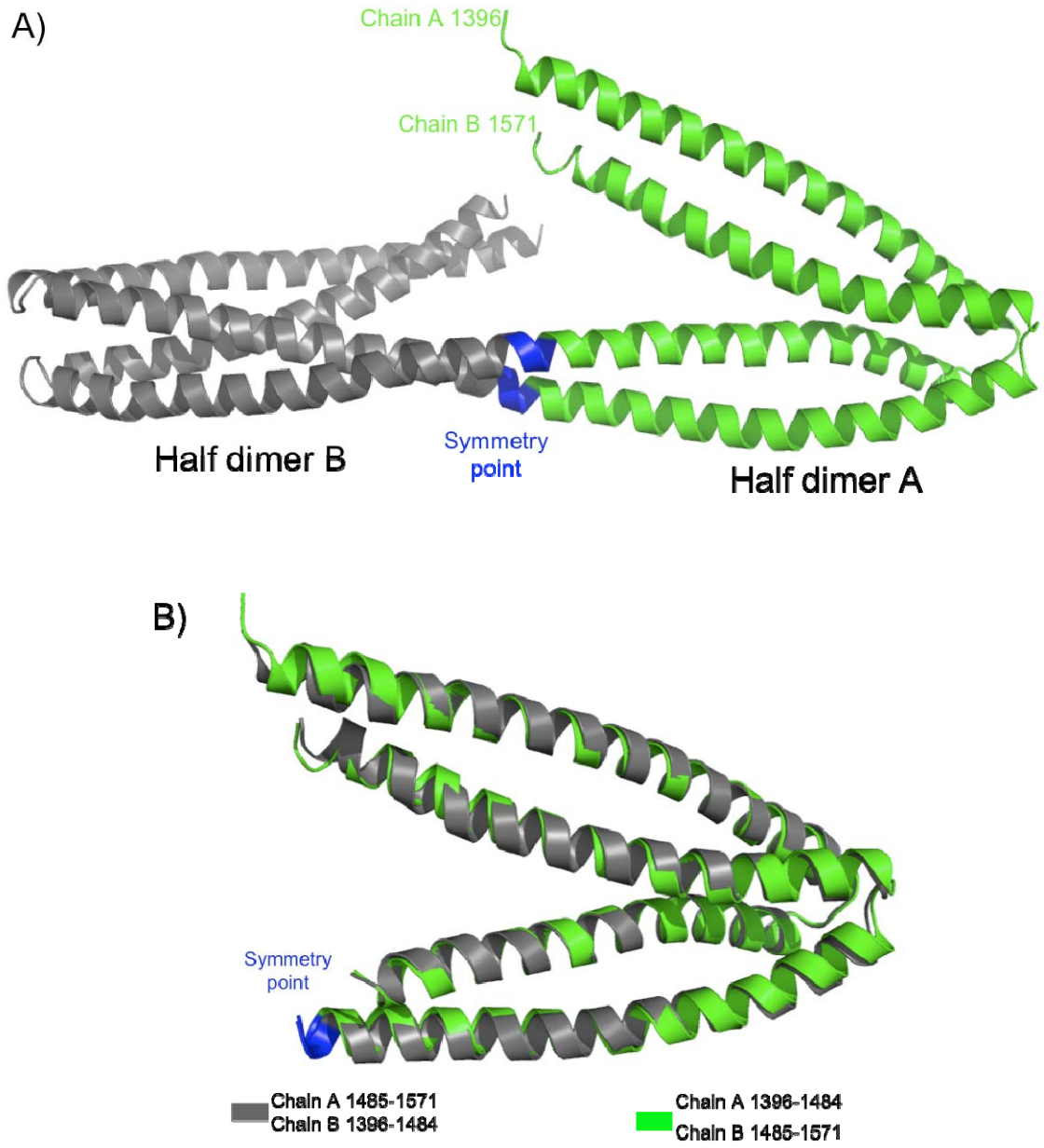

Figure 8: Symmetry in the dShroom SD2 domain.

(A) Ribbon diagram of the dShroom SD2 domain with the two half dimers shown in green (half dimer A) and gray (half dimer B). The symmetry point is highlighted in blue.

(B) Structural alignment of the SD2 half dimers with an r.m.s.d of 0.6 Å. The two half dimers were aligned using the DALI server and the r.m.s.d. was calculated over 178 Cα atoms.

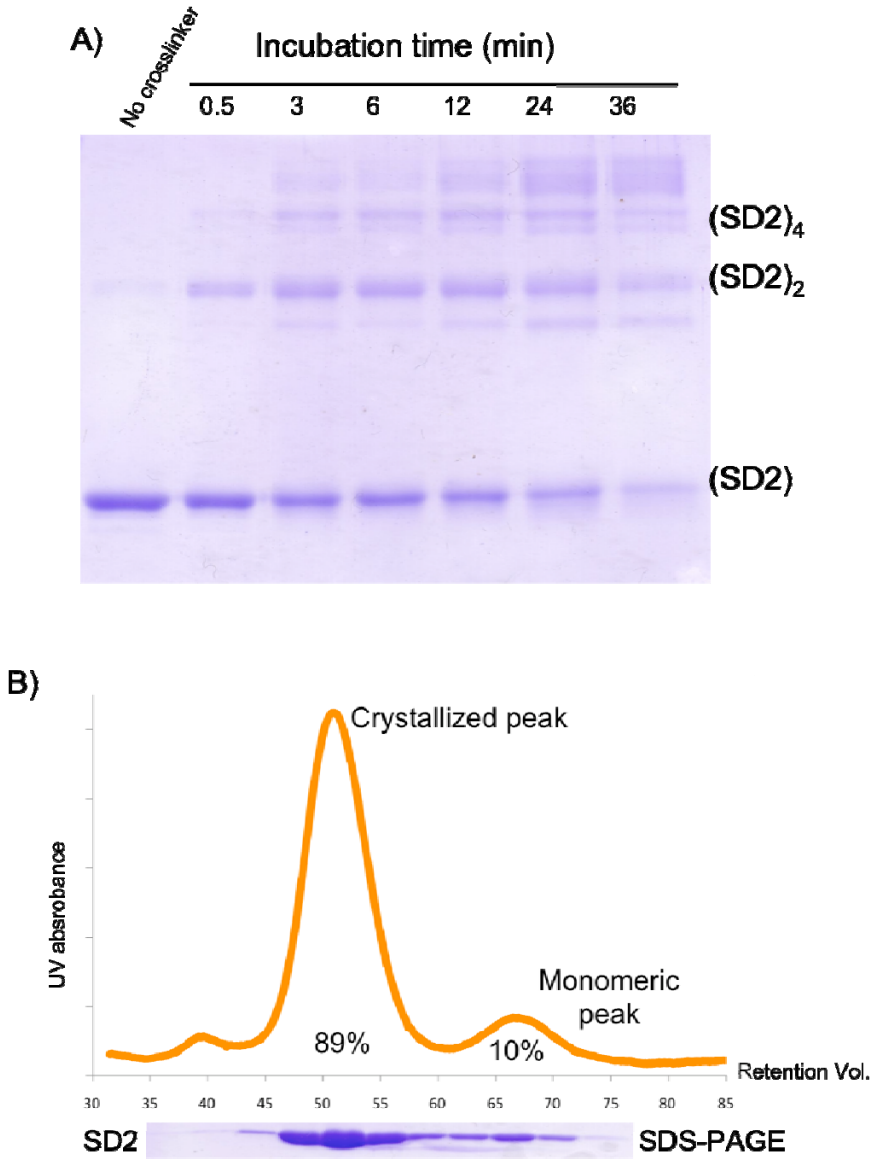

Figure 9: dShroom SD2 domain is a dimer in solution.

(A) Chemical crosslinking of dShroom SD2 domain. The SD2 domain was incubated with 0.009% glutaraldehyde for the indicated time and the resulting species were resolved with SDS-PAGE.

(B) Gel filtration profile of dShroom SD2 domain. Purified SD2 domain was subjected to size exclusion chromatography. The size exclusion trace is shown in orange. The peak areas of the dimeric (crystallized) and monomeric peaks are indicated. The fractions collected were analyzed by SDS-PAGE, which is indicated below the size exclusion trace.

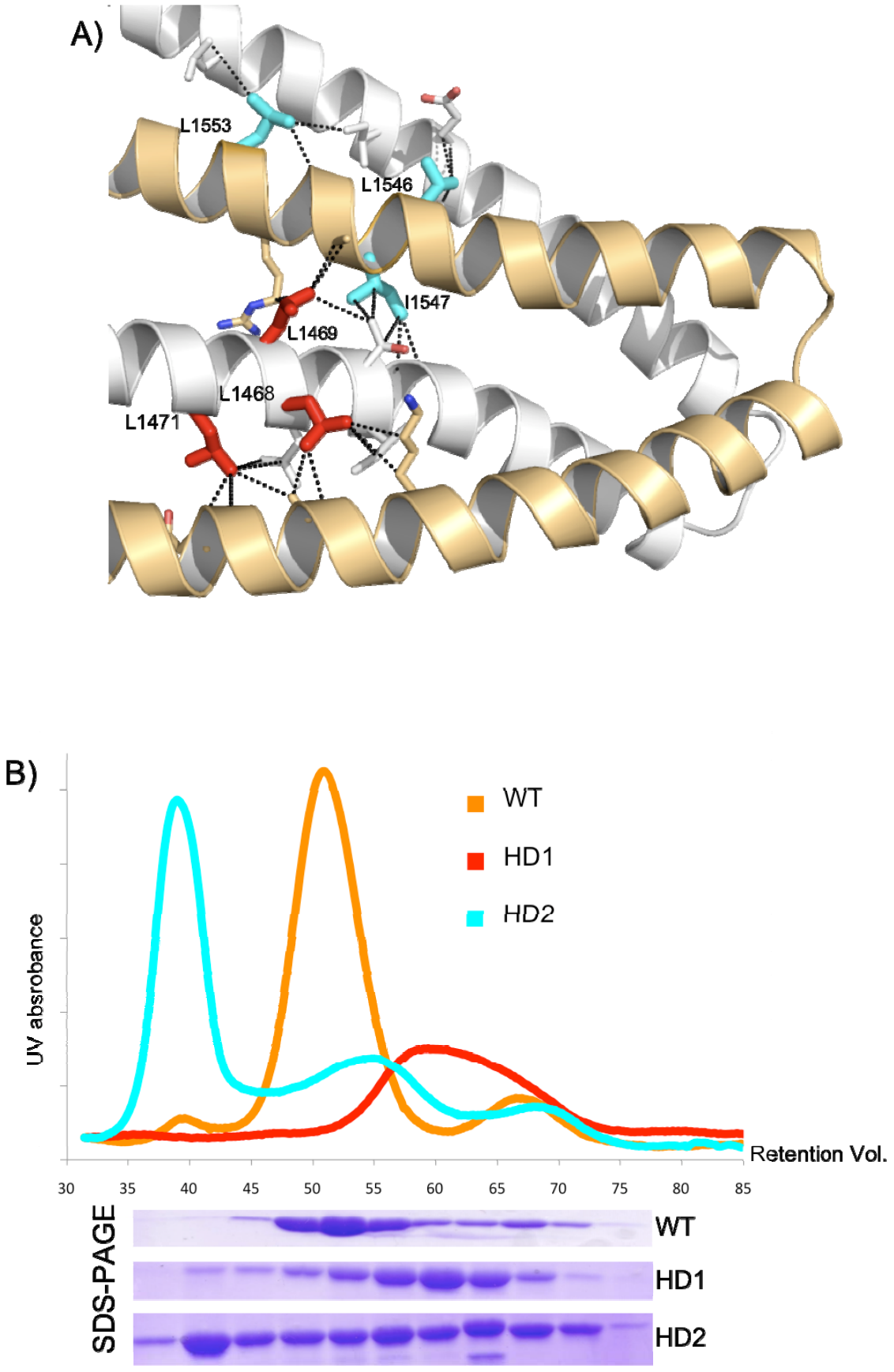
A)
L1553
L1546
I1547
L1469
L1468
L1471
B)
WT
HD1
HD2
UV absrobance
Retention Vol.
30
35
40
45
50
55
60
65
70
75
80
85
SDS-PAGE
WT
HD1
HD2

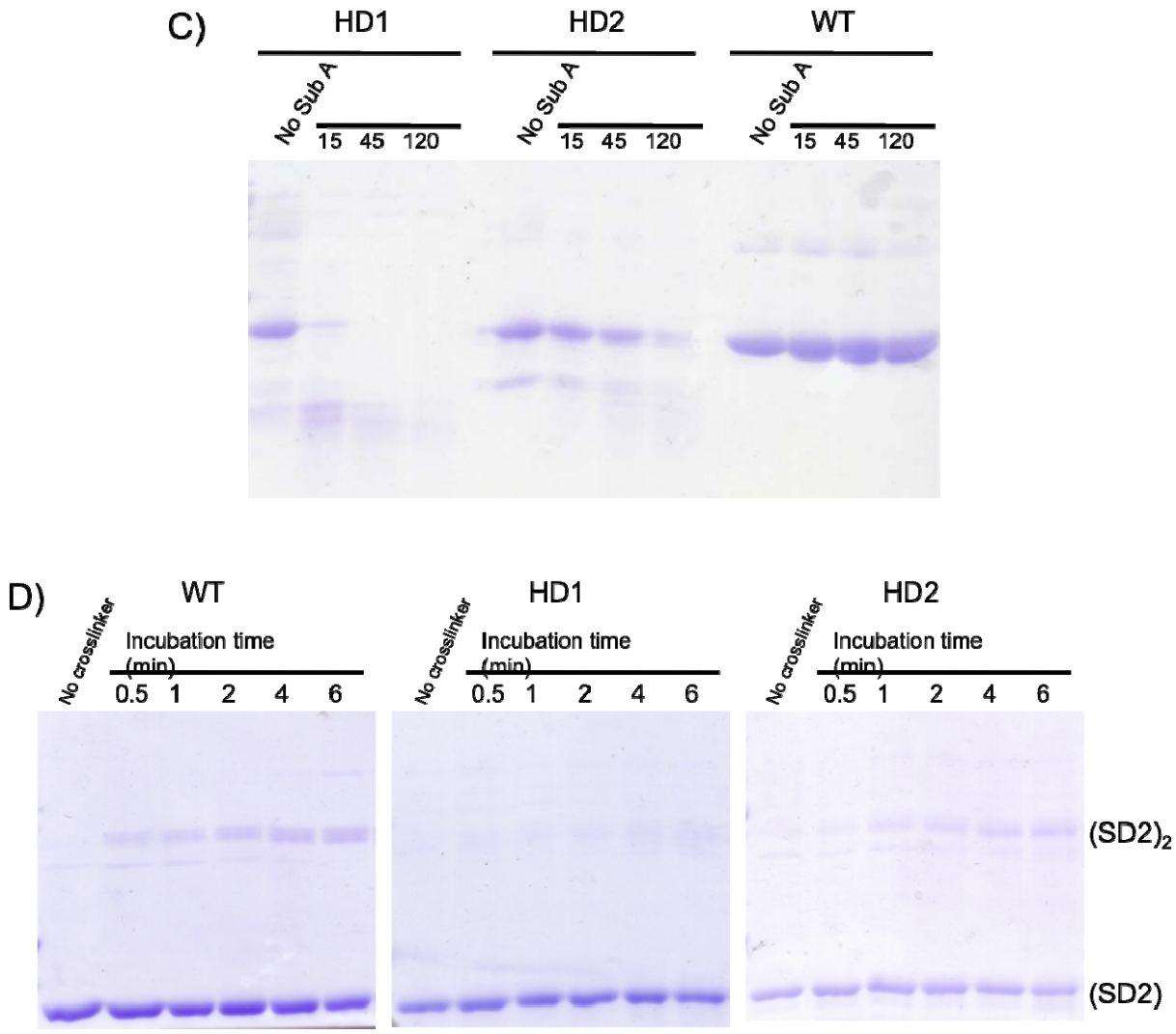

Figure 10: Mutations in the dimerization interface disrupt the stability and the fold of the SD2 domain.

(A) Ribbon diagram of the SD2 domain with the homodimerization (HD) mutants shown as stick diagrams in red (HD1) and cyan (HD2). The residues interacting the mutated residues are shown in gray or gold.

(B) Gel filtration profiles of the wild-type and HD mutant dShroom SD2 protieins. Purified wild-type and mutant SD2 domains were subjected to size exclusion chromatography. The size exclusion traces are shown in orange (wt), red (HD1), and cyan (HD2). The fractions collected were analyzed by SDS-PAGE, which is indicated below the size exclusion trace.

(C) Limited proteolysis of the HD mutants. Wild-type and mutant proteins were subjected to 13ng of the protease Subtilisin A for the indicated time. The reaction was stopped at the indicated time with PMSF and the digested fragments were visualized using SDS-PAGE.

(D) Chemical crosslinking of the HD mutants. The wild-type and mutant proteins were incubated with 0.002% glutaraldehyde for the indicated time. The reaction was stopped with 1M Tris pH 8.0 and the resulting species were resolved with SDS-PAGE.

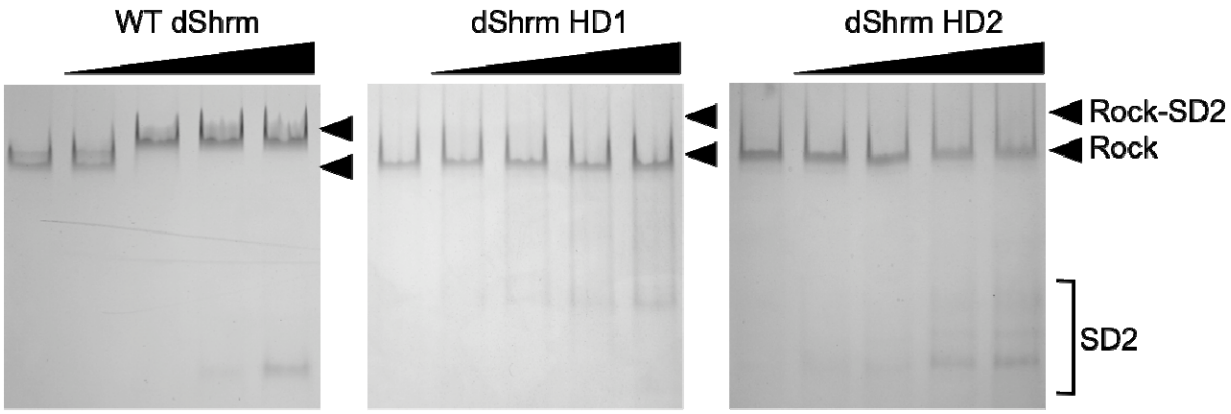

Figure 11: Mutations in the dimerization interface disrupt Rock binding.

Native gel electrophoresis of dRock SBD (724-938) with increasing concentrations of wild-type or HD mutant dShroom SD2 domains. dRock SBD was mixed with wild-type or SD2 domains and incubated at room temperature before subjecting the proteins to Native PAGE.

2.2.5 The central SD2 coiled coil segment is important for the Shroom-Rock interaction

I next took a mutational approach to identify surfaces in the SD2 domain that mediate interaction with Rock SBD. I first aligned 12 Shroom sequences using ClustalW to identify conserved patches [119]. Then, using the RISLER scoring matrix in the ESPRIPT program I scored and mapped the conserved residues on to the surface of the SD2 domain (Fig. 11A) [120, 121]. The SD2 domain has conserved residues throughout the sequence; however, there were three regions that had clusters of surface exposed conserved residues. I made three multiple substitution mutations, by site-directed mutagenesis, that targeted these three surface exposed conserved clusters (SC). All three SC mutants (^{1402}KMDEL^{1406} to AMDRA, ^{1470}SLSERLA^{1476} to ALEEDLE, ^{1509}LKSDIERR^{1516} to AASDIEDA) termed cluster 1, cluster 2 and cluster 3 have gel filtration elution profiles similar to the wild-type and show no increased sensitivity to proteases. Cluster 1 targets residues in the arm towards the N-terminus while cluster 2 and cluster 3 target conserved residues in the central body segment. The ability of these mutations to interact with Rock was tested via pull-downs and native gel electrophoresis. These biochemical experiments were performed in collaboration with the Hildebrand lab. Both the pull-down and gel shift assays indicated that while the cluster 1 mutant was still capable of binding Rock SBD, the cluster 2 and cluster 3 mutants were not (Fig. 11B and 11C). Binding to Rock SBD was greatly diminished for the cluster 2 mutant and completely abolished for the cluster 3 mutant. These results suggest that the Rock-binding surface in Drosophila Shroom lies in the central body segment of the SD2 domain with the conserved residues in cluster 3 playing a more significant role in binding Rock than residues in cluster 2.

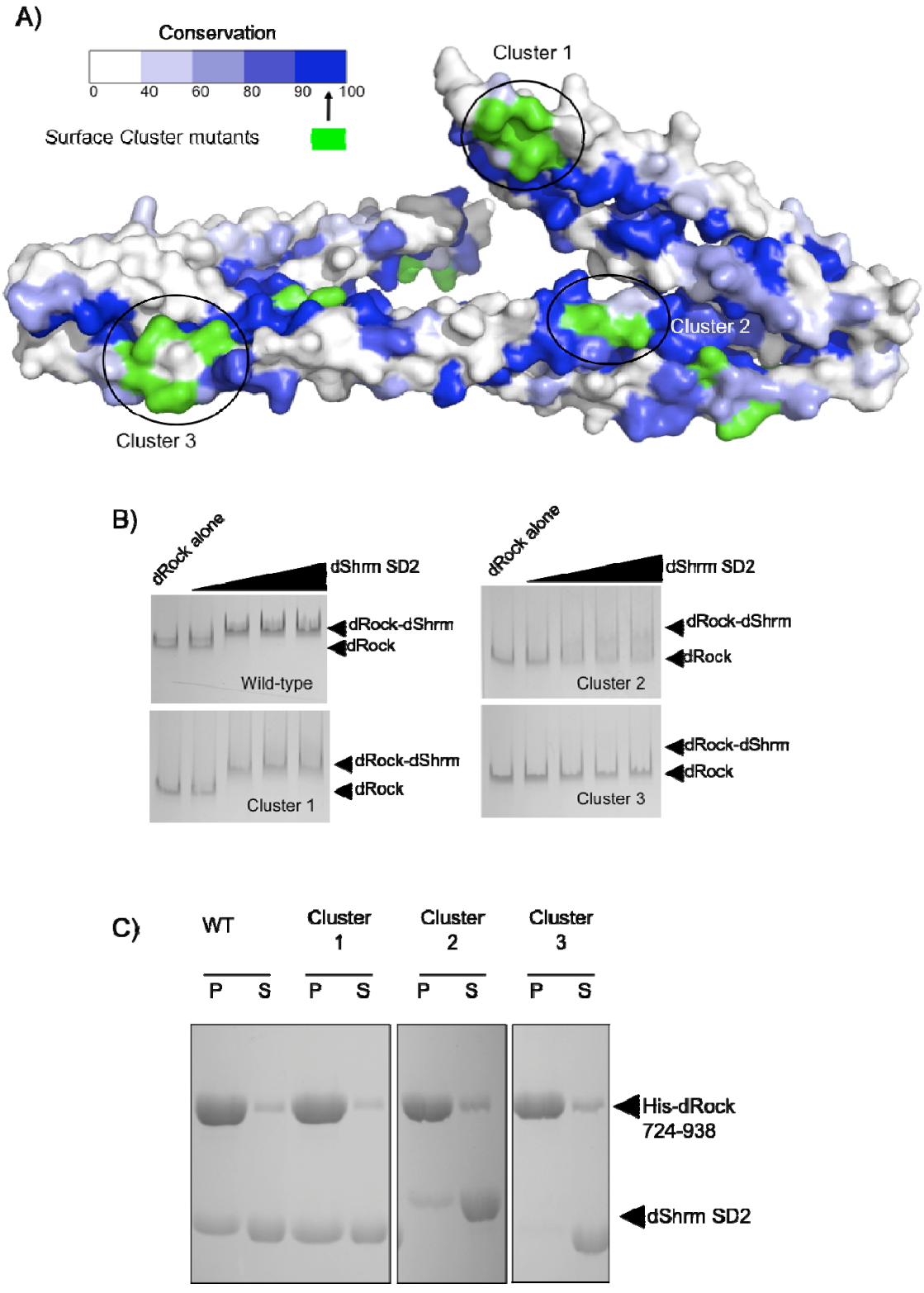

Figure 12: Conserved surfaces in the SD2 central coiled coil segment are important for the Shroom-Rock interaction.

(A) Surface view of the dShroom SD2 structure with conservation highlighted in shades of blue. Conservation was obtained from a multiple sequence alignment of 12 SD2 sequences and scored using the RISLER matrix in espript [120, 121]. The invariant residues targeted for mutation in each cluster are shown in green.

(B) Native gel electrophoresis of dRock (724-938) with increasing concentrations of wild-type or SC mutant dShroom SD2 domains. dRock SBD was mixed with wild-type or SD2 domains and incubated at room temperature before subjecting the proteins to Native PAGE.

(C) Pull-down assay using his-tagged dRock (724-938) and wild-type or mutant dShroom SD2 proteins. His-tagged dRock bound to nickel beads was incubated with an excess of untagged wild-type or mutant SD2. The ability of the wild-type and mutant SD2 to bind to dRock was assayed by resolving the nickel beads and the supernatant using SDS-PAGE.

2.2.6 The Rock binding surface is conserved in vertebrate Shroom

To determine if these conserved residues also play an important role in Rock binding in vertebrates, the Hildebrand lab made the surface cluster and homodimerization mutants in the mouse Shroom3 SD2 (mShroom3) domain. We assayed the ability of these mutants to bind Rock and induce apical constriction using biochemical and cell based assays. GST pull downs showed that the cluster 1 mutant could bind Rock SBD; however, the cluster 2, cluster 3 and both of the homodimerization mutants cannot (Fig. 12A). Through GST pull-downs we also determined that the mShroom3 homodimerization mutants could not dimerize (Fig. 12C). These results are consistent with the results seen with the Drosophila SD2 domain; however, it looks like the residues in cluster 2 might play a more significant role in binding Rock in vertebrates.

The ability of these mutations to induce apical constriction was tested in a cell-based assay using MDCK cells. The surface cluster and homodimerization mutations were introduced into an endolyn –Shroom3 chimeric protein construct and the mutant constructs were then transfected into MDCK cells. All of the mutant proteins localized to the apical junction as seen by co-localization with the apical junction marker ZO-1. Consistent with *in vitro* binding results only the cluster 1 mutant was able to apically constrict cells similar to wild-type and cluster 2, cluster 3 and the two homodimerization mutants could not induce apical constriction (Fig. 12B). Based on these results we can conclude that the Rock-binding surface is located in the body segment of the SD2 domain and is conserved in vertebrates.

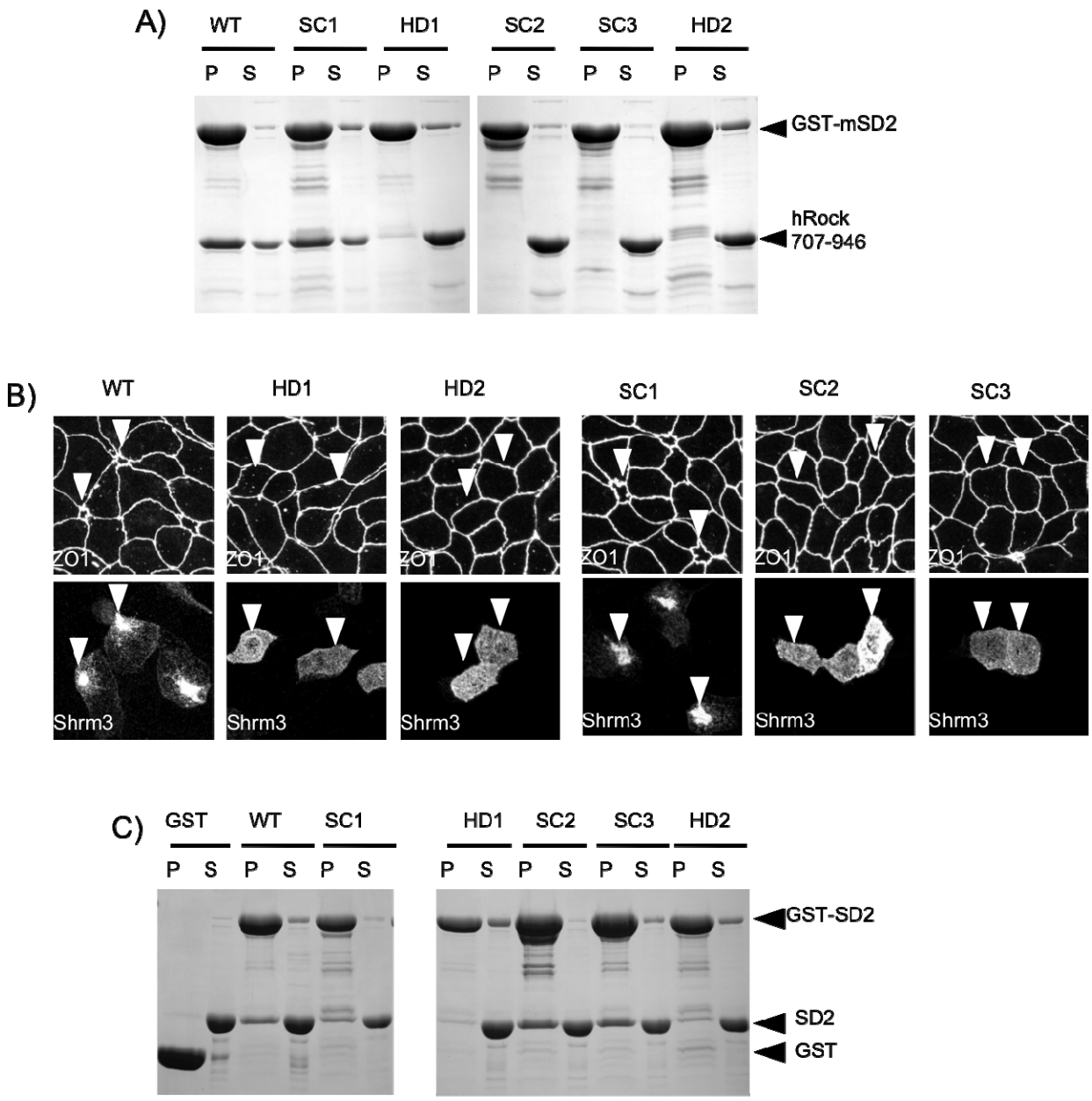

Figure 13: The SD2 Rock binding interface is conserved in the vertebrates.

(A) Pull-down assay with GST-tagged wild-type and mutant mouse Shroom3 SD2 domain and untagged hRock (707-946). Un-tagged hRock bound to GST beads was incubated with an of GST-tagged wild-type or mutant SD2. The ability of the wild-type and mutant SD2 to bind to hRock was assayed by resolving the GST beads (P) and the supernatant (S) using SDS-PAGE.

(B) Endolyn tagged wild-type or mutant mouse Shroom3 was expressed in MDCK cells and stained for ZO-1 and Shroom3. The transfected cells are indicated by arrow heads.

(C) Pull-down assay with wild-type or mutant GST tagged mouse Shroom3 and untagged wild-type Shroom3. Untagged mouse Shroom3 bound to GST beads was incubated with an of GST-tagged wild-type or mutant SD2. The ability of the wild-type and mutant SD2 to bind to untagged mouse Shroom3 was assayed by resolving the GST beads (P) and the supernatant using SDS-PAGE.

2.2.7 Attempts to crystallize SD2 domains from vertebrate Shroom proteins

In an effort to determine the structure of the mouse Shroom SD2 domain I designed an mShroom2 SD2 construct based on the Drosophila Shroom SD2 structure. We had previously made several mShroom2 and mShroom3 SD2 constructs and while these proteins purified easily, they did not yield crystals. The boundaries of the new mShroom2 SD2 construct were based on the ordered residues seen in the dShroom SD2 structure. The mShroom2 SD2 (1293-1476) was cloned into the expression vector pMCSG7 and transformed into BL21-CodonPlus *E. coli* cells. The protein expressed to a high degree (~200mg/L) and was easily purified (~98% purity) using nickel affinity chromatography, ion exchange and size exclusion chromatography. Peak fractions from gel filtration were dialyzed into buffer with 25mM NaCl, 20mM Tris pH 8.0, 1mM β-mercaptoethanol and concentrated to 15mg/ml and used to set up preliminary crystal screens at 23°C and 4°C. Thin rod shaped crystals formed in 35-39% 2-Methyl-2,4-pentanediol, 0.1 M Imidazole pH 8.0 and 0.2 M $MgCl_2$ at 4°C (Fig. 13A). After several rounds of optimization the

crystals only diffracted to ~8.0 Å. The new mShroom2 SD2 boundaries aided in the formation of crystals; however, these crystals were not diffraction quality crystals.

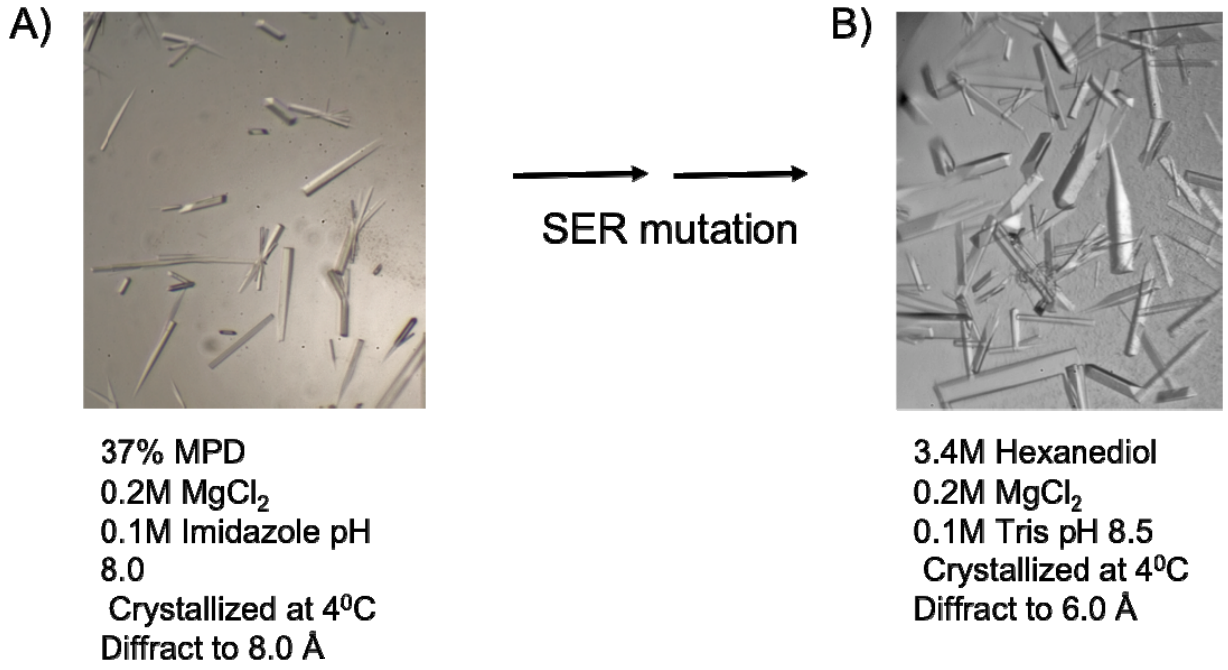

Figure 14: Mouse Shroom2 SD2 crystals.

(A) Optimized wild-type mouse Shroom2 SD2 (1293-1476) crystals. (B) Optimized SER mutant mouse Shroom2 SD2 crystals. The SER mutation did not significantly improve the quality of mShroom2 SD2 crystals.

In an effort to obtain crystals that diffract to a higher resolution I decided to use a technique called surface entropy reduction (SER) [122]. The SER technique attempts to improve crystal contact and form better quality crystals by identifying patches of large, flexible and charge/polar residues (K, E, Q) and mutating them to more inflexible residues (A, R). I identified one such patch in mShroom2 SD2 (^{1410}KELK^{1413}) and mutated all three residues to alanine. The SER mutant was easily purified to high degree using a scheme similar to wild-type. The pure and homogenous protein was dialyzed into buffer with 25mM NaCl, 20mM Tris pH 8.0, 1mM β-mercaptoethanol and concentrated to ~23mg/ml and used to set up crystal screens. The SER mutant only crystallized in one condition, 3.4M Hexanediol, 0.2M $MgCl_2$, and 0.1M Tris pH 8.5 at 4°C (Fig. 13B). After several rounds of optimization these SER mutant crystals did not diffract past 6.0 Å. The SER mutation did not significantly improve the diffraction of mShroom2 SD2 crystals.

I cloned the human Shroom2 SD2 domain (1427-1610) into the pET-151/D-TOPO expression vector and transformed into BL21-CodonPlus *E. coli* cells. hShroom2 SD2 was purified using nickel affinity chromatography followed by size exclusion chromatography. The pure, homogenous protein was concentrated and used to set up crystal trays. Small brick shaped crystals formed in buffer containing 20% PEG-8000, 0.2M $MgCl_2$, and 0.1M Tris pH 8.5. After the initial rounds of refinement these crystals diffracted to ~ 8Å. Upon further optimization these crystals should diffract to a higher resolution, and we should be able to determine the structure of hShroom SD2 via a technique called molecular replacement with the dShroom SD2 model.

2.3 CONCLUSIONS

Using x-ray crystallography I determined the structure of the *Drosophila* Shroom SD2 domain spanning residues 1393-1576. The crystal structure revealed that the SD2 domain is an anti-parallel dimer with a novel fold consisting of three coiled-coil segments. The SD2 domain is composed of two short arm segments that flank a larger central coiled-coil segment. Using biochemical assays I determined that dimerization of the SD2 domain is important for interaction with Rock SBD. Upon mapping conserved residues on to the surface of the structure I identified three loosely grouped patches of highly conserved residues. Two out of the three patches were located on the central coiled-coil segment while the third was located at the tip of the N-terminal arm. Using mutational analysis combined with biochemical and cell-based assays I determined, collaboration with the Hildebrand lab, that the conserved residues in the central coiled-coil segment are required for interaction with Rock and Shroom mediated apical constriction. The role of these residues is conserved in invertebrates and vertebrates. These results suggest that the SD2 domain interacts with Rock using conserved residues in the central coiled-coil segment.

3.0 STRUCTURE OF THE ROCK SHROOM BINDING DOMAIN

3.1 INTRODUCTION

Rock proteins are highly conserved Ser/Thr kinases that regulate cytoskeleton dynamics mainly by phosphorylating and activating myosin II [1]. They are involved in regulating various cellular processes including changes in cell shape, cell motility, and cytokinesis. Rock was initially identified as a Rho binding protein that acts downstream of Rho [48, 69]. Since then several other binding partners for Rock have been identified including the actin binding protein Shroom. Rock is required for most of Shroom mediated processes specifically for Shroom induced apical constriction [2, 89]. Rock binds the Shroom SD2 domain using a conserved, centrally located Shroom-binding domain (SBD). This domain is located in middle of the central coiled coil region and is independent of the Rho binding domain of Rock [2]. The Shroom-Rock interaction recruits Rock to the apical junction where it activates non-muscle myosin II and facilitates the formation of a contractile actomyosin network. Mutations in the SD2 domain that abolish Rock binding show a decrease in phosphorylated myosin II at apical junctions [123]. Rock activity is required for Shroom mediated apical constriction; however, it is still unclear how Rock is activated once it is recruited to the apical junctions.

The kinase domain of Rock is autoinhibited by the C-terminal region [76]. This inhibition can be relieved when rock binds to RhoA or arachodonic acid. Rock activation in the Shroom-

Rock pathway, however, occurs independent of Rho and is most likely a unique mechanism. Understanding how the SBD interacts with the SD2 domain will allow us to gain insight into how Rock is activated in during Shroom mediate apical constriction. For this purpose I chose to start by structurally characterizing the two domains individually. After determining the structure of the Shroom SD2 domain the next step was to determine the structure of the Rock SBD.

The VanDemark and the Hildebrand labs designed a series of SBD constructs from human and *Drosophila* Rock based on secondary structure predictions and conservation (Fig. 14). Based on results from limited proteolysis experiments we identified a stable core SBD construct that still interacts with Shroom SD2. The core SBD from hRock1 (834-913) and dRock (821-938) were used to set up crystallization trays. The dRock SBD did not form crystals but hRock SBD formed thin plate like crystals that were difficult to optimize. With the aid of a surface entropy reduction mutation I was able to obtain diffraction quality crystals and determine the crystal structure of hRock SBD using single wavelength anomalous dispersion. The structure revealed that Rock SBD is a parallel, coiled coil dimer with canonical knobs into holes packing interactions. There is a high degree of sequence conservation at the N-terminus of the structure and mutating residues in this conserved surface disrupts the Shroom-Rock interaction. There are conserved residues in the C-terminal portion that when mutated cause a moderate decrease in Shroom binding.

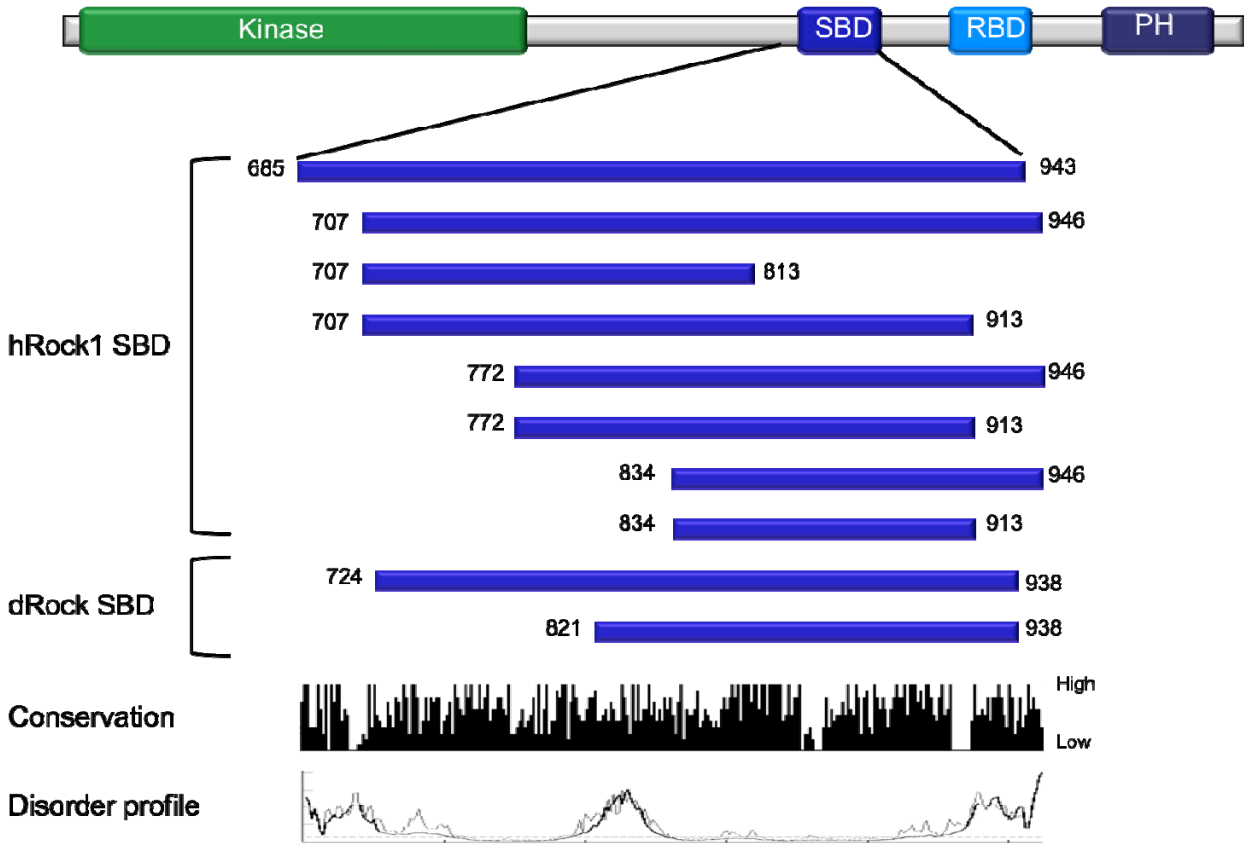

Figure 15: Rock SBD constructs.

SBD constructs from hRock1 and dRock designed for crystallographic screens. The boundaries of these constructs were determined based on conservation (indicated as black bars) and disorder predictions. The conservation was obtained by a multiple sequence alignment of 16 SBD sequences in ClustalW. The disorder profile was calculated using DISOPRED [119, 124].

3.2 RESULTS

3.2.1 Crystallizing the Human Rock SBD

The core hRock SBD (834-913) was cloned into the expression vector pET-151/D-TOPO expression vector and transformed into BL21-CodonPlus *E. coli* cells. Protein expression was induced via autoinduction and the protein yield was modest (15mg/L) [111]. hRock SBD was purified to ~99% purity using nickel affinity, ion exchange and size exclusion chromatography. Peak fractions from the size exclusion column were pooled, concentrated to 15mg/ml in buffer containing 8% glycerol, 500mM NaCl, 20mM Tris pH 8.0 and 1mM β-mercaptoethanol and used to set up crystallization screens. hRock SBD crystallized in a few conditions, however, even after several rounds of optimization these crystals only diffracted to ~8.0 Å. The initial crystallization attempts did not yield diffraction quality crystals so altering buffer conditions might improve crystal quality.

To aid with crystallization I dialyzed the purified hRock SBD into buffer containing 2% glycerol, 150mM Nacl, 20mM Tris pH 8.0 and 1mM β-mercaptoethanol. After dialysis the protein was once again concentrated to 15mg/ml and new crystallization screens were set up at 4°C and room temperature. The protein crystallized in several conditions at 4°C and at room temperature. The crystals at 4°C did not yield diffraction quality crystals. The conditions at room temperature were more promising yielding thin plate like crystals that crystallized in clusters (Fig. 15). These crystals also proved to be difficult to optimize. Apart from altering buffer conditions I also attempted to optimize these crystals with an additive screen and a technique called seeding. Seeding is used to improve crystal quality by trying to generate individual well-formed crystals. Usually poor quality crystals are crushed and made into "seeds"

that will serve as nucleation points. Ideally adding a dilute amount of these seeds to a drop that has no crystals should allow the protein to form individual better quality crystals. For hRock SBD I used to seeding to transform the plate clusters of crystals to thicker individual plates (Fig. 15). The additive screen, which involves the addition of a small amount of 96 different compounds to the crystallization buffer, also yielded improved crystals. Optimized crystals from seeding and the additive screens were transferred to a cryoprotectant buffer that contained the well solution plus 20% glycerol and then flash frozen. These optimized crystals unfortunately only diffracted to 3.5 Å. Altering buffer conditions and seeding improved the hRock SBD crystals; however, these crystals did not diffract to a resolution high enough for structure determination.

To improve the quality of the hRock SBD crystals I decided to turn to a technique called surface entropy reduction to improve crystal contact. Surface entropy reduction involves identifying patches of large, flexible, charged/polar residues (E, K, Q) in the protein sequence and mutating one of these patches to a more inflexible residue (A, R) [122]. I identified two such patches in the hRock SBD sequence and mutated the least conserved patch (^{884}EKE^{886}→AAA) using site directed mutagenesis. The plasmid encoding the SER mutant was transformed into BL21-CodonPlus *E. coli* cells and expression was induced using autoinduction. The SER mutant was purified (to ~99% purity) in a manner similar to the wild-type, and the peak fractions from size exclusion column were pooled and dialyzed into buffer containing 150mM NaCl, 20mM HEPES pH 7.5 and 1mM β-mercaptoethanol. After dialysis the SER mutant was concentrated to 15mg/ml and used for crystallization trials.

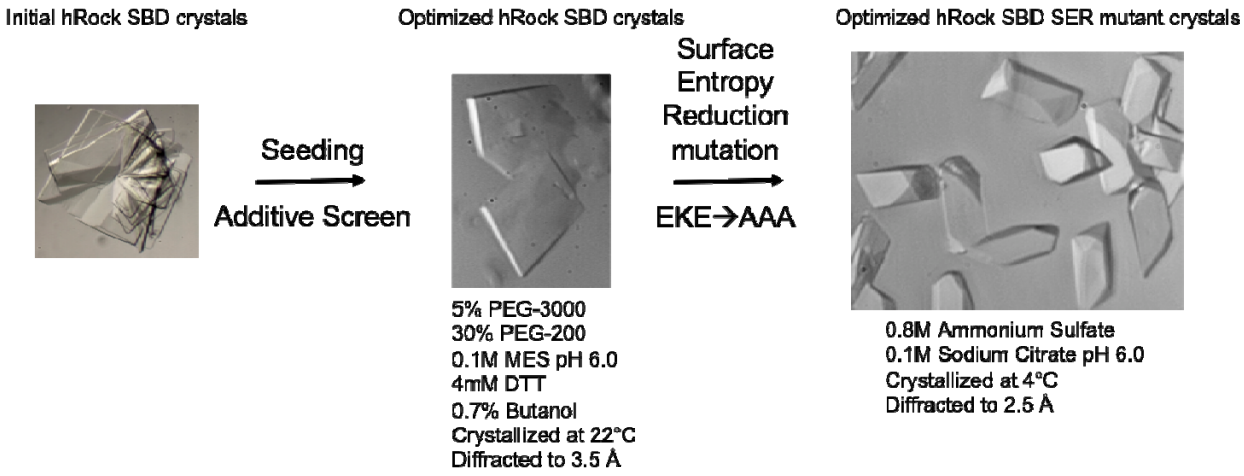

Figure 16: Human Rock SBD crystals.

Optimization of human Rock SBD (834-913) crystals with the use of seeding and surface entropy reduction (SER) mutation. The initial plate clusters crystals are shown in the first panel. The optimized SBD crystals obtained using a seeding and additive screens are shown in the middle panel. The high quality crystals obtained from SER mutations are shown in the last panel.

The protein crystallized in several conditions the most promising of which were in crystallization buffers containing 20% PEG 3350 and 0.2 $MgCl_2$, 2.0M ammonium sulfate and 0.1M sodium citrate pH 5.5, and lastly buffer containing 10% PEG-8000, 0.1M imidazole pH 8.0 and 0.2M calcium acetate. In all of these conditions the SER mutant protein formed thick bi-pyramidal crystals. In addition to optimizing the buffer conditions I once again used the additive screen and the seeding technique to improve crystal quality. While the additive screen did not improve crystal quality, the seeding technique produced diffraction quality crystals in crystallization buffer with 0.6-1.0M ammonium sulfate, and 0.1M sodium citrate pH 6.0 (Fig.

15). To solve the phase problem I purified selenomethionine substituted protein and crystallized it in conditions similar the native protein. The optimized native and selenomethionine crystals were transferred into a cryoprotectant buffer containing 2.5M ammonium sulfate, 20% glycerol, 150mM NaCl and 0.1M sodium citrate pH 6.0 and then flash frozen. I was able to obtain high diffraction quality hRock SBD crystals using SER mutations.

3.2.2 Determining the structure of hRock SBD

Native and anomalous data were collected using the X25 beamline at the National Synchrotron Light Source, Brookhaven National Laboratory. Both the native and anomalous datasets diffracted to 2.5 Å and diffraction data was processed using HKL2000 [125]. These crystals belong to the space group C2 with unit cell dimensions a = 142.4 Å, b = 56.2 Å, c = 80.7 Å and $\alpha = \gamma = 90°$ and $\beta = 119.2°$. In spite of high resolution of the anomalous dataset I was only able to use anomalous data up to 4.0 Å to calculate phases and get an electron density map using the SHELX program [115]. An initial model was built using COOT into this 4.0 Å map [114]. I had difficulty refining the model against the anomalous or the native datasets and the R-factors were high (R_{work}/R_{free} = 44.6/47.4). Even after I corrected the geometry, position and occupancy of all the residues in the model, the R-factors were higher than expected for a dataset of 2.5 Å (R_{work}/R_{free} = 34.7/40.1). Additionally the electron density map lacked the detail expected for a dataset of this resolution. There was poor density around the side chains and aberrant positive difference density where the model was already built in (Fig. 16A). This indicated that there was a problem with the datasets and not the model.

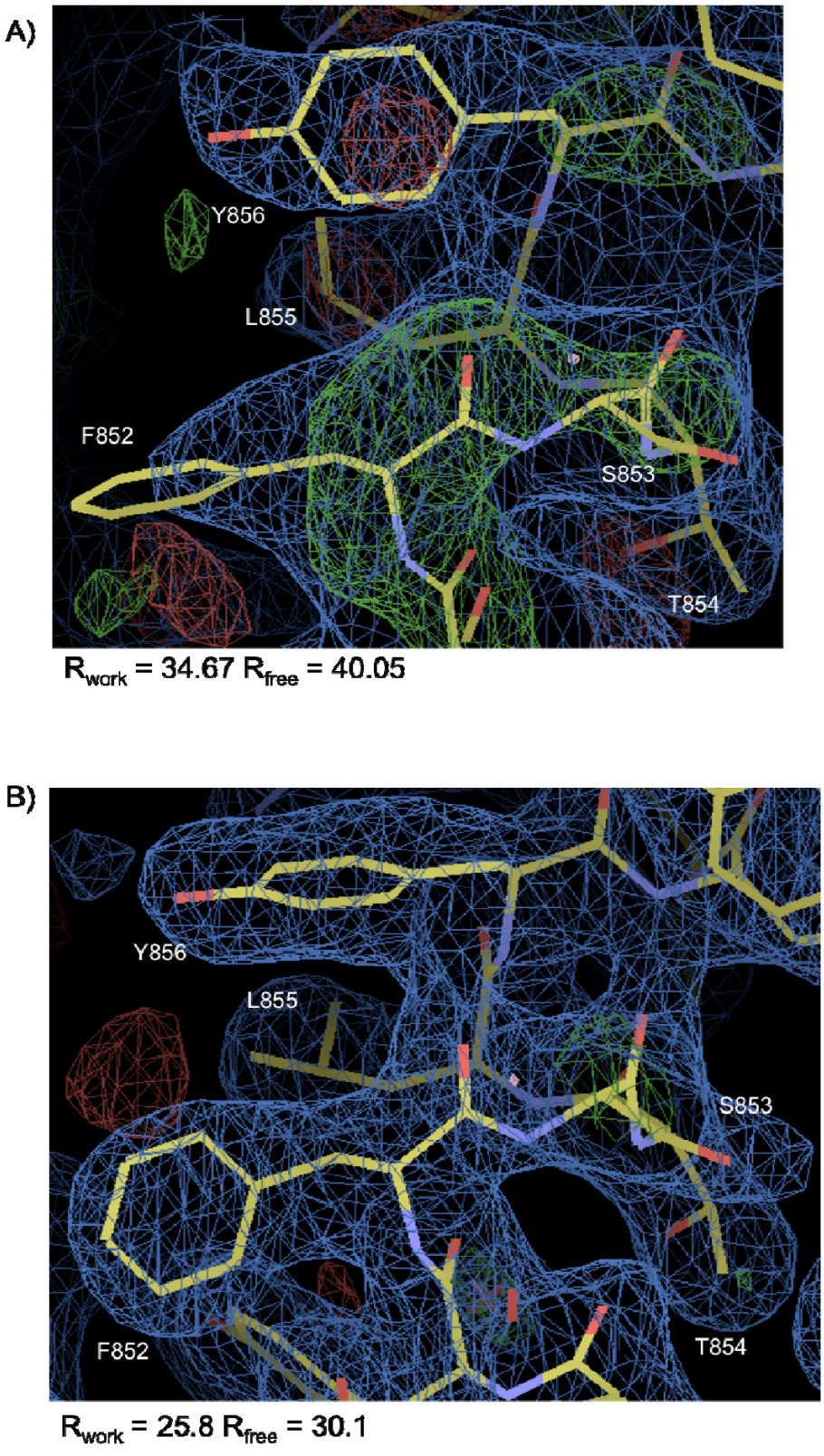

Figure 17: Ellipsoidal filtering improved electon density map quality.

(A) Electron density map (in blue), contoured at 1σ, of the hRock SER mutant data before ellipsoidal filtering to remove the poorly measured reflections. The positive difference density is shown in green and the negative difference density is shown in red. The model is represented as stick diagrams. There is poor electron density around several side chains and aberrant positive and negative electron density.

(B) Improved electron density map (blue), contoured at 1σ, of the hRock SER mutant after ellipsoidal filtering to remove the poorly measured reflections. The model is represented as stick diagrams. Ellipsoidal filtering improved the quality of the electron density map.

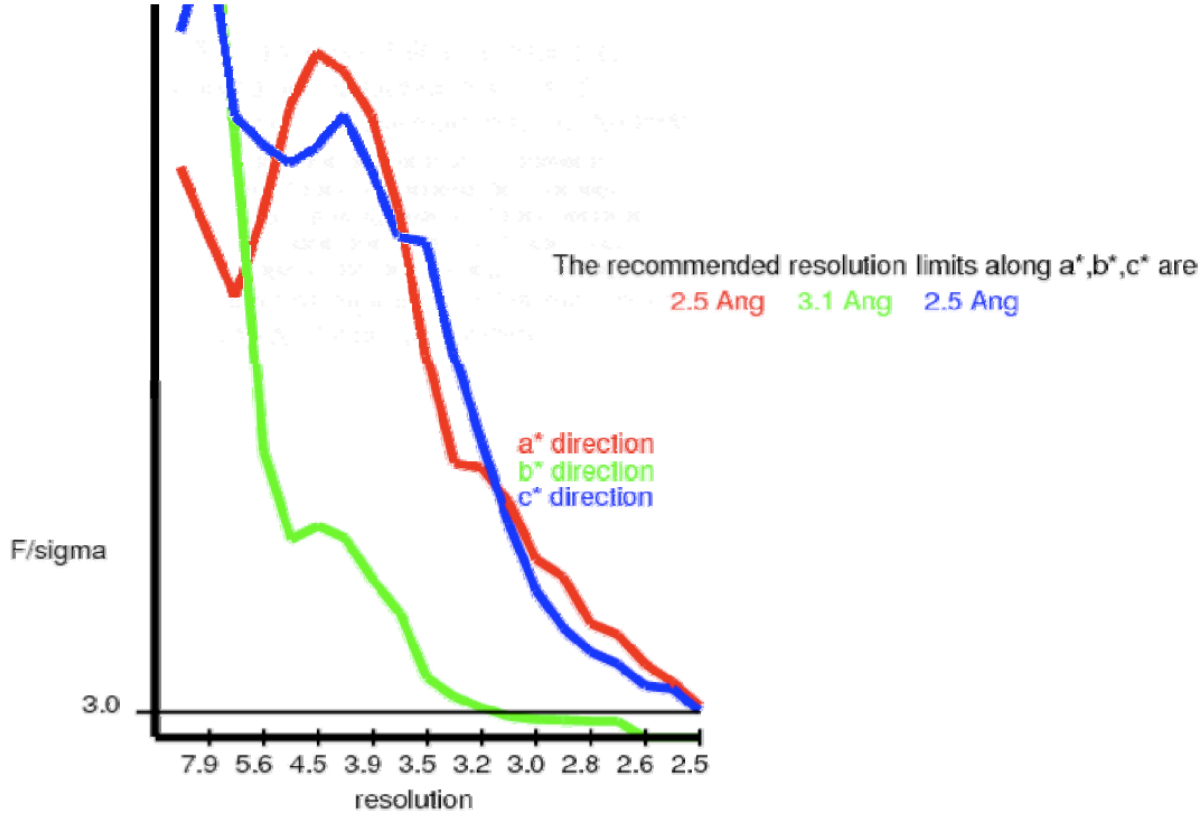

Figure 18: hRock SBD data has severe diffraction anisotropy.

F/sigma is plotted against resolution for the three directions of diffraction to determine at what resolution the F/sigma drops below 3 in each direction. This graph indicates that the diffraction data goes out 2.5 Å in the a* and the c* directions but only out to 3.1 Å in the b* direction.

Analysis of the processed datasets did not indicate the presence of more common problems such as merohedral twinning or pseudo-translational symmetry. So I decided to look at other crystallographic defects that could account for the issues seen with the data. Sometimes proteins pack more uniformly in one direction over another causing the crystal to diffract unequally in all directions. This is called diffraction anisotropy and in severe cases it can result in an ellipsoidal diffraction pattern instead of a spherical one. Current data processing programs cannot account for the ellipsoidal diffraction pattern and include poorly measured reflections in the data, specifically in the weakly diffracting direction, thus introducing a lot of noise into the dataset. Coiled coil proteins have been known to display diffraction anisotropy [126]. Since Rock SBD is predicted to be a coiled coil protein, I analyzed the diffraction data from the Rock SBD SER mutant crystals for diffraction anisotropy using the Diffraction Anisotropy Server [127]. This analysis indicated that the native data diffracted to 2.5 Å in the 'a' and 'c' directions but only to 3.1 Å in the 'b' direction (Fig. 17). After determining the resolution cut offs for each direction the server performed ellipsoidal truncation to remove most of the weakly measured reflections from the dataset. I used the truncated native data for further refinement and building and saw an immediate improvement in refinement statistics (R_{work}/R_{free} = 30.1/32.8) and the electron density map (Fig. 16B). After a few more rounds of refinement and building I was able to improve the R-factors to R_{work}/R_{free} = 25.8/30.1. There are four SBD molecules in the asymmetric unit and current structure contains residues 836-904 in molecule C, 838-902 in molecule D, 837-902 in molecule E, and 838-903 in molecule F. Analysis of the structure with Molprobity indicates that all of the residues in both chains lie in the favored regions of the Ramachandran plot [128]. The average B-factor for both molecules is 47.5 $Å^2$ (Table 2). Using

ellipsoidal truncation I was able to correct anisotropic diffraction in the data and determine the structure of the hRock SBD at 2.5 Å.

Table 2: Data collection and refinement statistics for hRock1 SBD

Data collection and refinement statistics for hRock1 SBD		
	SeMet (SAD)	Native
Data Collection		
Space Group	C2	C2
Cell Dimensions		
a (Å)	141.6	142.5
b (Å)	56.1	56.2
c (Å)	80.4	80.7
α = γ (°)	90	90
β (°)	119.0	119.1
Resolution (Å)	50.0-2.4 (2.44-2.40)	50.0-2.5 (2.54-2.50)
Unique Reflections	21426	17172
R_{merge}	8.7 (65.7)	7.6 (54.7)
$I/\sigma I$	27.0 (1.6)	30.7 (1.9)
Completeness (%)	98.9 (93.8)	88.6 (56.1)
Redundancy	6.1 (4.1)	5.7 (4.9)
Refinement		
Resolution (Å)		50.0-2.5
R_{work} / R_{free}		25.78/30.14
No. atoms		
Protein		2179
Solvent		9
R.m.s. deviations		
Bond lengths (Å)		0.009
Bond angles (°)		1.192
Average isotropic B values (Å^2)		47.51
Protein		47.41
Water		35.75
Ramachandran statistics		
Outliers		0
Allowed		0
Favored		100

Values in parentheses correspond to those in the outer resolution shell.
$R_{merge} = (|(\Sigma I - \langle I \rangle)|)/(\Sigma I)$, where <I> is the average intensity of multiple measurements.
$R_{work} = \Sigma_{hkl}||F_{obs}(hkl)|| - F_{calc}(hkl)||/\Sigma_{hkl}|F_{obs}(hkl)|$.
R_{free} = crossvalidation R factor for 7.3% of the reflections against which the model was not refined.

3.2.3 hRock SBD is a parallel coiled coil dimer

The crystal structure revealed that Rock SBD is a parallel-coiled coil dimer (Fig. 18A). There are two dimers in the asymmetric unit that pack in a tail to tail manner. This packing interaction causes the coiled-coil dimer to fray at the C- terminal ends and form a four helical bundle such that the N-terminal half forms a dimer and the C-terminal half forms a tetramer (Fig. 18B). The individual chains in each dimer align with an r.m.s.d of 2.8 Å with the highest level of similarity at the N-terminus (Fig. 19B). The two SBD dimers structurally align with an r.m.s.d of 1.0 Å indicating that the two SBD dimers are essentially identical (Fig. 19A). Since there are no major differences between the two dimers in the asymmetric unit the following analyses were carried out with the dimer composed of chains C and D.

Analysis of the structure with the program SOCKET indicates that all the coiled coil interactions at the dimerization interface and at the four-helix bundle interface are canonical knobs into holes packing interactions [129]. Even though the interactions mediating the tetramer interface resemble canonical coiled-coil interactions we believe that the four helical bundle formed by the two dimers is an artifact of crystal packing. Using the program TWISTER, I determined the average pitch, rise, and radius of the overall structure to be 178.7 Å, 1.63 Å, and 6.5 Å, respectively [130]. There is a sharp increase in the pitch where the four helices start to form the four-helical bundle (Fig. 20A and 20B). The rise of the coiled coil stays constant throughout the structure; however, there is a gradual increase in the radius of the coiled coil dimer from the N-termius to the C-terminus due to the helices splaying apart for the four helical bundle packing interaction (Fig. 20C and 20D). These results suggest that the hRock SBD dimer is a traditional coiled coil dimer and any deviations observed are due to the packing interactions between the two dimers.

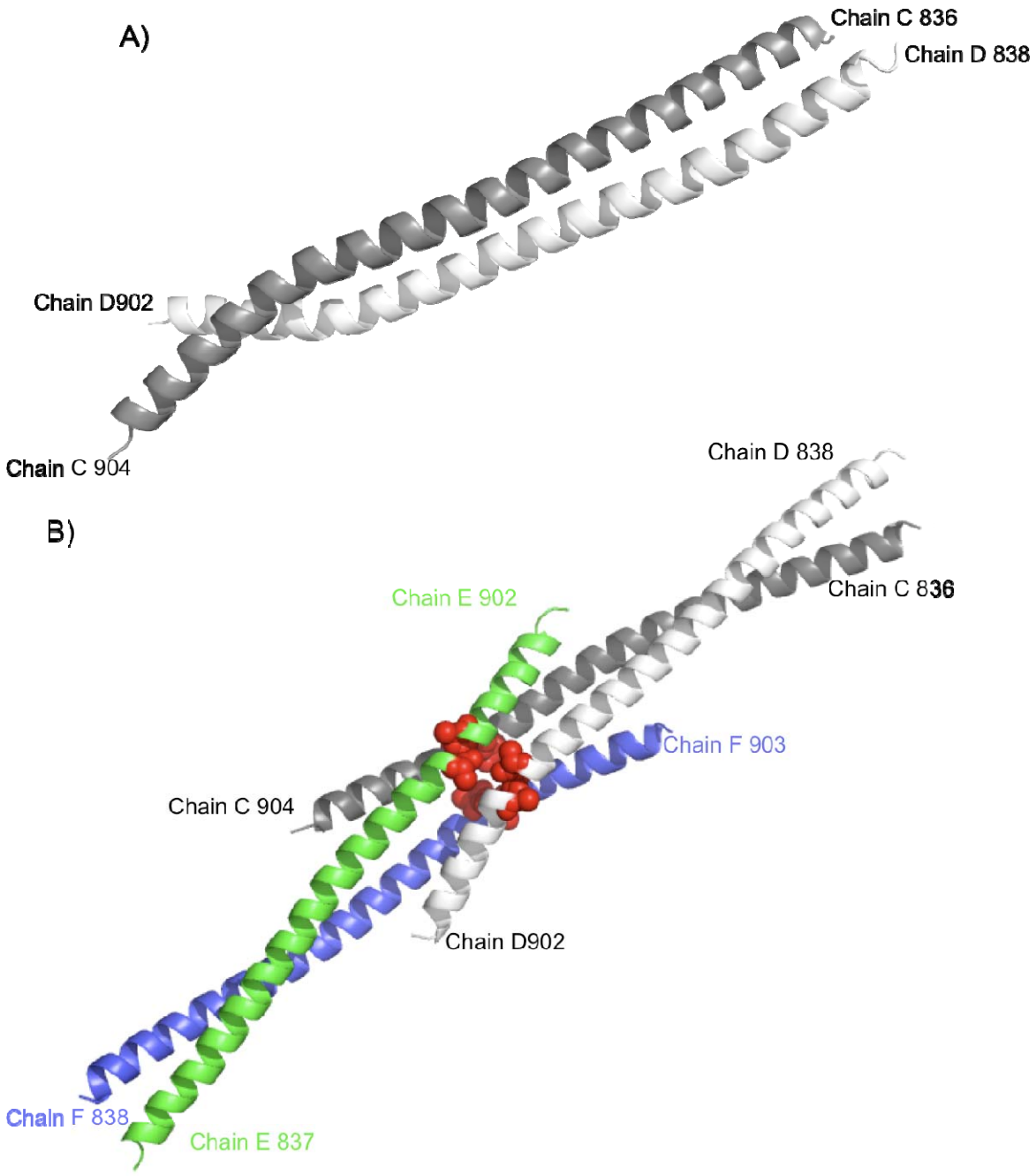

Figure 19: Structure of the hRock SBD.

(A) Ribbon diagram representing the Rock SBD parallel coiled coil dimer with Chain C in gray and Chain D in white.

(B) Ribbon diagram of the two Rock SBD dimers seen in the crystal asymmetric unit. Chains C and D are shown in gray and white and Chains E and F are shown in green and blue. The surface entropy reduction (SER) mutations are shown as red spheres. The SER mutant residues lie at the interface between the two SBD dimers.

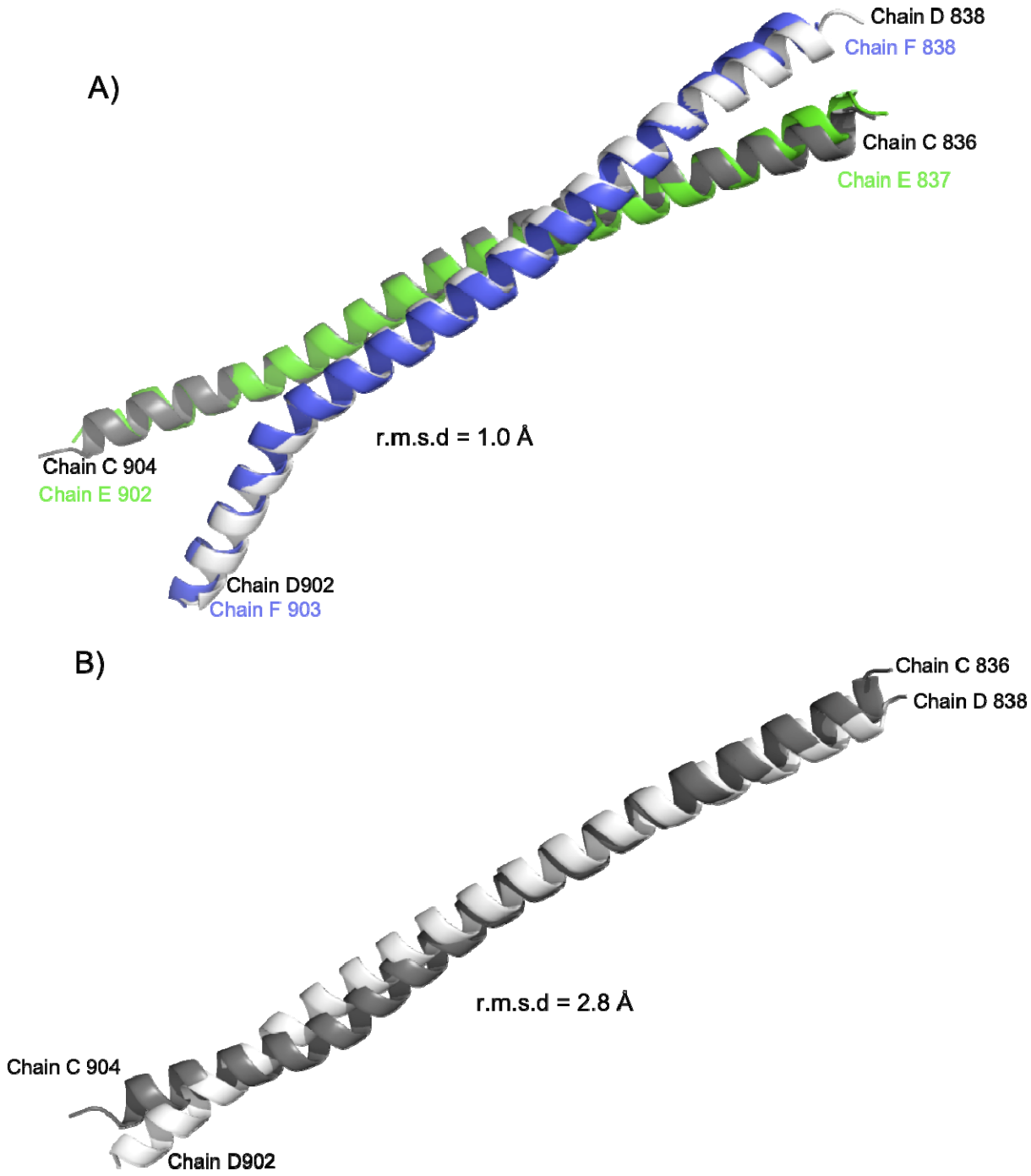

Figure 20 : Structural alignment of the hRock SBD.

(A) Structural alignment of the two SBD dimers. The two dimers align with an r.m.s.d of 1.0 Å over 70 Cα atoms. Alignment was done with PDB efold

(B) Structural alignment of the SBD monomers in each dimer. The two SBD monomers align with an r.m.s.d of 2.8 Å over 70 Cα atoms with highest degree of difference at the C-terminus. Alignment was done with PDB efold.

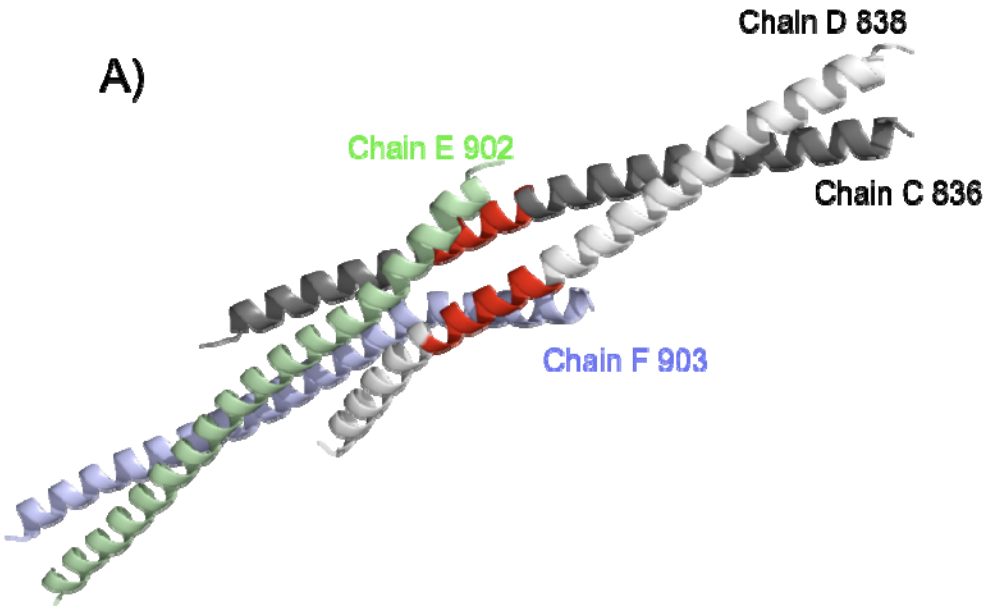

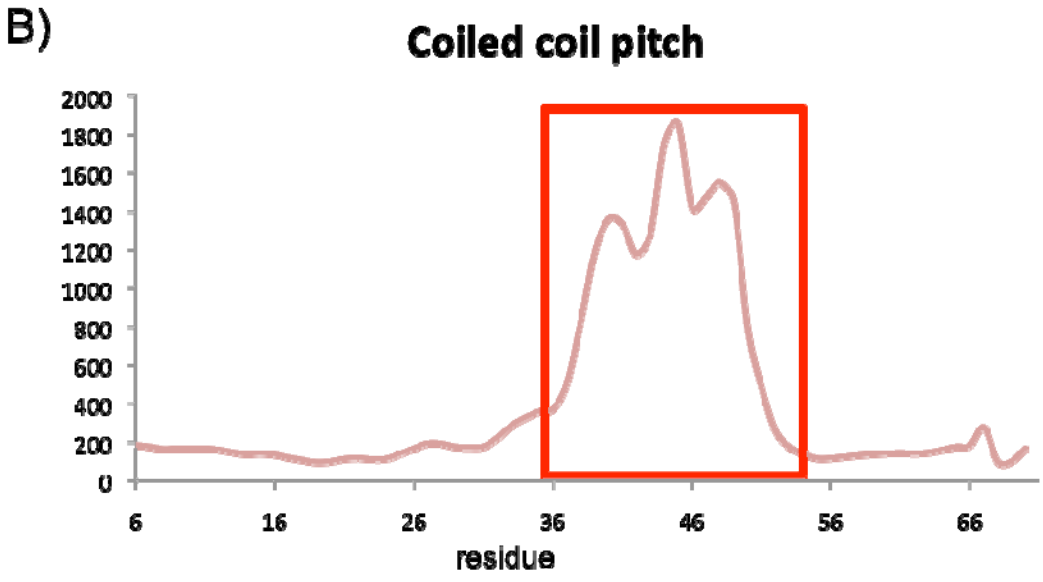

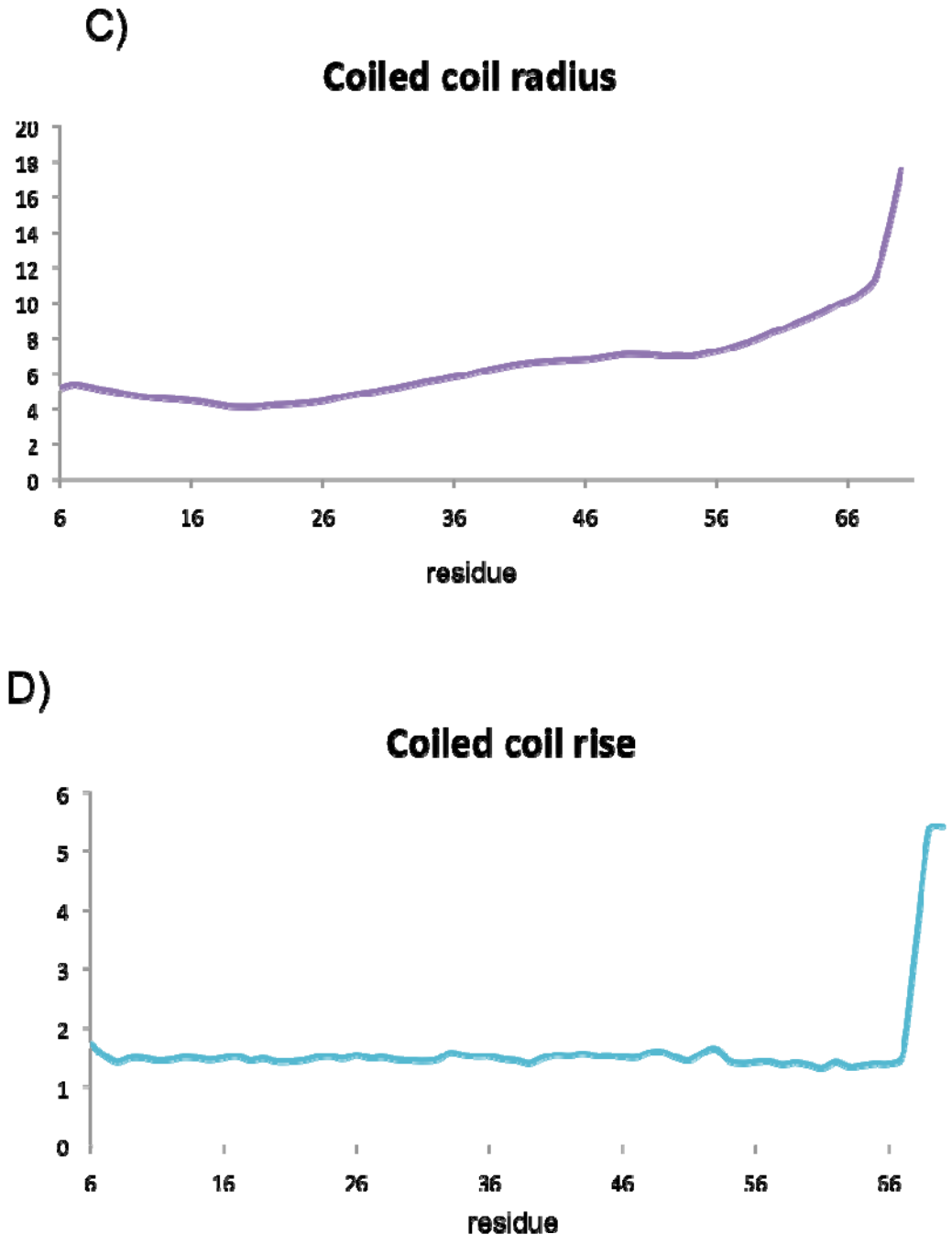

Figure 21: Analysis of the SBD coiled-coil.

(A) Cartoon representation of the two Rock SBD dimers with Chains C and D in black and white and Chains E and F in green and blue. The region where the coiled coil pitch increases due the four helical bundle packing is highlighted in red in the C and D chains. (B) Coiled coil pitch (Å) vs. residue graph. (C) Coiled coil radius (Å) vs. residue graph. (D) Coiled coil rise (Å) vs. residue graph. Graphs presented in (B), (C), and (D) were calculated in

the program TWISTER [130]. These graphs indicate that the packing interactions between the two dimers cause the coiled coil dimer to fray towards the C-terminal end.

3.2.4 Conserved patches in SBD that mediate the Shroom-Rock interaction

I took a mutational approach to identify residues in Rock SBD that mediate the Shroom-Rock interaction. Using a multiple sequence alignment of 18 Rock sequences and the RISLER matrix in the ESPRIPT program I identified and scored conserved residues in the Rock SBD [120, 121]. Upon mapping the conserved residues on to the surface of the SBD dimer it became immediately apparent that while there were a number of conserved patches throughout the structure the N-terminal region was mostly invariant (Fig. 21A). In collaboration with the Hildebrand lab I designed a series of multi-site substitution mutations that targeted the conserved surface exposed residues (Fig. 21B) and (Table 3). All of the targeted residues were mutated to alanine. The ability of these mutations to interact with hShroom SD2 domain was tested using gel shift and fluorescence anisotropy assays. Due to the difficulty in detecting the SD2-SBD complex using the minimal SBD construct (834-913) all of the mutations were made in a longer SBD construct (707-946) that extended into the coiled-coil region. The gel shift assays indicate that mutating residues in the highly conserved N-terminal patches, specifically ^{850}QYF^{852} and ^{857}KTQ^{859}, completely abolish SD2 binding (Fig. 22A). These observations are confirmed by the fluorescence anisotropy experiments (Fig. 22B). Additionally, the anisotropy experiments

indicate that disrupting some of the conserved residues at the C-terminus, ^{900}ESE^{902}, moderately disrupts the interaction with the SD2 domain. Both anisotropy and gel shift assays indicate that the SER mutation does not disrupt the Shroom-Rock interaction (Fig. 22A and B). These results suggest that there are two conserved regions, one at the N-terminus and one at the C-terminus, in the hRock SBD that mediate the Shroom-Rock interaction with the N-terminal region playing a more significant role than the C-terminal region (Fig. 22C).

Table 3: hRock1 Shroom binding domain mutations.

Mutant #	Residue #s	Sequence
1	850-852	QYF
2	865-866	EE
3	857-859	KTQ
4	872-879	RENLKKIQ
5	900-902	ESE
6	906	R
7	900-906	ESEQLAR

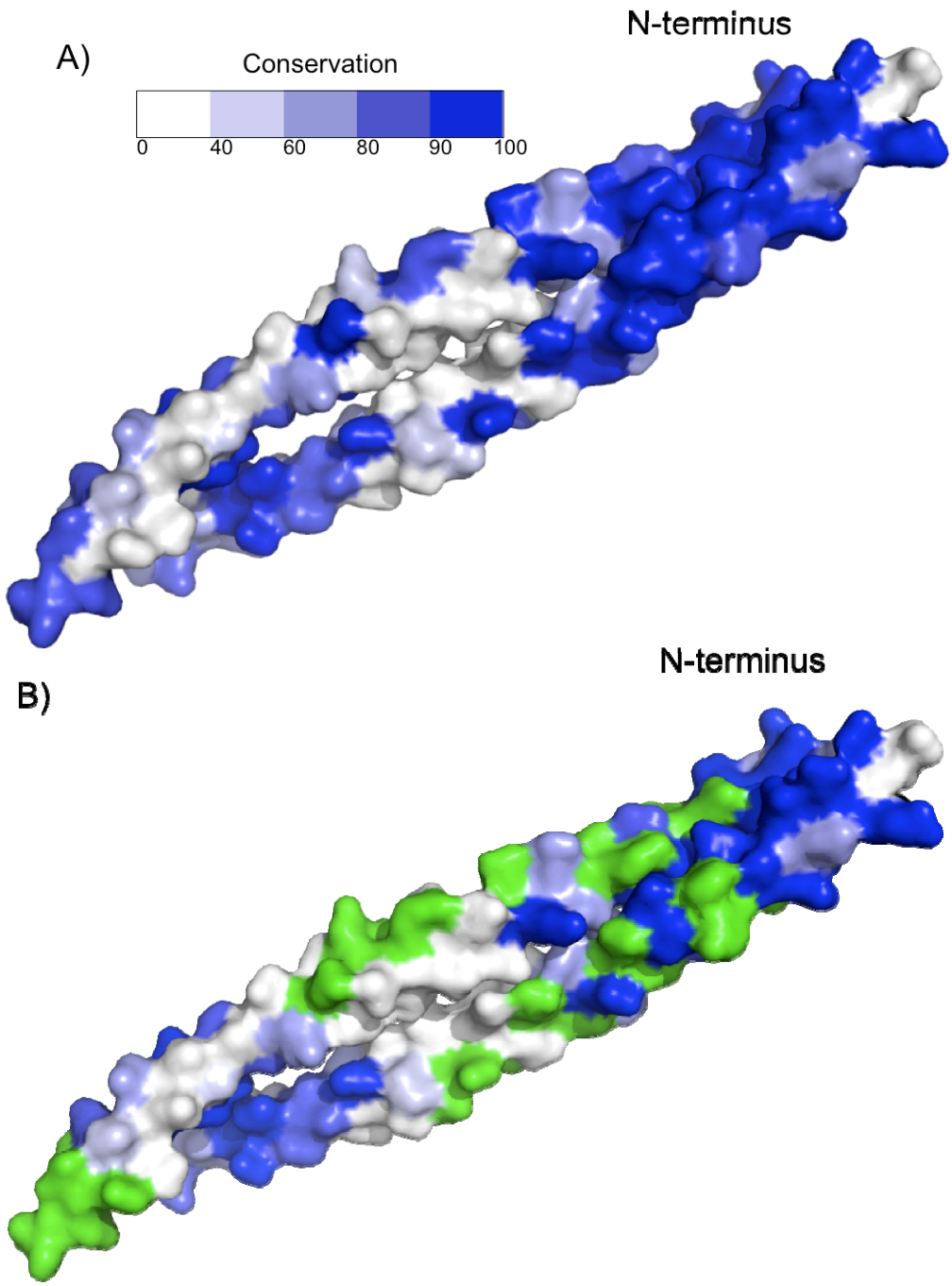

Figure 22 : The N-terminal half of hRock SBD is highly conserved.

(A) Surface view of the Rock SBD with the conserved residues highlighted in shades of blue. Conservation was obtained from a multiple sequence alignment of 16 SBD sequences and scored using the RISLER matrix in espript.

(B) The conserved residues targeted for mutational analysis are highlighted in green.

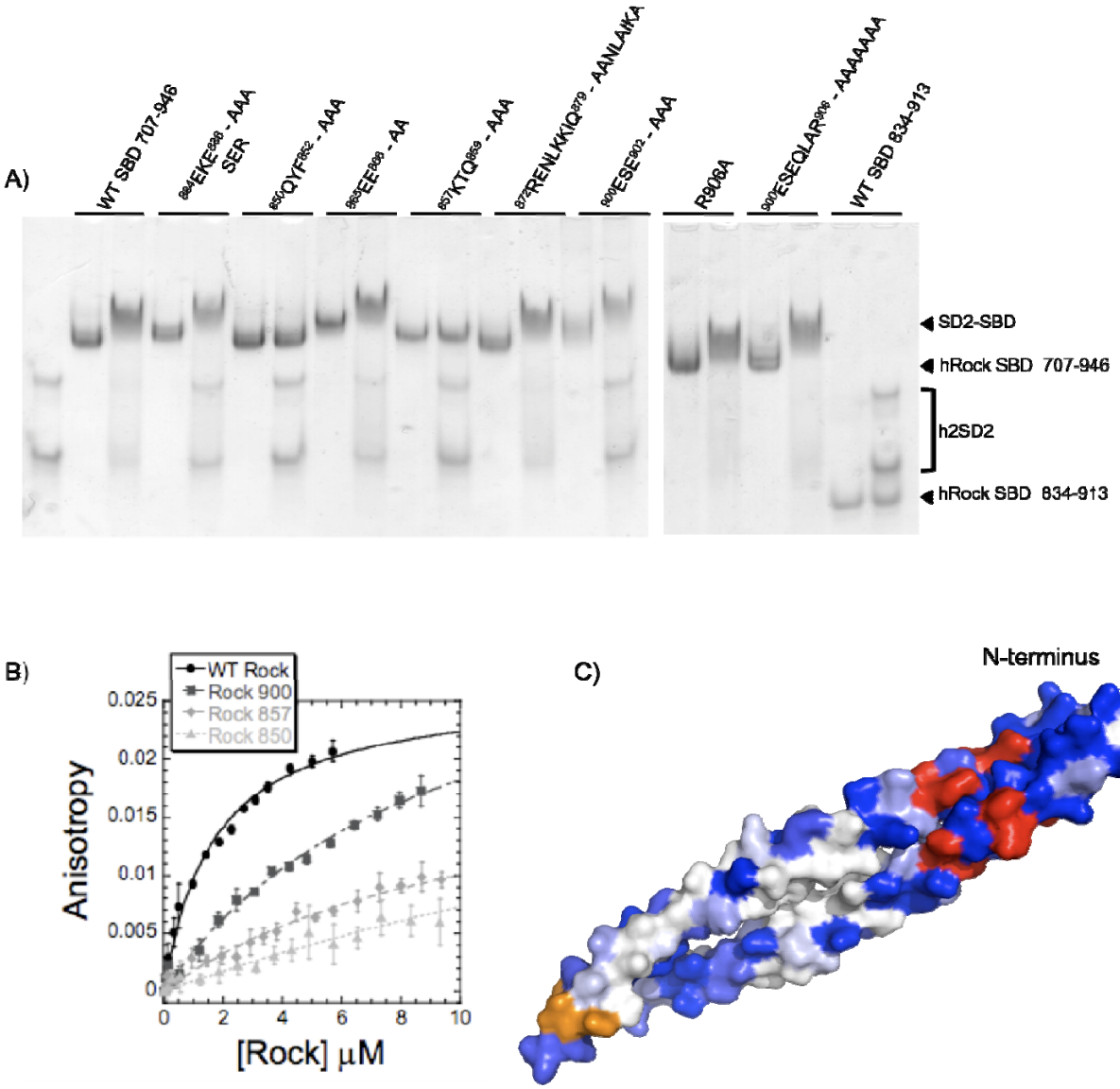

Figure 23: Disrupting conserved residues in hRock SBD disrupts SD2 interaction.

(A) Native gel electrophoresis with h2SD2 and wild-type or mutant hRock SBD. 10µM hShroom2 SD2 and wild-type or mutant hRock1 SBD were mixed and incubated at room temperature prior to subjecting the protein to Native PAGE.

(B) Fluorescence anisotropy of labeled hShroom2 SD2. Concentration of labeled hShroom2 SD2 was fixed at 20nM and increasing amounts of wild-type or mutant hRock SBD was titrated. The increase in anisotropy was measured at 595m.

(C) Surface view of the hRock SBD dimer with the conserved residues highlighted in blue. The conserved residues at the N-terminus that are required for SD2 interaction are highlighted in red. The conserved resides at the C-terminus that when mutated cause a moderate defect in SD2 interaction are highlighted in orange.

3.3 CONCLUSIONS

I determined the structure of the core human Rock1 SBD spanning residues 834-913 using x-ray crystallography. The structure revealed that hRock SBD is a parallel coiled-coil dimer. In the asymmetric unit of the crystal there are two SBD dimers that pack in a tail-to-tail manner. Analysis of the rise, pitch, and radius of the coiled-coil with the program TWISTER indicated that hRock SBD is a canonical coiled-coil dimer. Upon mapping the conserved residues to the surface of the SBD revealed that there is a high level of conservation at the N-terminus. Using a combination of mutational and biochemical analysis I identified two conserved patches that play an important role in mediating interactions with Shroom. One of the patches is on the highly conserved N-terminus and the second patch is located at the C-terminus of the hRock SBD structure. These results suggest that conserved residues at the N- and C-terminus of SBD mediate interaction with Shroom.

4.0 CHARACTERIZATION OF THE SHROOM-ROCK COMPLEX

4.1 INTRODUCTION

To understand the mechanistic details of the Shroom-Rock interaction and Shroom mediated apical constriction we need to structurally characterize the Shroom-Rock complex. The crystal structures of the individual domains indicate that both SD2 and SBD are coiled coil dimers. Biochemical assays with the SD2 domains suggest that dimerization is important for the Shroom-Rock interaction [123]. Structures of other portions of the Rock coiled-coil region have also been determined to be coiled coil dimers [83, 84, 126]. The structure of the Rho binding domain of Rock in complex with RhoA indicates that Rock binds to RhoA as a dimer [84]. Based on these observations I can hypothesize that the SD2-SBD complex is a heterotetramer.

To characterize the Shroom SD2-Rock SBD complex I used a series of biochemical assays with complexes from different species. I determined the dissociation constant of the *Drosophila* Shroom-Rock complex to be 0.58 ± 0.07 μM. Using a variety of biochemical techniques I was also able to determine that the molar ratio of the SD2-SBD complex is 1:1. I also attempted to determine the structure of the mShroom2 SD2-hRock1 SBD. Using surface entropy reduction mutations in both proteins I was able to obtain diffraction quality crystals. Upon optimization these crystals should provide high quality diffraction data that can be used to determine the structure of the complex using molecular replacement.

4.2 DROSOPHILA SHROOM-ROCK COMPLEX

4.2.1 Fluorescence Energy Transfer

In an effort to elucidate the molecular details of the Shroom-Rock complex, we first utilized fluorescence energy transfer (FRET) experiments to detect and quantify the interaction between dShroom and dRock SBD. These experiments were done in collaboration with Michael Trakselis in the Department of Chemistry at the University of Pittsburgh. We labeled dRock with Cy5 at its N-terminus while dShroom SD2 was labeled with Cy3 at a single cysteine (C1428) not believed to be located within the Rock-binding interface. There are two endogenous cysteines within this construct of dShroom SD2, so a conservative mutant of dShroom (C1533S) was generated to ensure labeling at a single position. Titration of dShroom with dRock resulted in a decrease in donor emission and increase in acceptor emission consistent with an increase in FRET due to a binding interaction. Assuming a single binding mode for this interaction, the equilibrium K_d is calculated to be 0.58 ± 0.07 μM (Fig. 23A).

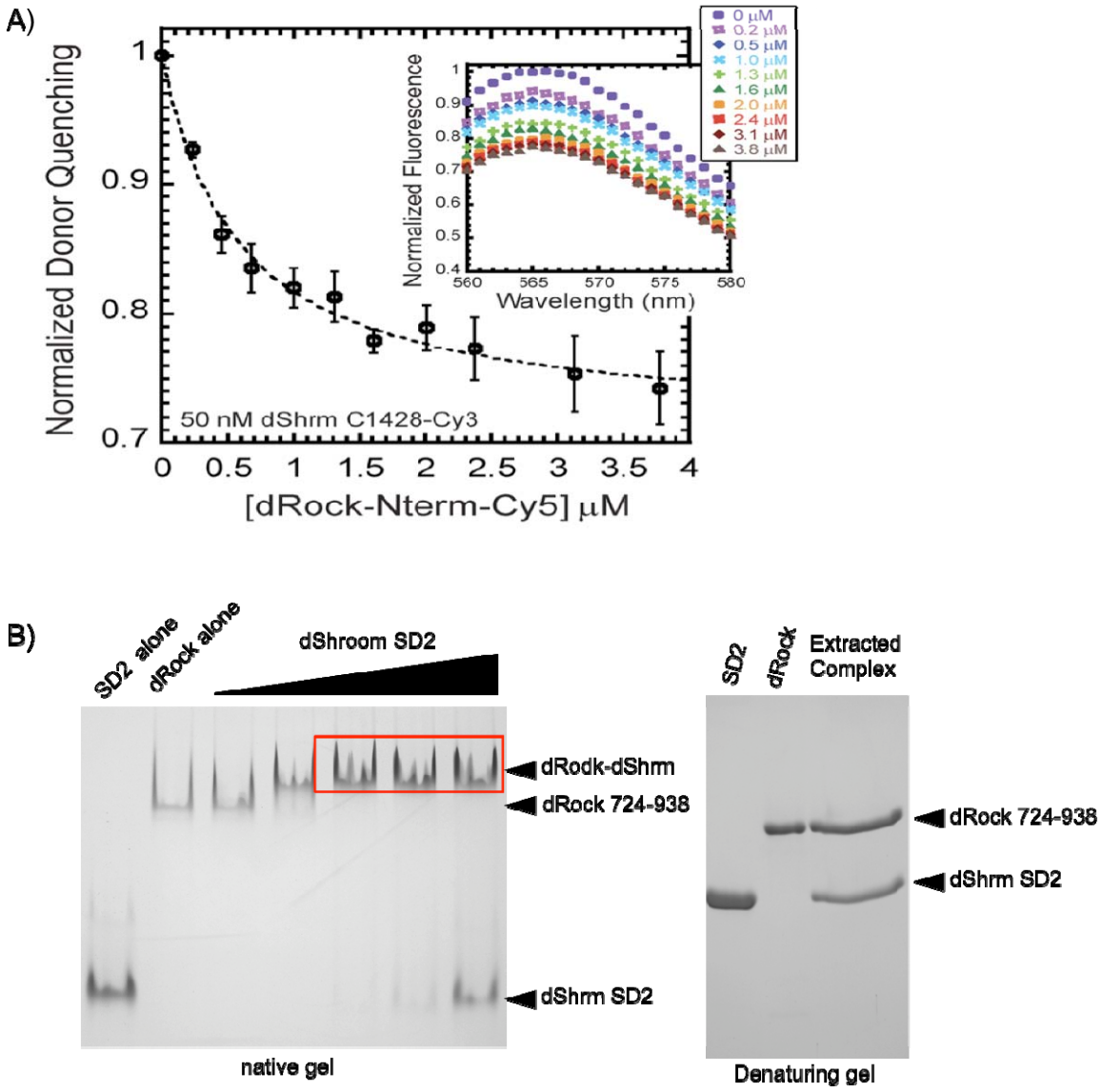

Figure 24: Characterizing the SD2-SBD complex.

(A) Donor quenching is plotted as a function of Rock and fitted to single binding mode to give a K_d of 0.58 ± 0.07 µM. Inset shows the decrease in donor fluorescence upon addition of different concentrations of Rock.

(B) 5µM SBD was mixed with increasing amounts of SD2 and the resulting SD2-SBD complex was first resolved via Native PAGE. Bands corresponding to the complex were excised and the resulting protein eluted from the gel slice was resolved using SDS-PAGE.

4.2.2 Stoichiometry of SD2-SBD complex

We next examined the stoichiometry of the dShroom-dRock complex. To determine this, purified dRock SBD and dShroom SD2 were mixed in solution to form a complex and then resolved on a native gel. Following electrophoresis, the complexes were excised from the gel, eluted, resolved by SDS-PAGE, and detected by Coomassie blue staining (Fig. 23B). Alternatively, purified SD2 and SBD were mixed at equimolar ratios and the complex was run on a gel filtration column and peak fractions were resolved by SDS-PAGE. The ratio of SD2 to SBD in the complex was measured by densitometry and corrected for the relative molecular masses of the two proteins. In all cases, isolated complexes were composed of SD2 and SBD in an approximately 1:1 molar ratio. While the possibility for a variety of higher-order species cannot be ruled out from this data, we feel that heterodimeric and heterotetrameric species are the most probable. I used a combination of SEC-MALS, mass spectrometry and crosslinking to determine if the SD2-SBD complex is a heterodimer or heterotetramer.

4.2.2.1 Chemical Crosslinking

Using chemical crosslinking I tried to determine the stoichiometry of the Shroom-Rock complex. The chemical crosslinking assay was performed with purified dShroom SD2 (1393-1576) and dRock SBD (724-938). Both proteins readily form dimers when exposed to small amounts of the crosslinker gluataraldehyde (Fig. 8A and Fig. 24). For all crosslinking experiments with the complex equimolar ratios of SD2 and SBD were mixed and incubated at room temperature before incubation with glutaraldehyde. Initial crosslinking experiments resulted in the formation of numerous mutlimers of varying Shroom-Rock composition that resolved as smears when subjected to SDS-PAGE (Fig. 25). Even after fine-tuning the crosslinking conditions I was

unable to resolve the SD2-SBD complex band (Fig. 26). In these crosslinking reactions the SD2 and SBD dimer bands still readily form and can be resolved via SDS-PAGE. The reason I am unable to resolve a crosslinked SD2-SBD band could be because these proteins react so readily with the crosslinker that they form multiple crosslinked species.

Since I was unable to resolve the complex by crosslinking dRock SBD (724-938) to dShroom SD2 I decided to use the minimal dRock SBD (821-938) that does not readily crosslink upon addition of glutaraldehyde (Fig. 27). The shorter SBD construct most likely does not crosslink because its reactive side chains are spaced too far apart to be crosslinked by glutaraldehyde. Since shorter SBD construct does not readily crosslink it is possible that the complex formed by this SBD and dShroomSD2 domain will be easier to resolve. Crosslinking experiments with SBD (821-938) and SD2 still resulted in multiple crosslinked species; however, there was one distinct band of ≈ 65kDa that was not present in the SD2 alone or SBD alone lane (Fig. 28). This band could correspond to one SD2 dimer and one SBD dimer suggesting that the SD2-SBD complex is a heterotetramer.

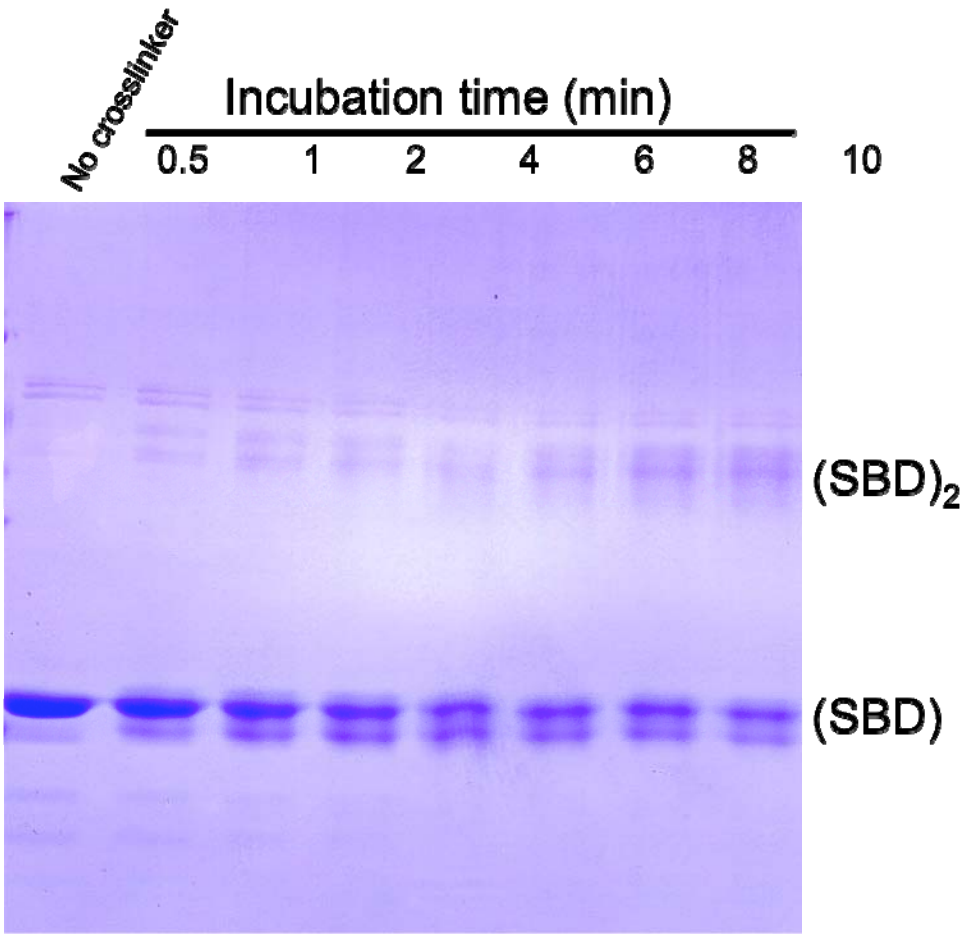

Figure 25: dRock SBD (724-938) readily dimerizes in solution.

Purified SBD (724-938) was incubated with 0.01% glutaraldehyde for the indicated time and the resulting species were resolved with SDS-PAGE.

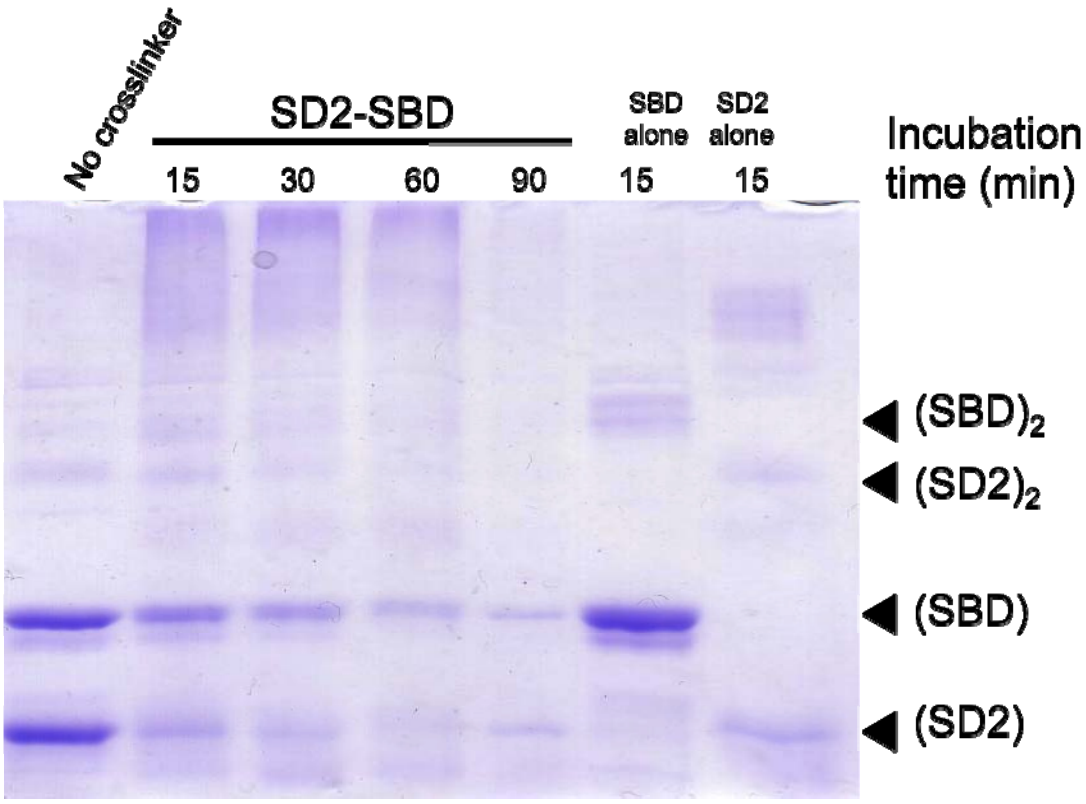

Figure 26: Initial crosslinking attempt of SD2-SBD complex.

Equimolar ratios of dShroomSD2 and dRockSBD were incubated with 0.01% glutaraldehyde for the indicated time and the resulting species were resolved with SDS-PAGE. The presence of various SD2-SBD multimers makes it difficult to resolve a single crosslinked complex band.

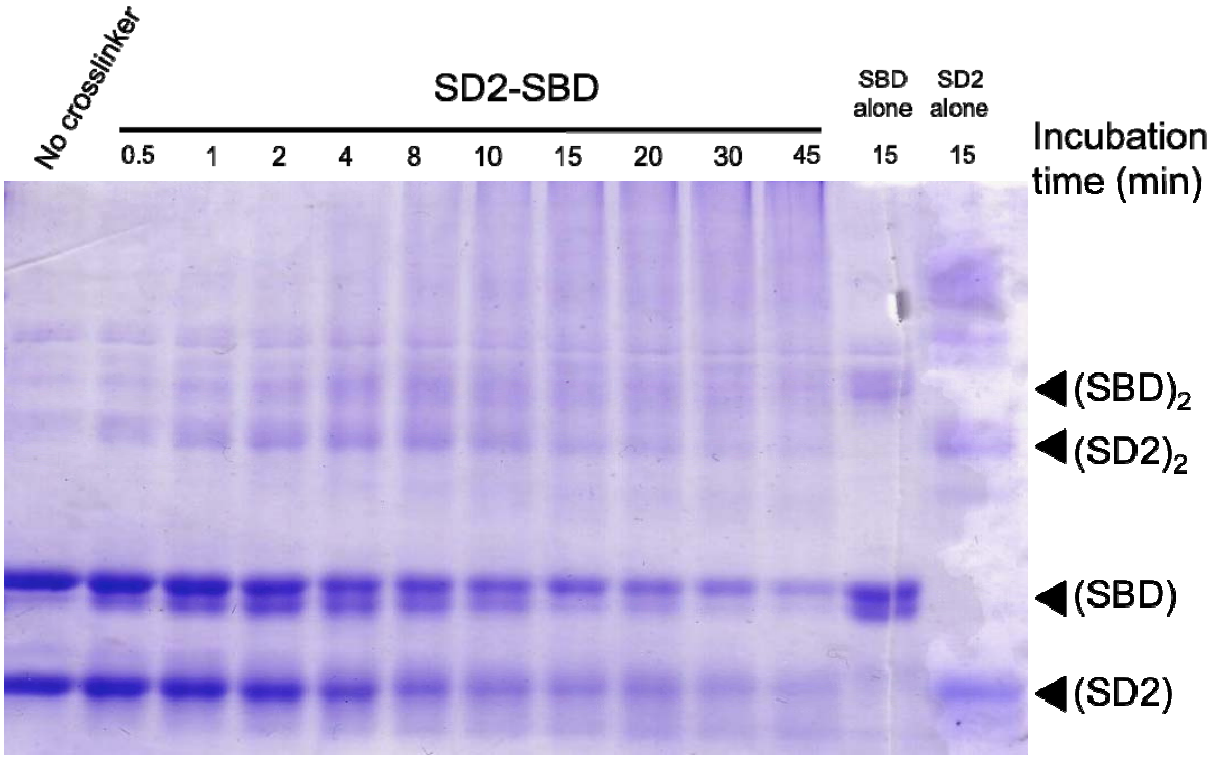

Figure 27: Crosslinking of SD2-SBD complex does not result in a single crosslinked complex band.

Equimolar ratios of dShroomSD2 and dRockSBD were incubated with 0.001% glutaraldehyde for the indicated time and the resulting species were resolved with SDS-PAGE. Fine-tuning the crosslinking conditions did not aid in resolving a single crosslinked complex band.

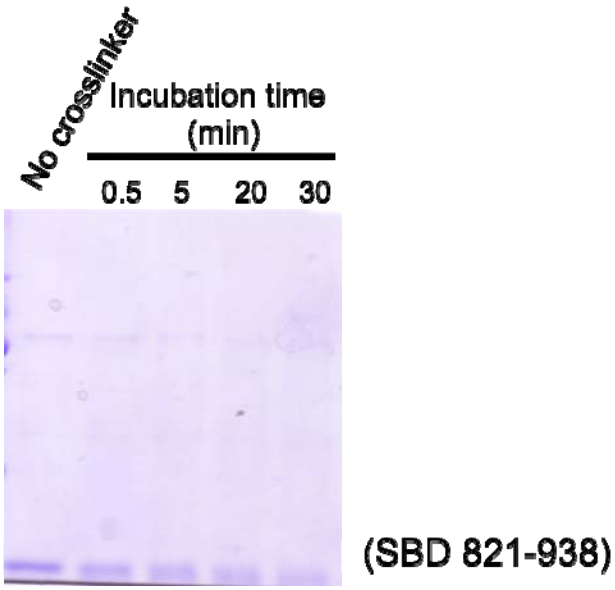

Figure 28: dRock SBD (821-938) does not readily crosslink in solution with glutaraldehyde.

Purified SBD (821-938) was incubated with 0.1% glutaraldehyde for the indicated time and the resulting species were resolved with SDS-PAGE. No crosslinked species was observed when dRock SBD (821-938) was subjected to crosslinking with glutaraldehyde.

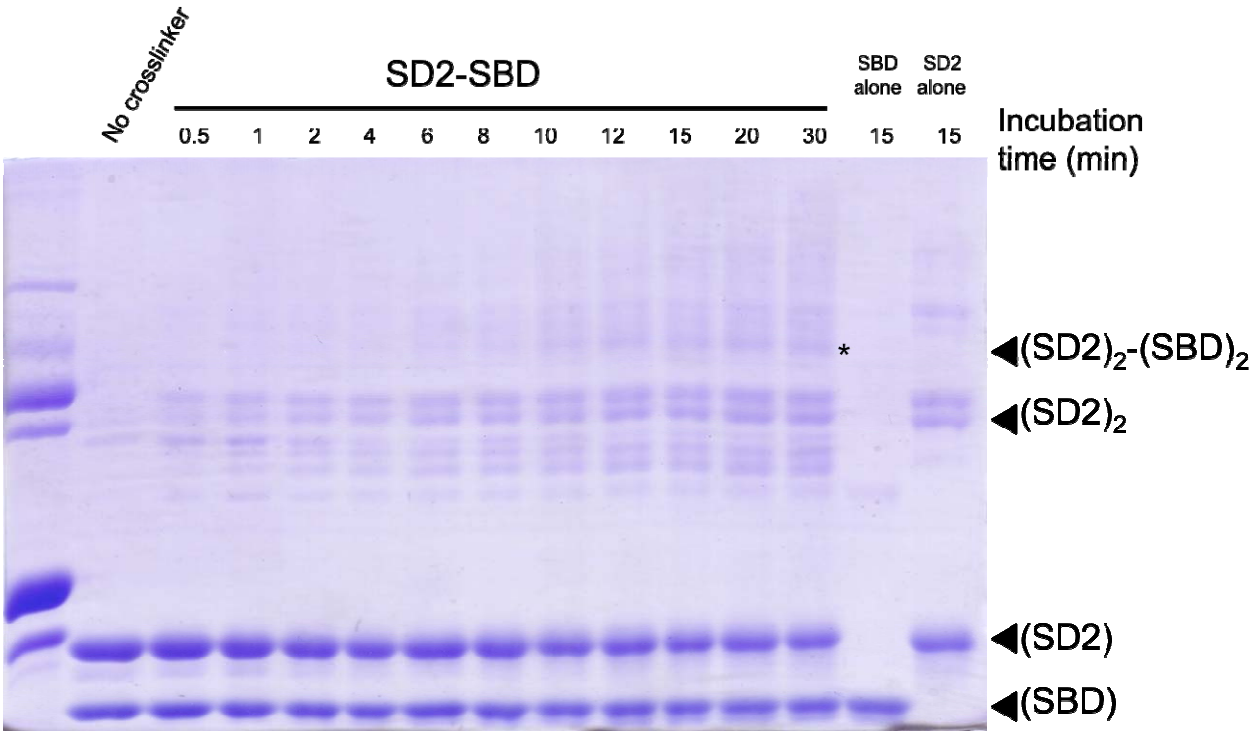

Figure 29: Crosslinking of dShroomSD2-dRock SBD (821-938).

Equimolar ratios of dShroomSD2 and dRockSBD were incubated with 0.005% glutaraldehyde for the indicated time and the resulting species were resolved with SDS-PAGE. The (*) indicates the crosslinked band not seen in either SD2 or SBD alone lanes. This band most likely corresponds to the SD2-SBD heterotetramer.

4.2.2.2 Size exclusion chromatography coupled with Multi-angle light scattering

To confirm the crosslinking results and to determine the stoichiometry with the longer SBD construct I analyzed the SD2-SBD (724-938) using multi-angle light scattering. Traditional light scattering techniques can be used to determine the molecular mass of globular proteins that scatter light uniformly. Light scattering from extended or large proteins or protein complexes on

the other hand varies greatly depending on the angle. Therefore the extended non-globular structures of SD2 domain and the SBD domain make them suboptimal candidates for traditional light scattering experiments. Instead we decided to use multi-angle light scattering (MALS), which measures the scattering from various angles and can determine the molecular weight of molecules independent of shape. Usually MALS is coupled with size exclusion chromatography to ensure the measurement of a single species. Purified dShroomSD2 and dRockSBD (724-938) were mixed at equilmolar ratios and subjected to an initial round of gel filtration. Fractions that contained both proteins in equal amounts were pooled and subjected to SEC-MALS (Fig. 29A). The SEC-MALS results indicated that the complex eluted off the size exclusion column in one peak with an apparent molecular weight of ≈80kDa (Fig. 29B). This molecular weight of the complex is much lower than the molecular weight for the tetramer, which would be around 93kDa. The molecular weight of 80kDa is slightly larger than the trimeric complex composed of two SBD molecules and one SD2 molecule. These results are not consistent with the results we previously observed. Additional experiments are required to properly analyze and interpret the results from SEC-MALS.

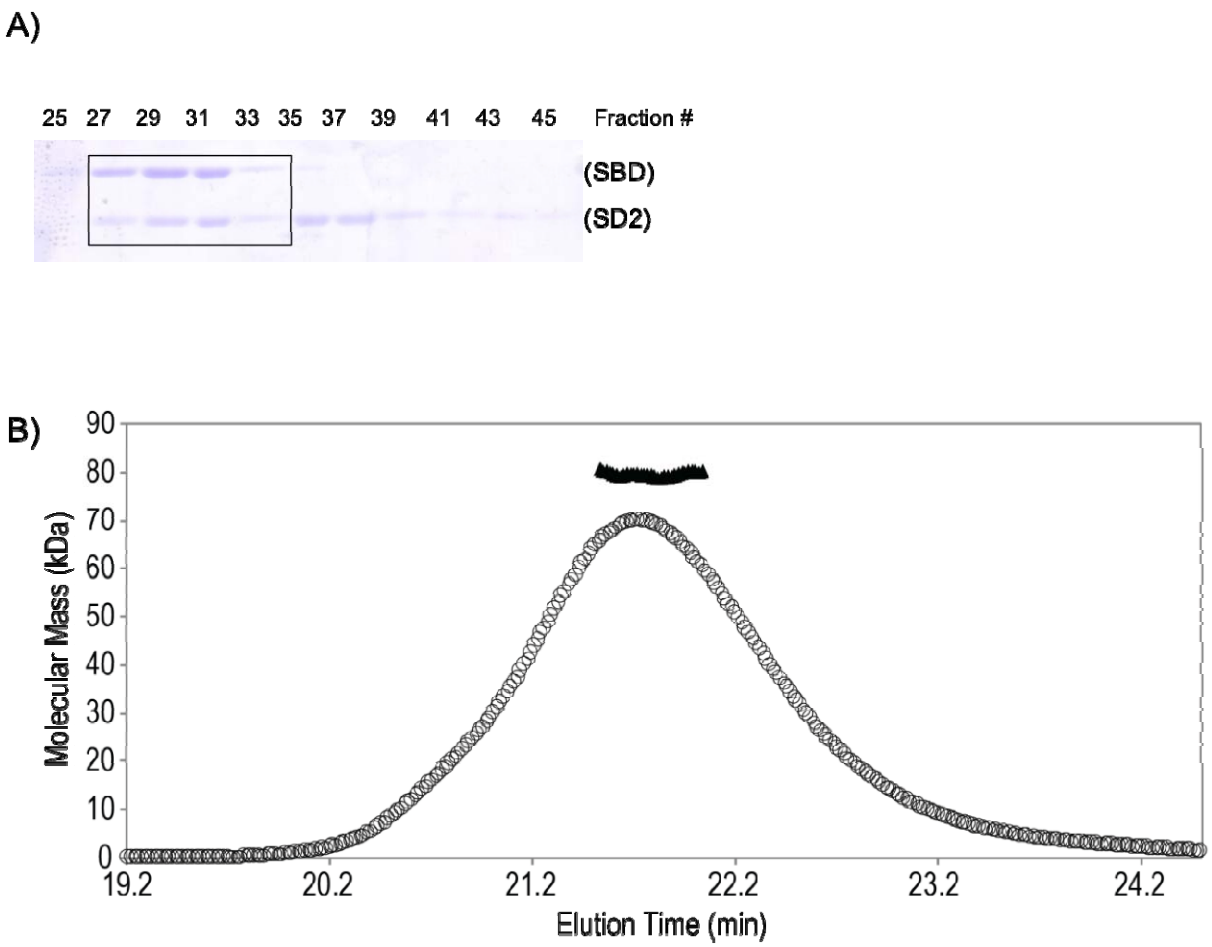

Figure 30: SEC-MALS with the dShroomSD2-dRock (724-938).

(A) Equimolar amounts of dShroom SD2-dRock SBD we mixed and subjection to a first round of gel filtration. Gel filtration fractions resolved by SDS-PAGE and the fractions pooled for SEC-MALS are highlighted by the black box.

(B) SEC-MALS chromatogram. The complex eluted off the column in peak between 20 and 23mls with the apparent M.W. weight of the complex is ≈80kDa. This molecular suggests that the SD2-SBD complex is a heterotrimer.

4.2.2.3 Mass Spectrometry

Mass spectrometry (MS) coupled with the soft ionization processes of electrospray ionization (ES) can be used to detect stoichiometry of complexes. To determine if I could resolve the discrepancy between the results from the crosslinking and the SEC-MALS experiments I performed ES-MS. Once again peak gel filtrations that contain both SD2 and SBD were pooled and concentrated to 42μM. The concentrated protein was dialyzed into buffer containing 100mM ammonium acetate and 20mM Tris pH 7.0. This buffer is ideal for MS, however, the SD2-SBD complex is not stable for very long in these conditions (Fig. 30). All the MS-ES experiments were performed on the complex within one week of dialysis into the acetate buffer. The protein was subjected to gel filtration using a C4 column immediately prior to ionization. The major peaks observed from ES-MS had a molecular weight of 21kDa, 25kDa, 42kDa and 51kDa (Fig. 31). These molecular weights correspond to SD2 and SBD monomers and dimers. These results suggest that ES-MS was not a gentle enough technique to keep the SD2-SBD complex intact. However, the presence of both SD2 and SBD dimers could suggest that the complex is a heterotetramer. Crosslinking the complex prior to ionization and using an even softer ionization technique called nanospray ES might aid in keeping the complex intact during ES-MS.

4.2.2.4 Crystallization of the SD2-SBD complex

The biochemical assays described above, with the exception of SEC-MALS, suggest that the molecular ratio of the Shroom-Rock complex is 1:1; however, it is still unclear if the complex is a heterodimer or a heterotetramer. To determine the composition of the complex I decided to determine the crystal structure of the complex. Co-expression and co-purification

attempts made by the VanDemark lab and the Hildebrand lab were not successful in purifying the large homogenous amounts of the SD2-SBD complex required for crystallography. Since I was able to easily purify large amounts of the individual proteins I mixed equimolar amounts of individually purified SD2 and SBD to generate the complex and the set up crystallization screens. Crystal screens with the Drosophila SD2-SBD complex did not yield any crystals; however, the mouse Shroom2 SD2- human Rock1 SBD complex formed crystals.

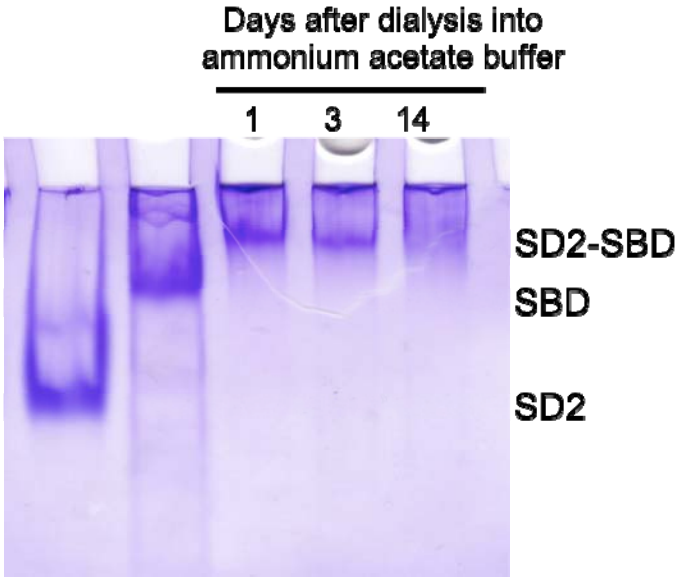

Figure 31: dShroomSD2-dRock SBD complex is not stable in the ammonium acetate buffer.

Native PAGE to resolve the dShroomSD2-dRock SBD (724-938) complex after gel filtration and dialysis into ammonium acetate buffer. The peak fractions containing the SD2-SBD complex from the size exclusion column were pooled and subjected to native PAGE before and after dialysis into the ammonium acetate buffer. The proteins degrade in the ammonium acetate approximately 2 weeks after dialysis.

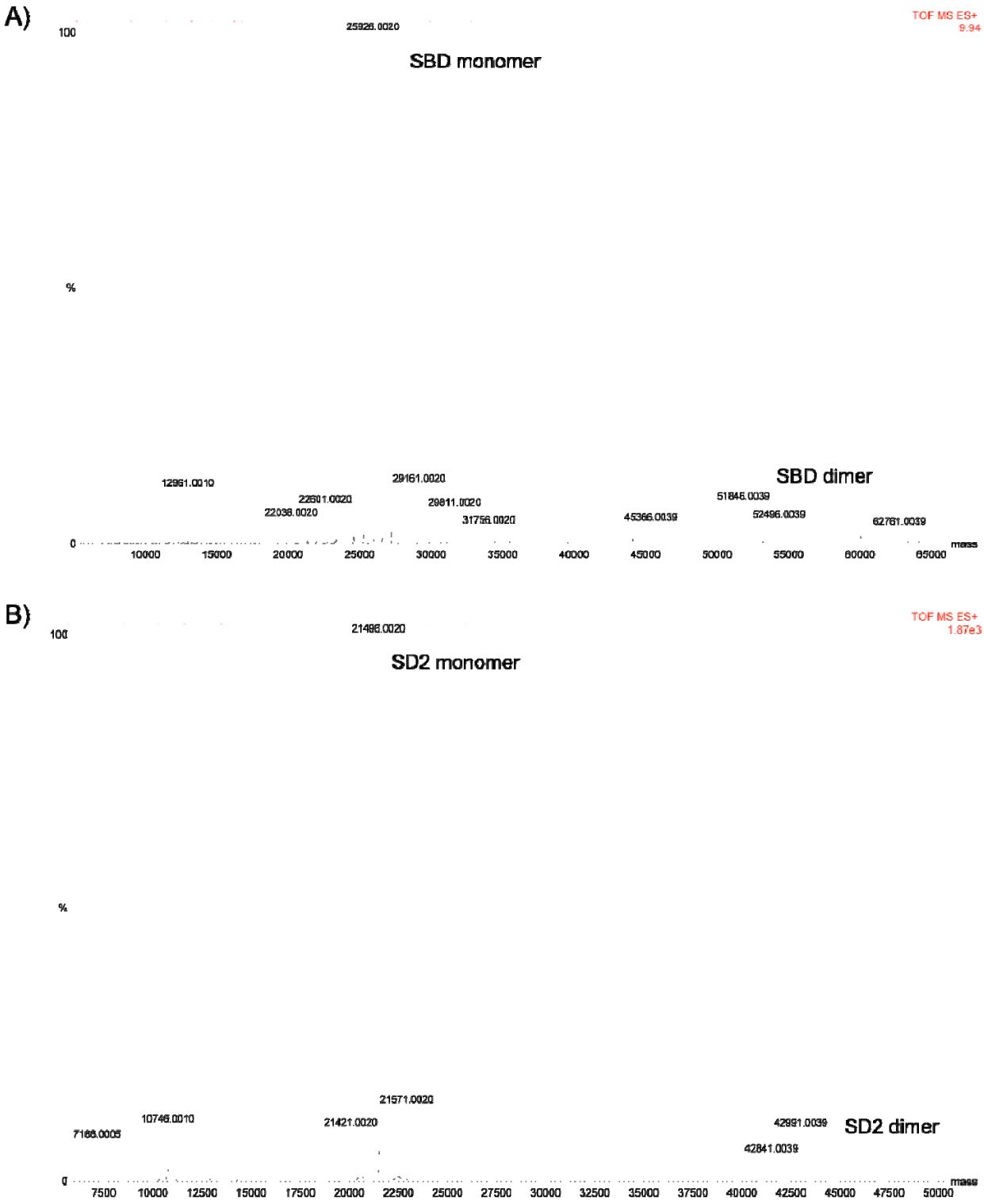

Figure 32: Electrospray-Mass Spectrometry of dShroomSD2-dRock SBD (724-938).

Major peaks corresponding to the dRock SBD monomer (25kDa) and dimer (51kDa) are shown in (A) and major peaks corresponding to the dShroom SD2 monomer (21kDa) and dimer (42kDa) are shown (B). The ES-MS spectrum indicate that this technique was not soft enough to keep the SD2-SBD complex intact.

4.3 MOUSE SHROOM2- HUMAN ROCK1 COMPLEX

Human Rock1 and mouse Rock1 share 96% percent identity therefore; mouse Shroom2-Human Rock1 complex is biologically significant (Fig. 32). Purified mShroom2 SD2 (1293-1476) and hRock1 SBD (834-913) mixed at equimolar ratios to concentration of 15mg/ml. The complex was allowed to sit at room temperature for 30min in buffer containing 100mM NaCl and 20mM Tris pH 8.0 before setting up crystallization trials. The mShroom2-hRock1 complex crystallized at room temperature in two conditions both of which contained 15% Ethanol, 0.2 $MgCl_2$ and either 0.1M Imidazole pH 8.0 or 0.1M HEPES pH 7.5. In both of these conditions the complex formed thin needle or rod shaped crystals that we very difficult to manipulate (Fig. 33A). I confirmed the presence of both proteins in the crystals by isolating the crystals and visualizing the proteins in them using SDS-PAGE and coomassie staining (Fig. 33B). I was able to crystallize the mShroom2 SD2-hRock1 SBD complex; however, the needle shaped crystals were difficult to optimize and manipulate.

```
hRock1_SBD      834 GNEGQMRELQDQLEAEQYFSTLYKTQVKELKEEIEEKNRE 873
mRock1_SBD      834 GNEGQMRELQDQLEAEQYFSTLYKTQVKELKEEIEEKNRE 873

hRock1_SBD      874 NLKKIQELQNEKETLATQLDLAETKAESEQLARGLLEEQY 913
mRock1_SBD      874 NLRKIQELQSEKETLSTQLDLAETKAESEQLARGILEEQY 913
```

Figure 33: Pairwise alignment of SBD from mouse and human Rock1.

Pariwise alignment of residues 834-913 from human Rock1 and mouse Rock 1. The alignment was was done using ClustalW and visualized using JalView [119]. Percent identity was calculated in JalView to be 96%.

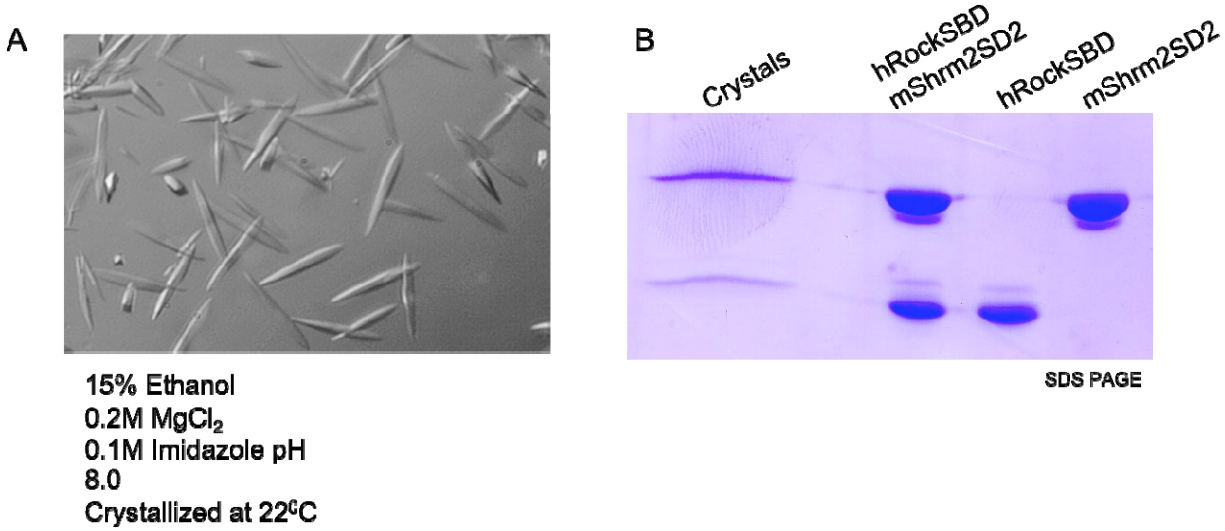

Figure 34: mShroom2 SD2-hRock1 SBD crystals.

(A) Optimized mShroom2 SD2-hRock1 SBD crystals.

(B) Crystals were extensively washed, dissolved and visualized using SDS-PAGE and coomassie staining. These crystals contained both mShroom2 SD2 and hRock1 SBD proteins.

To improve crystal quality I decided to use surface entropy reduction mutants of both proteins. Once again I mixed equimolar ratios of both the mutant SER proteins that were purified individually and set up crystallization trials. The SER mutant complex crystallized in several conditions forming mostly thick rods or plates (Fig. 34A). These crystals proved to be much easier to optimize and manipulate. I once again confirmed the presence of both proteins in the crystals using SDS-PAGE and coomassie staining (Fig. 34B). After initial rounds of optimization these crystals diffracted to ~ 7.5 Å. Upon further optimization these crystals should diffract to a higher resolution and the structure of the complex can be determined using molecular replacement with the structures of the SD2 domain or the SBD.

4.4 CONCLUSIONS

I characterized the Shroom SD2-Rock SBD complex using a variety of biochemical assays. These biochemical assays suggest that molar ratio of the SD2-SBD complex is 1:1. Additionally, the results from SEC-MALS and chemical crosslinking suggest that the stoichiometry for the SD2-SBD complex is 2:2 but we have not ruled out higher order complexes. The 2:2 stoichiometric ratio of the complex would be in agreement with the results observed with the SD2 domain and the SBD.

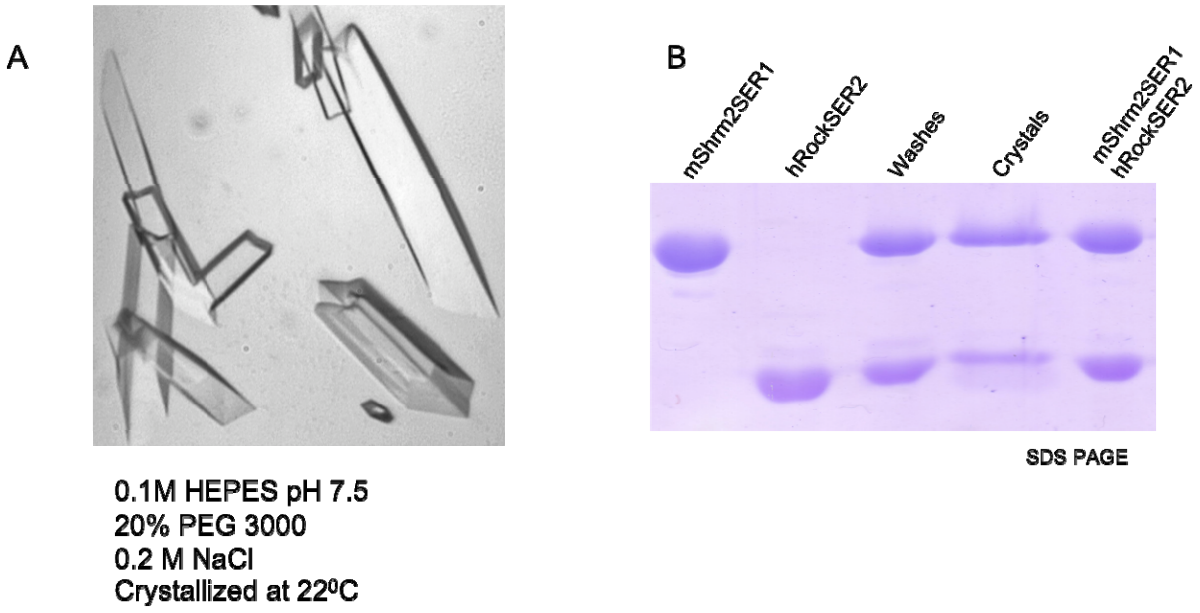

Figure 35: SER mutant mShroom2 SD2-hRock1 SBD crystals.

(A) Optimized SER mutant mShroom2 SD2-hRock1 SBD crystals. SER mutations significantly improved the quality of the complex crystals.

(B) Crystals were extensively washed, dissolved and visualized using SDS-PAGE and coomassie staining. These crystals contained both mShroom2 SD2 and hRock1 SBD SER mutant proteins.

5.0 DISCUSSION

I used structural and biochemical studies to gain insight into the mechanistic details of the Shroom-Rock interaction. First, I determined the structure of the Shroom SD2 domain. The crystal structure revealed that the SD2 domain is an anti-parallel coiled-coil dimer. The SD2 domain has a novel fold composed of two short arm segments that flank a longer central body segment. Using mutational analysis I identified two highly conserved patches in the central body segment that are important for Rock interaction and Shroom-mediated apical constriction. Due to the anti-parallel nature of the structure these two patches lie on opposite sides of the molecule. Through biochemical and cell based assays I also determined that dimerization is important for the Shroom-Rock interaction. These results suggest that the SD2 domain interacts with Rock as a dimer using residues in the central coiled-coil fragment.

The dShroom SD2 domain elutes off the size-exclusion column in two peaks, with the first peak accounting for the majority of the protein. The second peak consists of a smaller species and only accounts for approximately 9% of the protein. The protein from the first peak was used for the crystallographic and biochemical studies described above. The structure of the protein in the second peak has yet to be determined. This peak consists of a smaller species, possibly representing an SD2 monomer or an alternate conformation of the SD2 dimer that adopts a more compact fold. In an effort to differentiate between these two possibilities I designed mutations that cause localized disruptions to the dimerization interface. These

dimerization mutant proteins had unique elutions profiles that did not match wild-type peak 1 or peak 2. This made it difficult to interpret the exact effect of these mutations on the conformation of the SD2 domain. These results suggested that local perturbations at the dimerization interface disrupts the overall fold of the SD2 domain but does not necessarily shift the equilibrium towards the monomeric or smaller species. Further analysis of the protein in the second peak as well as the homodimerization mutant proteins is required. Techniques such as analytical ultracentrifugation or small-angle x-ray scattering could provide better insight into alternate conformations of the SD2 domain and the possible transition states between these conformations.

I next determined the structure of the Rock Shroom binding domain (SBD). To determine this structure I made surface entropy reduction (SER) mutations in hRock1 SBD. Ideally, the residues chosen for SER mutations would not be conserved. However, due to the high degree of conservation in the SBD one out of the three residues mutated for SER was highly conserved. This mutation, however, did not affect the ability of the SBD to bind the SD2 domain. The SER mutant diffraction data displayed diffraction anisotropy that lowered the quality of the data and hindered refinement of the model. To correct for diffraction anisotropy I used ellipsoidal truncation to remove poorly measured reflections from the dataset. This reduced the completeness of the data, however; removal of the poorly measured reflections improved data quality and model refinement.

The crystal structure revealed that the SBD is a parallel coiled-coil dimer. It is composed of a single coiled coil segment with canonical knobs into holes packing interactions at the coiled-coil interface. Mapping conserved residues to the surface of the SBD revealed that there is a large patch of highly conserved residues at the N-terminus of the structure. Once again I used mutational analysis to identify residues in the SBD that are important for Shroom interaction.

Detection of the SD2-SBD complex using the core hRock1 SBD construct used for crystallization (834-913) proved to be difficult as I was unable to detect a shift to the complex band via native PAGE. Since fluorescence anisotropy experiments with the core and the longer SBD (707-946) constructs indicate that they both bind to the SD2 domain with comparable affinity, the biochemical experiments described below were performed with a larger construct of hRock1 SBD. Biochemical assays with the hRock1 SBD mutants indicate that mutating the conserved residues at the N-terminus abolishes Shroom binding. There are also conserved residues at the C-terminus that when mutated cause a moderate defect in Shroom binding. These results indicate that there are two conserved surfaces in the SBD, one at the N-terminus and one at the C-terminus that are important for the Shroom-Rock interaction. Also, the conserved patch at the N-terminus plays a more significant role in Shroom binding than the conserved patch at the C-terminus.

Lastly I characterized the SD2-SBD complex using a variety of biochemical assays. Using FRET we determined the K_d of the SD2-SBD complex to be 0.58 μM. This affinity is comparable to that of RhoA, which has a reported K_d of 0.13 mM [131]. We believe the molar ratio of the SD2-SBD complex to be 1:1; however, it is still unclear if that corresponds to a heterodimer or a heterotetramer. Chemical crosslinking and mass spectrometry experiments were unable to provide us with a clear answer as to whether the composition of the complex is a heterodimer or a heterotertramer. With both of these techniques we were unable to identify a single species of the complex. Additionally, I performed a single SEC-MALS experiment with the dShroom-dRock complex to determine the molecular weight of the complex. The results from this experiment suggested a trimeric complex, which is not in agreement the results observed with crosslinking or mass spectrometry. The SEC-MALS experiment was only

performed on the dShroomSD2-dRock SBD complex without the inclusion of proper controls such as determining the profile of the individual proteins. Additionally, the dRock SBD construct used for this experiment was a longer construct that was prone to degradation. Repeating the experiment with the proper controls and a complex composed of core dRock SBD that is stable should give us a more reliable answer towards the molecular composition of the complex.

Results from structural, biochemical, and cell-based studies indicate that there are two binding surfaces in the SD2 domain and the SBD, with clear differences in the binding surfaces. In the SD2 domain the residues that make up the two binding surfaces are identical and come from both chains. Due to the anti-parallel nature of the SD2 domain, the two patches lay on opposite sides of the molecule. In the SBD dimer, however, each monomer contains one binding patch at the N-terminus and one at the C-terminus that are not identical. Due to the placement of these binding surfaces in the SD2 and SBD domains it is difficult to imagine a model where they interact without either protein going through a conformational change. If this were to happen then the identical binding surfaces in Shroom would be interacting with different binding surfaces in Rock (Fig. 36A). Instead we propose models where the Shroom-Rock interaction causes a conformational change in one or both domains.

It is possible that the Rock binding patches identified in the Shroom SD2 domain only interact with one of the two identified Shroom binding patches in the Rock SBD. Since, mutation of the N-terminal patch in the Rock SBD showed a great defect in Shroom binding than the C-terminal patch it is likely that Shroom binds to these residues in Rock. In this scenario, the Shroom SD2 domain would still have to go through a conformational change such that both of the Rock binding patches are on the same side. The Shroom SD2 domain could bend at the symmetry point and position the two binding patches on either side of the Rock SBD at the N-

terminus (Fig. 36B). This model leaves open the possibility that there might be additional Rock binding sites on the Shroom SD2 domain that need to be identified.

Other possible models could involve the unraveling of either the SD2 or the SBD coiled-coil dimers upon complex formation. If the Rock SBD coiled-coil dimer splits apart then each monomer could associate with the Shroom SD2 dimer on opposite sides in a manner where they are in an anti-parallel orientation with respect to each other. Most of the structural and biochemical data available for the other domains suggest that Rock is a parallel dimer and does not change to an anti-parallel dimer. Therefore, it is somewhat unlikely that the Rock SBD dimer will split apart to bind Shroom on opposite sides, however; this drastic conformational change in the Rock SBD could trigger the activation of the kinase domain. Instead of the Rock SBD, the Shroom SD2 domain could also unravel and bind Rock as two monomers. The Shroom SD2 dimer has a large protein interface and disrupting this interface could be highly unfavorable, however; binding to Rock could counteract this unfavorable conformational change. Alternatively, the two Shroom SD2 monomers could bend at the symmetry point to take on a conformation similar to the SD2 half dimer and then bind to Rock.

Further experiments that address the possibility of conformational change in both molecules are required. To this end structures of SD domains from vertebrate Shroom proteins might reveal alternate conformations of this domain. Additionally, determining the structure of the complex will provide us with a more definitive answer of how these two domains interact. We currently only have crystals from a mixed species complex (human Rock-mouse Shroom). Even though human Rock and mouse Rock share 96% sequence identity a complex of proteins from the same species would be more ideal.

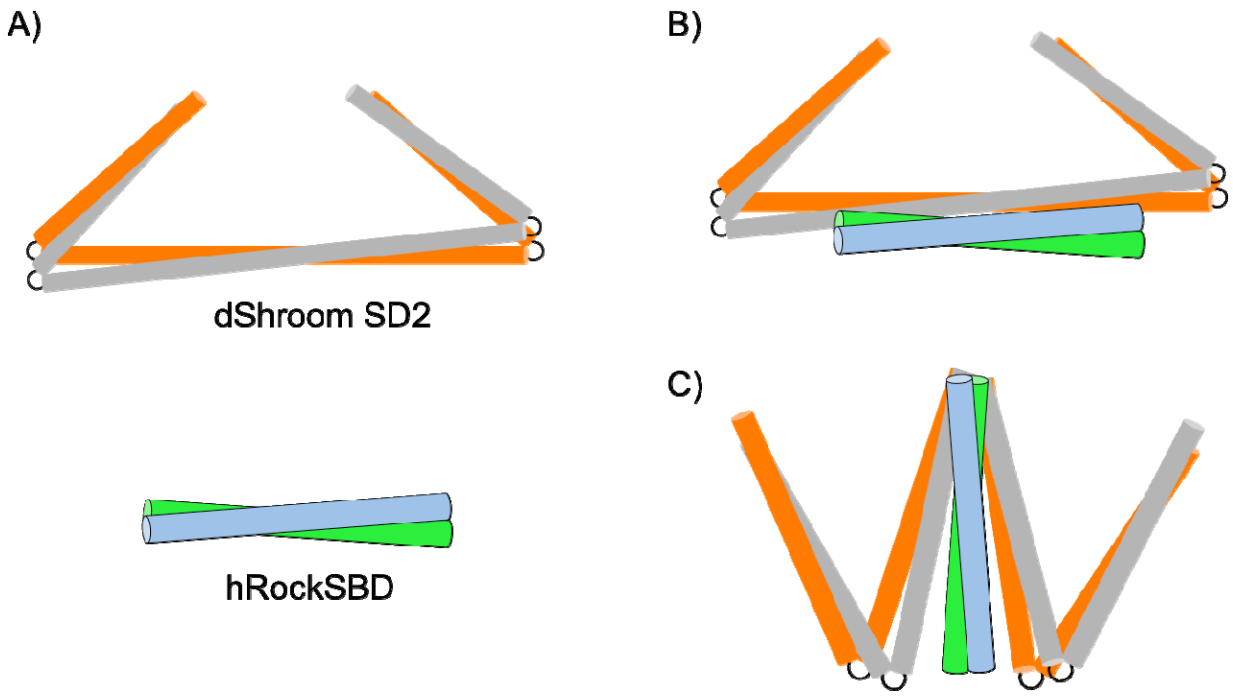

Figure 36: SD2-SBD interaction Models.

Possible models for how the Shroom SD2 domain and Rock SBD interact. The dShroom SD2 dimer is shown in orange and gray and the hRock1 SBD dimer is shown in blue and green. A) Cartoon illustrations of dShroom SD2 domain and hRock SBD. B) Model of the Shroom SD2-Rock SBD complex where neither domain goes through any conformational changes. C) Model of the Shroom SD2-Rock SBD complex where the SD2 domain goes through a conformational change and interacts with the N-terminal region of Rock SBD.

6.0 MATERIALS AND METHODS

6.1 PROTEIN EXPRESSION AND PURIFICATION

Coding sequences for all the Shroom SD2 domain constructs and all Rock SBD constructs were amplified by PCR and cloned into the bacterial expression vector pET151-D/Topo (Invitrogen). Protein expression was performed in codon plus BL21(DE3) *E.coli* cells using ZY autoinduction media at room temperature for ~24 hours, harvested by centrifugation, and lysed via homogenization in 25 mM Tris pH8.0, 500 mM NaCl, 10% glycerol, 5 mM Imidazole, 5 mM beta-mercaptoethanol [111]. The lysate was cleared by centrifugation at 100,000 x *g*.

All of the wild-type and mutant dShroom SD2 proteins were purified by nickel affinity chromatography (Qiagen), followed by overnight digestion with TEV protease, a second round of nickel affinity purification was performed to remove the liberated His-tag, TEV protease, and many non-specific contaminants. Gel filtration, using a Sephacryl S-200 gel filtration column (GE Healthcare) was performed and peak fractions were pooled and concentrated. Wild-type dShroom SD2 was concentrated to 9 mg/ml in 20 mM Tris pH 8.0, 0.5 M NaCl, 8% Glycerol and 5 mM dithiothreitol (DTT) using a Vivaspin concentrator (Millipore) prior to crystallization. The purity was typically >99% as verified by SDS-PAGE.

Purification of wild-type and mutant mouse Shroom SD2, dRock SBD (724-938) and willd-type and mutant human Rock SBD (834-913) was aided by the addition of an anion

exchange chromatography step prior to gel filtration. After gel filtration peak fractions of mShroom2 SD2 and hRock SBD were pooled and dialyzed into buffers more compatible for crystallization. Wild-type and mutant mShroom2 SD2 were concentrated to 16 mg/ml prior to crystallization. Wild-type and mutant hRock SBD were concentrated to 14 mg/ml prior to crystallization. Selenomethionine substituted dShroom SD2 and mutant hRock SBD were expressed using PASM media, and purification was essentially the same as the native protein [111].

6.2 MUTANT MOUSE SHROOM3, DROSOPHILA SHROOM SD2, AND HUMAN ROCK SBD PROTEINS

SC and HD mutations in mShrm3 and dShrm, were made using the QuikChange Site-Directed Mutagenesis kit (Stratagene). The surface entropy reduction mutations in mShroom2 SD2 and all of the mutations in hRock SBD (707-946, and 834-913) were also made using the QuikChange Site-Directed Mutagenesis kit (Stratagene). All biochemical assays with wild-type, SC and HD proteins were performed with the indicated protein fractions from gel filtration. For mShroom3 mutants, mutagenesis was performed on mShrm3 in the pCS2-Endolyn-Shrm3 expression plasmid. For in vitro expression of mShrm3 SD2 mutant proteins, the mutated sequence encoding amino acids 1562-1986 were cloned from the Endolyn-Shrm3 vectors in pGex-2TK for expression in *E.coli* Codon+ (RIPL) cells. Recombinant proteins were expressed and purified as described [7].

6.3 CRYSTALLIZATION OF DROSOPHILA SHROOM SD2 DOMAIN

Single, thick rod shaped crystals were obtained for dShrm SD2 via the vapor diffusion method with a reservoir solution containing 0.1 M MES at pH 6.0, 1.35 M K/Na tartrate, 0.7 M sodium thiocynate, 11% glycerol (v/v) and 4 mM DTT. Crystals grew at 4°C in 7-10 days with a typical size of 80 x 40 x 500 μm, and were cryoprotected by transition of the crystal into a buffer containing 0.1 M MES, 1.4 M K/Na tartrate, 0.9 M sodium thiocynate, 15% glycerol and 4 mM DTT. The cryoprotected crystals were flash frozen under liquid nitrogen prior to data collection. The same procedure was used to crystallize and cryoprotect selenomethionine (SeMET) substituted SD2.

6.4 CRYSTALLIZATION OF HUMAN ROCK SBD

Initial plate clusters of crystals formed at room temperature in buffers containing 20% PEG-8000, 0.2M Calcium Acetate, and 0.1M 2-(N-morpholino)ethanesulfonic acid pH 6.0 or, 5% PEG-3000, 30% PEG-200 and 2-(N-morpholino)ethanesulfonic acid pH 6.0, or 30% 2-Methyl-2,4-pentanediol, 0.1M Sodium Acetate pH 4.6, and 0.2 M $CaCl_2$ or, 20% 2-Methyl-2,4-pentanediol and 0.1M 2-(N-morpholino)ethanesulfonic acid pH 5.0. Upon optimization single plate like crystals with a typical size of 400 x 300 x 10 μm were obtained for hRock SBD at 22°C with a reservoir solution containing 5% PEG-3000, 30% PEG 200, 0.1 M MES pH 6.0, 2mM DTT, 0.7% butanol. Crystals were cryoprotected by transition into a cryoprotectant buffer containing 7% PEG-3000, 35% PEG 200, 0.1 M MES pH 6.0, 200mM NaCl, 2mM DTT and 20% glycerol and flash frozen under liquid nitrogen prior to data collection.

Single bipyramidal crystals with a typical size of 300 x 80 x 40 μm were obtained for hRock SBD SER2 via streak seeding at 4°C with a reservoir solution containing 0.1 M Citrate pH 6.0, and 1.0 M ammonium sulfate. Crystals were cryoprotected by transition into a buffer containing 0.1 M citrate pH 6.0, 2.5 M ammonium sulfate, 0.15 M NaCl, and 20% glycerol and flash frozen under liquid nitrogen prior to data collection. The same procedure was used to crystallize and cryoprotect selenomethionine (SeMET) substituted hRock SBD SER2.

6.5 SINGLE WAVELENGTH ANOMALOUS DISPERSION

Without any know structural homologs to guide structural determination, I used single-wavelength anomalous dispersion to calculate phases and obtain an electron density map. Certain elements such as selenium have anomalous scattering patterns at certain wavelengths that can be used calculate the phases for the selenium atoms. Upon calculating the phases for the selenium atoms, phases for the rest of the atoms in the crystals can be estimated. For this purpose I purified and crystallized selenomethionine substituted proteins. This was done by simply growing up cells expressing the SD2 or SBD construct that crystallize in PASM media [111]. The addition of selenomethionine did not alter the crystallization conditions therefore the selenomethione substituted crystals were optimized using the same conditions as the native crystals. Data on the selenomethionine crystals were collected at the synchrotron using x-rays tuned to the selenium anomalous peak wavelength.

6.6 STRUCTURE DETERMINATION OF DSHROOM SD2 DOMAIN

SD2 crystals belong to space group $P2_12_12$ with a = 72.6 Å, b = 85.6 Å, c = 93.0 Å. Diffraction data from both native and SeMET dShrm SD2 crystals were collected at beamline X25 at the National Synchrotron Light Source. Diffraction data integration, scaling, and merging were performed using HKL2000 [125]. Initial phases were estimated via the SAD method using SHELX C/D/E [115] which found 6 of the possible 8 selenium sites. An initial model was built into these experimental maps using Coot [114]. This model was then further refined against native data and the model improved using a combination of simulated annealing, as well as positional, B-factor refinement, and TLS refinement [132] within Phenix [133]. Model quality was monitored using MolProbity [117]. All structural images in this paper were generated using PyMol (W. Delano; http://). The coordinates and structure factors for the Drosophila SD2 domain structure presented in this publication have been submitted to the PDB (www.rcsb.org) and assigned the identifier 3THF.

6.7 STRUCTURE DETERMINATION OF HROCK SBD

SBD crystals belong to space group C2 with a = 142.4 Å, b = 56.2 Å, c = 80.7 Å and $\alpha = \gamma = 90°$ and $\beta = 119.2°$. Analysis of the native dataset using the diffraction anisotropy server [127] indicated that it was severely anisotropic diffracting to 2.5 Å in the a and c direction but only 3.1 Å in the b direction. Diffraction data from both native and SeMET hRock SBD SER mutant crystals were collected at beamline X25 at the National Synchrotron Light Source. Diffraction data integration, scaling, and merging were performed using HKL2000 [125]. Initial

phases were estimated via the SAD method at 4.0 Å using SHELX C/D/E which found all four possible selenium sites [115]. An initial model was built into these experimental maps using Coot [114]. The native dateset was subjected to ellipsoidal truncation using the diffraction anisotropy sever and 1231 reflections were rejected. The model was refined against this truncated native data and the model improved using a combination of simulated annealing, as well as positional, B-factor refinement, and rigid body refinement [132] within Phenix [133]. Model quality was monitored using MolProbity [117].

6.8 CHEMICAL CROSSLINKING

For all crosslinking reactions the purified proteins were incubated with the indicated concentration of glutaraldehyde in a reaction buffer containing 25 mM HEPES pH 7.5, 8% Glycerol, 500 mM NaCl and 5 mM β-ME, with a final protein concentration of 8 μM. For the SD2-SBD complex crosslinking reactions the individual proteins were mixed at equimolar ratios and incubated at room temperature for 20 minutes prior to adding the crosslinker. At each time point, 20μl of the crosslinking reaction was removed and the reaction stopped with 2 μl of 1.0 M Tris at pH 8.0 and the sample subjected to SDS-PAGE and visualized using Coomassie blue staining.

6.9 APICAL CONSTRICTION ASSAYS

These assays were performed by Ryan Rizaldy and Debamitra Das from the Hildebrand lab. MDCK cells were grown in EMEM supplemented with 10% FBS, pen/strep, and L-Glutamine. Apical constriction assays using Endolyn-dShrm, Endo-Shrm3, Endo-mShrm3 dlSD2, or Endo-Shrm3 harboring SC or HD were performed and imaged as described [4]. Cells were attained with the following antibodies: UPT132 (1:250, rabbit anti-Shrm3, [4]), Rat anti-ZO1 (1:500, Chemicon), Rabbit anti-pThr18/pSer19 MLC2 (1:50, Cell Signaling). Primary antibodies were detected using Alexa-488 or 568 conjugated secondary antibodies (1:400, Invitrogen). Images were acquired using a Biorad Radiance 2000 Laser Scanning System mounted on a Nikon E800 microscope with 40 and 60X oil objectives and processed using either ImageJ or Photoshop. The fluorescent intensity of ppMLC was determined using ImageJ and was achieved by measuring the average fluorescent intensity of a fixed ROI at the apical surface of sub-saturated confocal images from expressing and non-expressing cells. Fluorescent intensity of the ROI was then corrected for the decrease in area of apically constricted cells (n = at least 20 cells/variant). Change in fluorescent intensity was then determined as the ratio of the corrected intensity of constricted versus non-constricted cells.

6.10 LIMITED PROTEOLYSIS

Approximately 20µg of wild-type or mutant dShroom SD2 proteins were incubated with 13ng of the protease Subtilisin A in a reaction buffer with 8% glycerol, 500mM NaCl, Tris pH 8.0 and 5mM βME. At each time point 20 µl of the proteolysis reaction was stopped

with 2µl PMSF and the proteolyzed product was subjected to SDS-PAGE and visualized using coomassie blue staining.

6.11 COMPLEX FORMATION

For native gel electrophoresis with *Drosophila* proteins, a fixed concentration (5 µM) of dRock 724-938 was mixed with increasing concentration of dShrmSD2 (1-10 µM) and incubated for 1 hour. Samples were then loaded on 8% PAGE gels and resolved by electrophoresis at 4^{O} C. For native gel electrophoresis with human proteins, a fixed concentration (10 µM) of wild-type oro mutant hRock 707-946 was mixed with a fixed conentration of hShroomSD2 (10 µM). Samples were then loaded on 12% PAGE gels and resolved by electrophoresis at 4^{O} C. Proteins were detected with Coomassie blue. For GST pull-down assays using mShrm3, either wild type GST-Shrm3 SD2 or SC and HD mutant versions (spanning amino acids 1562-1986) bound to beads were mixed with soluble, untagged mShrm3 SD2 (residues 1762-1952) or hRock1 (residues 707-948). Complexes were washed with NETN, resuspended in SDS-PAGE sample buffer, resolved by SDS-PAGE, and detected using Coomassie Blue.

6.12 FLUORESCENT LABELING OF HUMAN SHROOM2 SD2

hShroom2 SD2 was labeled at the N-terminus with Oregon Green 488 Succinimidyl ester (Invitrogen) in amino labeling buffer (20 mM Hepes pH 7.4, 100 mM NaCl, 5% Glycerol).

Labeling reactions included 10× molar excess of fluorophore at room temperature for 2 h. Excess fluorophore was removed from the samples through extensive dialysis with labeling buffer. The labeling efficiency was quantified using the extinction coefficient of the dye compared with the protein concentration determined from a standard curve using a Bradford assay and found to be essentially 1:1.

6.13 FLUORESCENCE ANISOTROPY BINDING EXPERIMENTS

These experiments were performed by Robert Bauer in the Trakselis lab in the Chemistry Department at the Univeristy of Pittsburgh. Fluorescence anisotropy measurements were performed in hShroom reaction buffer (20 mM Hepes pH 7.4, 100 mM NaCl, 5% Glycerol) using 20 nM of N-terminally labeled hShroom-Oregon Green 488 and increasing concentrations of hRock. Measurements were collected as described previously using a Floromax-3 fluorimeter (Horiba Jobin Yvon) [134]. Labeled proteins were excited at 496 nm and emission was monitored at 524 nm using 5-second integration times for three consecutive readings. The reported values are the average of at least three independent experiments and fit by a non-linear least squares analysis using Kaleidagraph (Synergy, Reading, PA) to a single binding model:

$d+[\mathrm{P}]$ (1)

where A is the amplitude, K_d is the dissociation constant and [P] is the concentration of the titrated protein.

6.14 FLUORESCENT LABELING

These experiments were performed by Robert Bauer in the Trakselis lab in the Chemistry Department at the Univeristy of Pittsburgh. dShroom was labeled at the N-terminus with Alexa 594 succinimidyl ester (Invitrogen), in amino labeling buffer (20 mM Hepes pH 7.0, 100 mM NaCl, 8% Glycerol), or at C1428 of the C1533S mutant with Cy3 or Cy5 maleimide (GE Healthcare) in cysteine labeling buffer (20 mM HEPES pH 7.6, 100 mM NaCl, 8% Glycerol). Small (821-938) dRock was labeled at C862 with Cy3 maleimide as above. Large dRock (724-938) was labeled at the N-terminus with Cy5 succinimidyl ester (GE Healthsciences) in amino labeling buffer. All labeling reactions included 10X molar excess of fluorophore, at room temperature for two hours. Excess fluorophore was removed from the samples through extensive dialysis with labeling buffer. The labeling efficiency was quantified using the extinction coefficient of the dye compared to the protein concentration determined from a standard curve using a Bradford assay and found to be essentially 1:1.

6.15 FLUORESCENCE RESONANCE ENERGY TRANSFER (FRET) BINDING EXPERIMENTS

These experiments were performed by Robert Bauer in the Trakselis lab in the Chemistry Department at the Univeristy of Pittsburgh. FRET titrations were performed in dShrm reaction buffer, using a 50 nM of Cy3-labeled dShrm or dRok and increasing concentrations of Cy5-labelled dRok or dShrm. Cy3 was excited at 552 nM and the donor emission maxima (563 nM) was corrected for dilution, normalized, and plotted as a function of protein concentration as the

average of three independent experiments. Fluorescence quenching (F_Q) titrations were fit to a single binding equation:

$$F_Q = \frac{\Delta F_Q \times [dRock]}{K_D + [dRock]} \qquad (2)$$

where ΔF_Q is the normalized change in donor fluorescence intensity and K_D is the dissociation constant.

6.16 MULTIANGLE LIGHT SCATTERING AND ELECTROSPRAY MASS SPECTROMETRY

Purified dShroom SD2 and dRock SBD (724-938) were mixed at equimolar ratios and subjected to size exclusion chromatography. Fractions from gel filtration that contained both proteins in equal amounts were pooled and concentrated to 40μM. Prior to ES-MS the concentrated complex was dialyzed into buffer containing 100mM ammonium acetate and 20mM Tris pH 7.0. ES-MS was performed using the Q-TOF-2 instrument in Mark Bier's lab at Carnegie Mellon University. The complex was subjected to a C4 gel filtration column prior to ionization. The size exclusion chromatography multiangle light scattering experiments were carried out in the Gronenborn laboratory in the Department of Structural Biology at the University of Pittsburgh.

6.17 ISOLATION OF COMPLEX CRYSTALS

Wild-type and mutant mShroom2 SD2-hRock1 SBD crystals were washed with the well solution multiple times to remove any uncrystallized protein. The washed crystals in well solution were

transferred to an eppendorf tube and dissolved using SDS-PAGE loading dye and visualzed using SDS-PAGE and coomassie staining.

APPENDIX A

STRUCTURAL CHARACTERIZATION OF THE CAC1 SUBUNIT OF CHROMATIN ASSOCIATION FACTOR 1

A.1 INTRODUCTION

In eukaryotic cells, DNA is wrapped around histones into nucleosomes to form a highly condensed but dynamic structure known as chromatin. Nucleosomes consist of approximately 147bp of DNA wrapped around an octamer of histone proteins (two copies each of histones H2A, H2B, H3 and H4) that help condense DNA Nucleosomes are compacted to form higher order structures via interactions with proteins such as linker histones [135]. These higher order chromatin structures play a key role in stably packaging large amounts of genetic material into the relatively small nucleus. This compact organization however greatly limits accessibility of the DNA to other proteins. Even a single nucleosome is a significant barrier for all DNA templated processes, including transcription, DNA repair, and recombination [136, 137]. To overcome this barrier all these processes require the assistance of a host of other factors such as histone chaperones. These regulate chromatin structure by directly binding to histones and mediating nucleosome assembly and transport [138]. Histone chaperones can function as

monomers or as part of multisubunit complexes and can bind histone octamers, the H3/H4 tetramer or the H2A/H2B tetramer [139].

The most striking example of chromatin rearrangement occurs during replication, which causes global disruption of chromatin to allow the passage of replication machinery [137]. During replication the cell needs access to all its genetic material to not only replicate its genome but also to faithfully convert both genomes into an organized chromatin structure that is suitable for the biology of that organism [137]. After the progression of the replication fork, nucleosomes are assembled onto both replicated strands of DNA by histone chaperones. This nucleosome assembly occurs in a step-wise fashion where a histone chaperone first deposits histone H3/H4 dimers onto DNA, then a different chaperone adds histones H2A/H2B to complete the nucleosome [140]. The histone chaperone responsible for carrying out the first step in nucleosome assembly during replication is a three protein complex conserved from yeast to humans, known as chromatin assembly factor 1 (CAF) [140-142].

CAF was identified from HeLa nuclear extracts in an assay looking for factors that had chromatin assembly activity coupled to DNA replication [143]. The identified complex could assemble correctly spaced nucleosomes preferentially on DNA undergoing replication [143]. The CAF complex is made up of three proteins Cac1, Cac2, and Cac3 (Msi1) in yeast (p150, p60, p48 respectively in humans [144]). Cac1 is the largest subunit of the complex and plays a scaffolding role where Cac2 and Cac3 both bind Cac1 to form the CAF complex [145]. Cac2 and Cac3 are both WD-40 domain containing proteins that are homologous over the entire length of the WD-40 repeats [145]. Cac3 is a member of a large group of proteins (p48 family) that is also part of other chromatin modifying complexes such as Nucleosome Remodeling Factor (NURF) and Nucleosome Remodeling and Deacetylase (NuRD) [145, 146]. Of the three

subunits, Cac1 is most the elusive, as it has no recognized domains. The chromatin assembly activity of CAF is stimulated Asf1, a monomeric chaperone for histones H3 and H4. In yeast, Asf1 along with newly synthesized H3 and H4 forms a complex called RCAF (Replication Coupling Assembly Factor) [147]. RCAF promotes the chromatin assembly activity of CAF by a direct interaction, conserved from yeast to humans, between Asf1 and Cac2 [147-149].

In humans, nucleosome assembly by the CAF complex is required for progression through S-phase [150], and knockdown of CAF induces programmed cell death in proliferating cells [151]. In yeast, deletion of CAF is not lethal but does cause severe growth defects and loss of silencing at telomeres and mating loci [145]. CAF has been shown to localize to replication foci during S phase and to interact specifically with newly synthesized histones H3/H4 [152] [153]. CAF mediates its preference for newly synthesized histones by an interaction between Cac1 and histone H3 acetylated at lysine 36, a post-translational modification associated with newly synthesized histones [154]. CAF is not known to bind to DNA [143], instead, through a conserved interaction between Cac1 and PCNA, the replication processivity factor, CAF is recruited to replication foci [155-157]. Yeast Cac1 contains a PCNA binding motif (residues 227 and 234) and mutating this motif abolishes PCNA binding and the preference of CAF for newly replicated DNA [158]. The CAF complex is involved not only in chromatin assembly during DNA replication, but also in DNA repair pathways [145, 159-162], where CAF is recruited to damaged DNA via the interactions with PCNA and/or RecQ helicases [155, 163, 164]. CAF is also implicated to be important for heterochromatin formation at silenced regions of the genome [165]. In yeast and humans CAF interacts with proteins such as Sir1, Sas2 and HP1 that are involved in heterochromatin formation and epigenetic inheritance [166-170]. These interactions result in global changes in chromatin but their specific role nucleosome assembly is still

unknown [165, 171, 172]. The Cac1 subuint mediates all of these interactions, thus making it a central player in coordinating various functions of CAF.

In spite of the wealth of information provided by genetic and biochemical studies on the various interactions with CAF very little is known about mechanism underlying CAF function. Since Cac1 is the central player mediating CAF interactions, determining the structure of Cac1 will allow us to coordinate this wealth of existing data, generating testable models for nucleosome assembly that will be the first step towards a long-term goal of elucidating the mechanism of CAF function.

A.2 RESULTS

Numerous binding partners of Cac1 have been identified such as PCNA[158] Cac2, Cac3, histone H3, Sir1, Sgs1 Sas2 [151, 154, 158, 170], however the precise binding sites for most of these proteins have not been determined. The binding sites for Cac2 and Cac3 have been mapped to the C-terminal region of Cac1 specifically, between residues 215 and 429 for Cac3 and Cac2 [141] [158]. Yeast Cac1 (yCac1) was identified as RLF2 (Rap1p localization factor-2) and contains the highly charged KER and ED regions but is missing the N-terminus PEST box that is found in the human homolog p150 [145] (Fig 2). Previous studies have shown that the KER and ED regions are required for nucleosome assembly activity but the PEST box is not [141]. Previous studies in the VanDemark lab have shown that full-length yCac1, by itself or in a co-expression system with Cac2 and Cac3, is not expressed in detectable levels from bacteria so we chose to go after protein fragments instead (A. VanDemark, unpublished).

We analyzed Cac1 primary sequence using the web-based algorithms, PSIPRED and DISOPRED to predict likely secondary structure elements and regions of disorder [173, 174] [175]. Both algorithms predict that Cac1 has distinct structured and unstructured regions, however the DISOPRED analysis is surprisingly different from the PSIPRED analysis (Fig 3). There is no functional data to support either prediction so we have a number of options to choose from when designing Cac1 expression constructs. Initially I chose to use domain predictions from PSIPRED to guide designing our constructs for expression. In spite of the overall discrepancy, both algorithms predicted that the KER region of Cac1 is mostly likely unstructured.

PSIPRED analysis predicts secondary structure in three distinct regions of Cac1 (residues 1-125, 220-389, 418-606, 220-606) that we will call D1, D2, D3, NΔ220 respectively (Fig 3). All Cac1 fragments were cloned into the pET151-DTopo vector and transformed into codon(+) *E.coli*. Protein expression was induced via the autoinduction technique [111]. While Cac1D1 has only modest expression in bacteria, Cac1D2 and Cac1NΔ220 are well expressed but largely insoluble. Cac1D3 however was well expressed and very soluble (Fig. 35A). Limited proteolysis assays indicate that this Cac1 fragment is stable and therefore is an ideal candidate for crystallography (Fig. 35B). Cac1D3 was purified using a combination nickel affinity, and gel filtration chromatography. Peak fractions from the size exclusion column were pooled and concentrated to 9mg/ml and used for crystallization trials. Unfortunately, this Cac1 fragment did not yield any crystals. Additional constructs can be designed based on DISOPRED analysis that might prove to be more prone to crystallization.

In spite of its various advantages, the bacterial expression system lacks the cellular machinery that is sometimes required to fold and/or modify eukaryotic proteins. Eukaryotic

proteins expressed in bacteria requiring post-translational modifications and/or chaperone assisted folding can misfold and form insoluble aggregates. Expression of eukaryotic proteins particularly misfolded protein can also result in degradation. To overcome the problems with expression and solubility seen with the Cac1 fragments, I choose to try to purify them using a yeast expression system. The yCac1 fragments described above were cloned into the galactose inducible yeast expression vector pTF197, which adds a 12x his-tag to the N-terminus of the protein that can be used to detect protein expression via Western blotting. Preliminary expression tests indicate that all of the Cac1 fragments express very poorly in yeast. Other eukaryotic protein expression systems such as the bacculovirus expression system might aid in expression and purification of Cac1 fragments. In fact structures of the smallest CAF subunit Cac3 has been determined with protein expressed from a bacculovirus expression system [146].

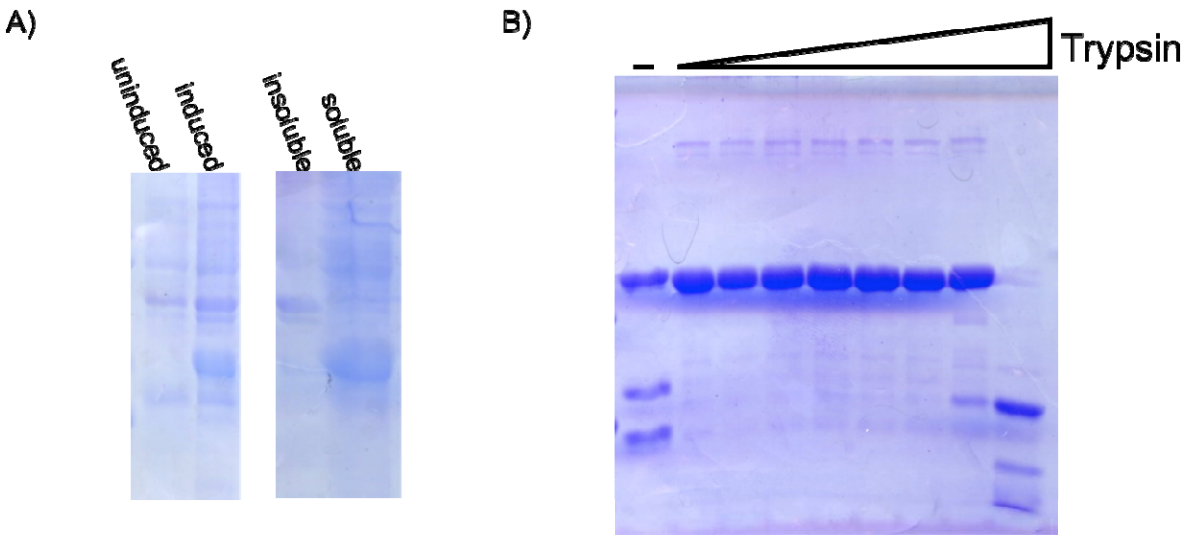

Figure 37: Cac1D3 expression and limited proteolysis.

(A) Expression and solubility of Cac1D3 after cell lysis was assayed via SDS-PAGE.

(B) Limited proteolysis of Cac1D3. Purified protein was incubated with increasing amounts of trypsin (0.004% - 0.5%) for 20min . The digested fragments were visualized using SDS-PAGE.

BIBLIOGRAPHY

1. Amano, M., et al., Phosphorylation and activation of myosin by Rho-associated kinase (Rho-kinase). J Biol Chem, 1996. **271**(34): p. 20246-9.

2. Nishimura, T. and M. Takeichi, Shroom3-mediated recruitment of Rho kinases to the apical cell junctions regulates epithelial and neuroepithelial planar remodeling. Development, 2008. **135**(8): p. 1493-502.

3. Hildebrand, J.D. and P. Soriano, Shroom, a PDZ domain-containing actin-binding protein, is required for neural tube morphogenesis in mice. Cell, 1999. **99**(5): p. 485-97.

4. Hildebrand, J.D., Shroom regulates epithelial cell shape via the apical positioning of an actomyosin network. J Cell Sci, 2005. **118**(Pt 22): p. 5191-203.

5. Plageman, T.F., Jr., et al., Pax6-dependent Shroom3 expression regulates apical constriction during lens placode invagination. Development. **137**(3): p. 405-15.

6. Fairbank, P.D., et al., Shroom2 (APXL) regulates melanosome biogenesis and localization in the retinal pigment epithelium. Development, 2006. **133**(20): p. 4109-18.

7. Farber, M.J., R. Rizaldy, and J.D. Hildebrand, Shroom2 regulates contractility to control endothelial morphogenesis. Mol Biol Cell. **22**(6): p. 795-805.

8. Quintin, S., C. Gally, and M. Labouesse, Epithelial morphogenesis in embryos: asymmetries, motors and brakes. Trends Genet, 2008. **24**(5): p. 221-30.

9. Lee, J.Y. and R.M. Harland, Actomyosin contractility and microtubules drive apical constriction in Xenopus bottle cells. Dev Biol, 2007. **311**(1): p. 40-52.

10. Kimberly, E.L. and J. Hardin, Bottle cells are required for the initiation of primary invagination in the sea urchin embryo. Dev Biol, 1998. **204**(1): p. 235-50.

11. Hardin, J. and R. Keller, The behaviour and function of bottle cells during gastrulation of Xenopus laevis. Development, 1988. **103**(1): p. 211-30.

12. Lee, J.Y. and B. Goldstein, Mechanisms of cell positioning during C. elegans gastrulation. Development, 2003. **130**(2): p. 307-20.

13. Solon, J., et al., Pulsed forces timed by a ratchet-like mechanism drive directed tissue movement during dorsal closure. Cell, 2009. **137**(7): p. 1331-42.

14. Costa, M., E.T. Wilson, and E. Wieschaus, A putative cell signal encoded by the folded gastrulation gene coordinates cell shape changes during Drosophila gastrulation. Cell, 1994. **76**(6): p. 1075-89.

15. Leptin, M. and B. Grunewald, Cell shape changes during gastrulation in Drosophila. Development, 1990. **110**(1): p. 73-84.

16. Sweeton, D., et al., Gastrulation in Drosophila: the formation of the ventral furrow and posterior midgut invaginations. Development, 1991. **112**(3): p. 775-89.

17. Tomlinson, A., The cellular dynamics of pattern formation in the eye of Drosophila. J Embryol Exp Morphol, 1985. **89**: p. 313-31.

18. Bush, K.T., et al., Neural tube formation in the mouse: a morphometric and computerized three-dimensional reconstruction study of the relationship between apical constriction of neuroepithelial cells and the shape of the neuroepithelium. Anat Embryol (Berl), 1990. **181**(1): p. 49-58.

19. Karfunkel, P., The mechanisms of neural tube formation. Int Rev Cytol, 1974. **38**(0): p. 245-71.

20. Schoenwolf, G.C. and J.L. Smith, Mechanisms of neurulation: traditional viewpoint and recent advances. Development, 1990. **109**(2): p. 243-70.

21. Brodu, V. and J. Casanova, The RhoGAP crossveinless-c links trachealess and EGFR signaling to cell shape remodeling in Drosophila tracheal invagination. Genes Dev, 2006. **20**(13): p. 1817-28.

22. Barrett, K., M. Leptin, and J. Settleman, The Rho GTPase and a putative RhoGEF mediate a signaling pathway for the cell shape changes in Drosophila gastrulation. Cell, 1997. **91**(7): p. 905-15.

23. Homem, C.C. and M. Peifer, Diaphanous regulates myosin and adherens junctions to control cell contractility and protrusive behavior during morphogenesis. Development, 2008. **135**(6): p. 1005-18.

24. Beane, W.S., J.M. Gross, and D.R. McClay, RhoA regulates initiation of invagination, but not convergent extension, during sea urchin gastrulation. Dev Biol, 2006. **292**(1): p. 213-25.

25. Kolsch, V., et al., Control of Drosophila gastrulation by apical localization of adherens junctions and RhoGEF2. Science, 2007. **315**(5810): p. 384-6.

26. Corrigall, D., et al., Hedgehog signaling is a principal inducer of Myosin-II-driven cell ingression in Drosophila epithelia. Dev Cell, 2007. **13**(5): p. 730-42.

27. Escudero, L.M., M. Bischoff, and M. Freeman, Myosin II regulates complex cellular arrangement and epithelial architecture in Drosophila. Dev Cell, 2007. **13**(5): p. 717-29.

28. Xu, N., B. Keung, and M.M. Myat, Rho GTPase controls invagination and cohesive migration of the Drosophila salivary gland through Crumbs and Rho-kinase. Dev Biol, 2008. **321**(1): p. 88-100.

29. Karfunkel, P., The role of microtubules and microfilaments in neurulation in Xenopus. Dev Biol, 1971. **25**(1): p. 30-56.

30. Haigo, S.L., et al., Shroom induces apical constriction and is required for hingepoint formation during neural tube closure. Curr Biol, 2003. **13**(24): p. 2125-37.

31. Plageman, T.F., Jr., et al., Shroom3 and a Pitx2-N-cadherin pathway function cooperatively to generate asymmetric cell shape changes during gut morphogenesis. Dev Biol. **357**(1): p. 227-34.

32. Menzies, A.S., et al., Mena and vasodilator-stimulated phosphoprotein are required for multiple actin-dependent processes that shape the vertebrate nervous system. J Neurosci, 2004. **24**(37): p. 8029-38.

33. Kwiatkowski, A.V., et al., Ena/VASP Is Required for neuritogenesis in the developing cortex. Neuron, 2007. **56**(3): p. 441-55.

34. Roffers-Agarwal, J., et al., Enabled (Xena) regulates neural plate morphogenesis, apical constriction, and cellular adhesion required for neural tube closure in Xenopus. Dev Biol, 2008. **314**(2): p. 393-403.

35. Nandadasa, S., et al., N- and E-cadherins in Xenopus are specifically required in the neural and non-neural ectoderm, respectively, for F-actin assembly and morphogenetic movements. Development, 2009. **136**(8): p. 1327-38.

36. Ruff, C., et al., Single-molecule tracking of myosins with genetically engineered amplifier domains. Nat Struct Biol, 2001. **8**(3): p. 226-9.

37. Ruegg, C., et al., Molecular motors: force and movement generated by single myosin II molecules. News Physiol Sci, 2002. **17**: p. 213-8.

38. Davidson, L., M. von Dassow, and J. Zhou, Multi-scale mechanics from molecules to morphogenesis. Int J Biochem Cell Biol, 2009. **41**(11): p. 2147-62.

39. Martin, A.C., M. Kaschube, and E.F. Wieschaus, Pulsed contractions of an actin-myosin network drive apical constriction. Nature, 2009. **457**(7228): p. 495-9.

40. Rauzi, M., P.F. Lenne, and T. Lecuit, Planar polarized actomyosin contractile flows control epithelial junction remodelling. Nature. **468**(7327): p. 1110-4.

41. Martin, A.C., et al., Integration of contractile forces during tissue invagination. J Cell Biol. **188**(5): p. 735-49.

42. Ma, X., et al., Probing embryonic tissue mechanics with laser hole drilling. Phys Biol, 2009. **6**(3): p. 036004.

43. Somlyo, A.P. and A.V. Somlyo, Ca2+ sensitivity of smooth muscle and nonmuscle myosin II: modulated by G proteins, kinases, and myosin phosphatase. Physiol Rev, 2003. **83**(4): p. 1325-58.

44. Hirose, M., et al., Molecular dissection of the Rho-associated protein kinase (p160ROCK)-regulated neurite remodeling in neuroblastoma N1E-115 cells. J Cell Biol, 1998. **141**(7): p. 1625-36.

45. Goto, H., et al., Phosphorylation of vimentin by Rho-associated kinase at a unique amino-terminal site that is specifically phosphorylated during cytokinesis. J Biol Chem, 1998. **273**(19): p. 11728-36.

46. Amano, M., et al., Formation of actin stress fibers and focal adhesions enhanced by Rho-kinase. Science, 1997. **275**(5304): p. 1308-11.

47. Leung, T., et al., The p160 RhoA-binding kinase ROK alpha is a member of a kinase family and is involved in the reorganization of the cytoskeleton. Mol Cell Biol, 1996. **16**(10): p. 5313-27.

48. Ishizaki, T., et al., p160ROCK, a Rho-associated coiled-coil forming protein kinase, works downstream of Rho and induces focal adhesions. FEBS Lett, 1997. **404**(2-3): p. 118-24.

49. Kureishi, Y., et al., Rho-associated kinase directly induces smooth muscle contraction through myosin light chain phosphorylation. J Biol Chem, 1997. **272**(19): p. 12257-60.

50. Kosako, H., et al., Phosphorylation of glial fibrillary acidic protein at the same sites by cleavage furrow kinase and Rho-associated kinase. J Biol Chem, 1997. **272**(16): p. 10333-6.

51. Amano, M., et al., Myosin II activation promotes neurite retraction during the action of Rho and Rho-kinase. Genes Cells, 1998. **3**(3): p. 177-88.

52. Oshiro, N., Y. Fukata, and K. Kaibuchi, Phosphorylation of moesin by rho-associated kinase (Rho-kinase) plays a crucial role in the formation of microvilli-like structures. J Biol Chem, 1998. **273**(52): p. 34663-6.

53. Fukata, Y., et al., Phosphorylation of adducin by Rho-kinase plays a crucial role in cell motility. J Cell Biol, 1999. **145**(2): p. 347-61.

54. Chisholm, A.A. and P. Cohen, The myosin-bound form of protein phosphatase 1 (PP-1M) is the enzyme that dephosphorylates native myosin in skeletal and cardiac muscles. Biochim Biophys Acta, 1988. **971**(2): p. 163-9.

55. Ito, M., et al., Myosin phosphatase: structure, regulation and function. Mol Cell Biochem, 2004. **259**(1-2): p. 197-209.

56. Feng, J., et al., Dephosphorylation of distinct sites on the 20 kDa myosin light chain by smooth muscle myosin phosphatase. FEBS Lett, 1999. **448**(1): p. 101-4.

57. Kimura, K., et al., Regulation of myosin phosphatase by Rho and Rho-associated kinase (Rho-kinase). Science, 1996. **273**(5272): p. 245-8.

58. Kawano, Y., et al., Phosphorylation of myosin-binding subunit (MBS) of myosin phosphatase by Rho-kinase in vivo. J Cell Biol, 1999. **147**(5): p. 1023-38.

59. Feng, J., et al., Inhibitory phosphorylation site for Rho-associated kinase on smooth muscle myosin phosphatase. J Biol Chem, 1999. **274**(52): p. 37385-90.

60. Ichikawa, K., M. Ito, and D.J. Hartshorne, Phosphorylation of the large subunit of myosin phosphatase and inhibition of phosphatase activity. J Biol Chem, 1996. **271**(9): p. 4733-40.

61. Tsukita, S. and S. Yonemura, ERM proteins: head-to-tail regulation of actin-plasma membrane interaction. Trends Biochem Sci, 1997. **22**(2): p. 53-8.

62. Bretscher, A., Regulation of cortical structure by the ezrin-radixin-moesin protein family. Curr Opin Cell Biol, 1999. **11**(1): p. 109-16.

63. Matsui, T., et al., Rho-kinase phosphorylates COOH-terminal threonines of ezrin/radixin/moesin (ERM) proteins and regulates their head-to-tail association. J Cell Biol, 1998. **140**(3): p. 647-57.

64. Kimura, K., et al., Regulation of the association of adducin with actin filaments by Rho-associated kinase (Rho-kinase) and myosin phosphatase. J Biol Chem, 1998. **273**(10): p. 5542-8.

65. Ohashi, K., et al., Rho-associated kinase ROCK activates LIM-kinase 1 by phosphorylation at threonine 508 within the activation loop. J Biol Chem, 2000. **275**(5): p. 3577-82.

66. Maekawa, M., et al., Signaling from Rho to the actin cytoskeleton through protein kinases ROCK and LIM-kinase. Science, 1999. **285**(5429): p. 895-8.

67. Hashimoto, R., et al., Domain- and site-specific phosphorylation of bovine NF-L by Rho-associated kinase. Biochem Biophys Res Commun, 1998. **245**(2): p. 407-11.

68. Matsui, T., et al., Rho-associated kinase, a novel serine/threonine kinase, as a putative target for small GTP binding protein Rho. EMBO J, 1996. **15**(9): p. 2208-16.

69. Ishizaki, T., et al., The small GTP-binding protein Rho binds to and activates a 160 kDa Ser/Thr protein kinase homologous to myotonic dystrophy kinase. EMBO J, 1996. **15**(8): p. 1885-93.

70. Leung, T., et al., A novel serine/threonine kinase binding the Ras-related RhoA GTPase which translocates the kinase to peripheral membranes. J Biol Chem, 1995. **270**(49): p. 29051-4.

71. Nakagawa, O., et al., ROCK-I and ROCK-II, two isoforms of Rho-associated coiled-coil forming protein serine/threonine kinase in mice. FEBS Lett, 1996. **392**(2): p. 189-93.

72. Yoneda, A., H.A. Multhaupt, and J.R. Couchman, The Rho kinases I and II regulate different aspects of myosin II activity. J Cell Biol, 2005. **170**(3): p. 443-53.

73. Fujisawa, K., et al., Identification of the Rho-binding domain of p160ROCK, a Rho-associated coiled-coil containing protein kinase. J Biol Chem, 1996. **271**(38): p. 23022-8.

74. Jacobs, M., et al., The structure of dimeric ROCK I reveals the mechanism for ligand selectivity. J Biol Chem, 2006. **281**(1): p. 260-8.

75. Zheng, J., et al., Crystal structure of the catalytic subunit of cAMP-dependent protein kinase complexed with MgATP and peptide inhibitor. Biochemistry, 1993. **32**(9): p. 2154-61.

76. Amano, M., et al., The COOH terminus of Rho-kinase negatively regulates rho-kinase activity. J Biol Chem, 1999. **274**(45): p. 32418-24.

77. Tan, I., et al., Intermolecular and intramolecular interactions regulate catalytic activity of myotonic dystrophy kinase-related Cdc42-binding kinase alpha. Mol Cell Biol, 2001. **21**(8): p. 2767-78.

78. Chen, X.Q., et al., Characterization of RhoA-binding kinase ROKalpha implication of the pleckstrin homology domain in ROKalpha function using region-specific antibodies. J Biol Chem, 2002. **277**(15): p. 12680-8.

79. Turner, M.S., et al., Characterization and purification of truncated human Rho-kinase II expressed in Sf-21 cells. Arch Biochem Biophys, 2002. **405**(1): p. 13-20.

80. Sebbagh, M., et al., Caspase-3-mediated cleavage of ROCK I induces MLC phosphorylation and apoptotic membrane blebbing. Nat Cell Biol, 2001. **3**(4): p. 346-52.

81. Coleman, M.L., et al., Membrane blebbing during apoptosis results from caspase-mediated activation of ROCK I. Nat Cell Biol, 2001. **3**(4): p. 339-45.

82. Bishop, A.L. and A. Hall, Rho GTPases and their effector proteins. Biochem J, 2000. **348 Pt 2**: p. 241-55.

83. Shimizu, T., et al., Parallel coiled-coil association of the RhoA-binding domain in Rho-kinase. J Biol Chem, 2003. **278**(46): p. 46046-51.

84. Dvorsky, R., et al., Structural insights into the interaction of ROCKI with the switch regions of RhoA. J Biol Chem, 2004. **279**(8): p. 7098-104.

85. Morreale, A., et al., Structure of Cdc42 bound to the GTPase binding domain of PAK. Nat Struct Biol, 2000. **7**(5): p. 384-8.

86. Lei, M., et al., Structure of PAK1 in an autoinhibited conformation reveals a multistage activation switch. Cell, 2000. **102**(3): p. 387-97.

87. Feng, J., et al., Rho-associated kinase of chicken gizzard smooth muscle. J Biol Chem, 1999. **274**(6): p. 3744-52.

88. Wen, W., et al., Structure basis and unconventional lipid membrane binding properties of the PH-C1 tandem of rho kinases. J Biol Chem, 2008. **283**(38): p. 26263-73.

89. Bolinger, C., et al., Specific isoforms of drosophila shroom define spatial requirements for the induction of apical constriction. Dev Dyn. **239**(7): p. 2078-93.

90. Plageman, T.F., Jr., et al., A Trio-RhoA-Shroom3 pathway is required for apical constriction and epithelial invagination. Development. **138**(23): p. 5177-88.

91. Lee, C., M.P. Le, and J.B. Wallingford, The shroom family proteins play broad roles in the morphogenesis of thickened epithelial sheets. Dev Dyn, 2009. **238**(6): p. 1480-91.

92. Hagens, O., et al., Disruptions of the novel KIAA1202 gene are associated with X-linked mental retardation. Hum Genet, 2006. **118**(5): p. 578-90.

93. Dietz, M.L., et al., Differential actin-dependent localization modulates the evolutionarily conserved activity of Shroom family proteins. J Biol Chem, 2006. **281**(29): p. 20542-54.

94. Yoder, M. and J.D. Hildebrand, Shroom4 (Kiaa1202) is an actin-associated protein implicated in cytoskeletal organization. Cell Motil Cytoskeleton, 2007. **64**(1): p. 49-63.

95. Hayashi, T. and R.W. Carthew, Surface mechanics mediate pattern formation in the developing retina. Nature, 2004. **431**(7009): p. 647-52.

96. Job, D., O. Valiron, and B. Oakley, Microtubule nucleation. Curr Opin Cell Biol, 2003. **15**(1): p. 111-7.

97. Lee, C., H.M. Scherr, and J.B. Wallingford, Shroom family proteins regulate gamma-tubulin distribution and microtubule architecture during epithelial cell shape change. Development, 2007. **134**(7): p. 1431-41.

98. Taylor, J., et al., The scaffold protein POSH regulates axon outgrowth. Mol Biol Cell, 2008. **19**(12): p. 5181-92.

99. Schnorr, J.D., et al., Ras1 interacts with multiple new signaling and cytoskeletal loci in Drosophila eggshell patterning and morphogenesis. Genetics, 2001. **159**(2): p. 609-22.

100. Grindley, J.C., D.R. Davidson, and R.E. Hill, The role of Pax-6 in eye and nasal development. Development, 1995. **121**(5): p. 1433-42.

101. Chung, M.I., et al., Direct activation of Shroom3 transcription by Pitx proteins drives epithelial morphogenesis in the developing gut. Development. **137**(8): p. 1339-49.

102. Fischer, R.S., et al., Local cortical tension by myosin II guides 3D endothelial cell branching. Curr Biol, 2009. **19**(3): p. 260-5.

103. Raposo, G. and M.S. Marks, The dark side of lysosome-related organelles: specialization of the endocytic pathway for melanosome biogenesis. Traffic, 2002. **3**(4): p. 237-48.

104. Barral, D.C. and M.C. Seabra, The melanosome as a model to study organelle motility in mammals. Pigment Cell Res, 2004. **17**(2): p. 111-8.

105. Raposo, G., et al., Lysosome-related organelles: a view from immunity and pigmentation. Cell Struct Funct, 2002. **27**(6): p. 443-56.

106. Etournay, R., et al., Shroom2, a myosin-VIIa- and actin-binding protein, directly interacts with ZO-1 at tight junctions. J Cell Sci, 2007. **120**(Pt 16): p. 2838-50.

107. Staub, O., et al., Primary structure of an apical protein from Xenopus laevis that participates in amiloride-sensitive sodium channel activity. J Cell Biol, 1992. **119**(6): p. 1497-506.

108. Zuckerman, J.B., et al., Association of the epithelial sodium channel with Apx and alpha-spectrin in A6 renal epithelial cells. J Biol Chem, 1999. **274**(33): p. 23286-95.

109. Schiaffino, M.V., et al., Cloning of a human homologue of the Xenopus laevis APX gene from the ocular albinism type 1 critical region. Hum Mol Genet, 1995. **4**(3): p. 373-82.

110. McGuffin, L.J., K. Bryson, and D.T. Jones, The PSIPRED protein structure prediction server. Bioinformatics, 2000. **16**(4): p. 404-5.

111. Studier, F.W., Protein production by auto-induction in high density shaking cultures. Protein Expr Purif, 2005. **41**(1): p. 207-34.

112. Adams, P.D., et al., PHENIX: a comprehensive Python-based system for macromolecular structure solution. Acta Crystallogr D Biol Crystallogr. **66**(Pt 2): p. 213-21.

113. Otwinowski, Z. and W. Minor, Processing of X-ray Diffraction Data Collected in Oscillation Mode. Methods in Enzymology, 1997. **276**(Macromolecular Crystallography, part A): p. 307-326.

114. Emsley, P. and K. Cowtan, Coot: model-building tools for molecular graphics. Acta Crystallogr D Biol Crystallogr, 2004. **60**(Pt 12 Pt 1): p. 2126-32.

115. Sheldrick, G.M., A short history of SHELX. Acta Crystallogr A, 2008. **64**(Pt 1): p. 112-22.

116. Zucker, F., P.C. Champ, and E.A. Merritt, Validation of crystallographic models containing TLS or other descriptions of anisotropy. Acta Crystallogr D Biol Crystallogr. **66**(Pt 8): p. 889-900.

117. Davis, I.W., et al., MolProbity: all-atom contacts and structure validation for proteins and nucleic acids. Nucleic Acids Res, 2007. **35**(Web Server issue): p. W375-83.

118. Holm, L. and C. Sander, Touring protein fold space with Dali/FSSP. Nucleic Acids Res, 1998. **26**(1): p. 316-9.

119. Waterhouse, A.M., et al., Jalview Version 2--a multiple sequence alignment editor and analysis workbench. Bioinformatics, 2009. **25**(9): p. 1189-91.

120. Gouet, P., et al., ESPript: analysis of multiple sequence alignments in PostScript. Bioinformatics, 1999. **15**(4): p. 305-8.

121. Risler, J.L., et al., Amino acid substitutions in structurally related proteins. A pattern recognition approach. Determination of a new and efficient scoring matrix. J Mol Biol, 1988. **204**(4): p. 1019-29.

122. Goldschmidt, L., et al., Toward rational protein crystallization: A Web server for the design of crystallizable protein variants. Protein Sci, 2007. **16**(8): p. 1569-76.

123. Mohan, S., et al., Structure of the Shroom Domain 2 reveals a three-segmented coiled-coil required for dimerization, Rock binding, and apical constriction. Mol Biol Cell.

124. Ward, J.J., et al., Prediction and functional analysis of native disorder in proteins from the three kingdoms of life. J Mol Biol, 2004. **337**(3): p. 635-45.

125. Minor, Z.O.a.W., Processing of X-ray Diffraction Data Collected in Oscillation Mode. Methods in Enzymology, 1997. **276**: p. 307-326.

126. Tu, D., et al., Crystal structure of a coiled-coil domain from human ROCK I. PLoS One. **6**(3): p. e18080.

127. Strong, M., et al., Toward the structural genomics of complexes: crystal structure of a PE/PPE protein complex from Mycobacterium tuberculosis. Proc Natl Acad Sci U S A, 2006. **103**(21): p. 8060-5.

128. Davis, I.W., et al., MOLPROBITY: structure validation and all-atom contact analysis for nucleic acids and their complexes. Nucleic Acids Res, 2004. **32**(Web Server issue): p. W615-9.

129. Walshaw, J. and D.N. Woolfson, Socket: a program for identifying and analysing coiled-coil motifs within protein structures. J Mol Biol, 2001. **307**(5): p. 1427-50.

130. Strelkov, S.V. and P. Burkhard, Analysis of alpha-helical coiled coils with the program TWISTER reveals a structural mechanism for stutter compensation. J Struct Biol, 2002. **137**(1-2): p. 54-64.

131. Blumenstein, L. and M.R. Ahmadian, Models of the cooperative mechanism for Rho effector recognition: implications for RhoA-mediated effector activation. J Biol Chem, 2004. **279**(51): p. 53419-26.

132. Zucker, F., P.C. Champ, and E.A. Merritt, Validation of crystallographic models containing TLS or other descriptions of anisotropy. Acta Crystallogr D Biol Crystallogr, 2010. **66**(Pt 8): p. 889-900.

133. Adams, P.D., et al., PHENIX: a comprehensive Python-based system for macromolecular structure solution. Acta Crystallogr D Biol Crystallogr, 2010. **66**(Pt 2): p. 213-21.

134. Mikheikin, A.L., et al., A trimeric DNA polymerase complex increases the native replication processivity. Nucleic Acids Res, 2009. **37**(21): p. 7194-205.

135. Bednar, J., et al., Nucleosomes, linker DNA, and linker histone form a unique structural motif that directs the higher-order folding and compaction of chromatin. Proc Natl Acad Sci U S A, 1998. **95**(24): p. 14173-8.

136. Orphanides, G., et al., FACT, a factor that facilitates transcript elongation through nucleosomes. Cell, 1998. **92**(1): p. 105-16.

137. Groth, A., et al., Chromatin challenges during DNA replication and repair. Cell, 2007. **128**(4): p. 721-33.

138. Loyola, A. and G. Almouzni, Histone chaperones, a supporting role in the limelight. Biochim Biophys Acta, 2004. **1677**(1-3): p. 3-11.

139. De Koning, L., et al., Histone chaperones: an escort network regulating histone traffic. Nat Struct Mol Biol, 2007. **14**(11): p. 997-1007.

140. Smith, S. and B. Stillman, Stepwise assembly of chromatin during DNA replication in vitro. EMBO J, 1991. **10**(4): p. 971-80.

141. Kaufman, P.D., et al., The p150 and p60 subunits of chromatin assembly factor I: a molecular link between newly synthesized histones and DNA replication. Cell, 1995. **81**(7): p. 1105-14.

142. Kamakaka, R.T., et al., Postreplicative chromatin assembly by Drosophila and human chromatin assembly factor 1. Mol Cell Biol, 1996. **16**(3): p. 810-7.

143. Smith, S. and B. Stillman, Purification and characterization of CAF-I, a human cell factor required for chromatin assembly during DNA replication in vitro. Cell, 1989. **58**(1): p. 15-25.

144. Smith, S. and B. Stillman, Immunological characterization of chromatin assembly factor I, a human cell factor required for chromatin assembly during DNA replication in vitro. J Biol Chem, 1991. **266**(18): p. 12041-7.

145. Kaufman, P.D., R. Kobayashi, and B. Stillman, Ultraviolet radiation sensitivity and reduction of telomeric silencing in Saccharomyces cerevisiae cells lacking chromatin assembly factor-I. Genes Dev, 1997. **11**(3): p. 345-57.

146. Song, J.J., J.D. Garlick, and R.E. Kingston, Structural basis of histone H4 recognition by p55. Genes Dev, 2008. **22**(10): p. 1313-8.

147. Tyler, J.K., et al., The RCAF complex mediates chromatin assembly during DNA replication and repair. Nature, 1999. **402**(6761): p. 555-60.

148. Mello, J.A., et al., Human Asf1 and CAF-1 interact and synergize in a repair-coupled nucleosome assembly pathway. EMBO Rep, 2002. **3**(4): p. 329-34.

149. Tyler, J.K., et al., Interaction between the Drosophila CAF-1 and ASF1 chromatin assembly factors. Mol Cell Biol, 2001. **21**(19): p. 6574-84.

150. Hoek, M. and B. Stillman, Chromatin assembly factor 1 is essential and couples chromatin assembly to DNA replication in vivo. Proc Natl Acad Sci U S A, 2003. **100**(21): p. 12183-8.

151. Nabatiyan, A. and T. Krude, Silencing of chromatin assembly factor 1 in human cells leads to cell death and loss of chromatin assembly during DNA synthesis. Mol Cell Biol, 2004. **24**(7): p. 2853-62.

152. Verreault, A., et al., Nucleosome assembly by a complex of CAF-1 and acetylated histones H3/H4. Cell, 1996. **87**(1): p. 95-104.

153. Krude, T., Chromatin assembly factor 1 (CAF-1) colocalizes with replication foci in HeLa cell nuclei. Exp Cell Res, 1995. **220**(2): p. 304-11.

154. Li, Q., et al., Acetylation of histone H3 lysine 56 regulates replication-coupled nucleosome assembly. Cell, 2008. **134**(2): p. 244-55.

155. Moggs, J.G., et al., A CAF-1-PCNA-mediated chromatin assembly pathway triggered by sensing DNA damage. Mol Cell Biol, 2000. **20**(4): p. 1206-18.

156. Zhang, Z., K. Shibahara, and B. Stillman, PCNA connects DNA replication to epigenetic inheritance in yeast. Nature, 2000. **408**(6809): p. 221-5.

157. Shibahara, K. and B. Stillman, Replication-dependent marking of DNA by PCNA facilitates CAF-1-coupled inheritance of chromatin. Cell, 1999. **96**(4): p. 575-85.

158. Krawitz, D.C., T. Kama, and P.D. Kaufman, Chromatin assembly factor I mutants defective for PCNA binding require Asf1/Hir proteins for silencing. Mol Cell Biol, 2002. **22**(2): p. 614-25.

159. Gaillard, P.H., et al., Chromatin assembly coupled to DNA repair: a new role for chromatin assembly factor I. Cell, 1996. **86**(6): p. 887-96.

160. Linger, J. and J.K. Tyler, The yeast histone chaperone chromatin assembly factor 1 protects against double-strand DNA-damaging agents. Genetics, 2005. **171**(4): p. 1513-22.

161. Martini, E., et al., Recruitment of phosphorylated chromatin assembly factor 1 to chromatin after UV irradiation of human cells. J Cell Biol, 1998. **143**(3): p. 563-75.

162. Game, J.C. and P.D. Kaufman, Role of Saccharomyces cerevisiae chromatin assembly factor-I in repair of ultraviolet radiation damage in vivo. Genetics, 1999. **151**(2): p. 485-97.

163. Green, C.M. and G. Almouzni, Local action of the chromatin assembly factor CAF-1 at sites of nucleotide excision repair in vivo. EMBO J, 2003. **22**(19): p. 5163-74.

164. Jiao, R., et al., The Werner syndrome protein is required for recruitment of chromatin assembly factor 1 following DNA damage. Oncogene, 2007. **26**(26): p. 3811-22.

165. Monson, E.K., D. de Bruin, and V.A. Zakian, The yeast Cac1 protein is required for the stable inheritance of transcriptionally repressed chromatin at telomeres. Proc Natl Acad Sci U S A, 1997. **94**(24): p. 13081-6.

166. Reese, B.E., et al., The methyl-CpG binding protein MBD1 interacts with the p150 subunit of chromatin assembly factor 1. Mol Cell Biol, 2003. **23**(9): p. 3226-36.

167. Huang, S., et al., Rtt106p is a histone chaperone involved in heterochromatin-mediated silencing. Proc Natl Acad Sci U S A, 2005. **102**(38): p. 13410-5.

168. Quivy, J.P., et al., A CAF-1 dependent pool of HP1 during heterochromatin duplication. EMBO J, 2004. **23**(17): p. 3516-26.

169. Huang, S., et al., A novel role for histone chaperones CAF-1 and Rtt106p in heterochromatin silencing. EMBO J, 2007. **26**(9): p. 2274-83.

170. Meijsing, S.H. and A.E. Ehrenhofer-Murray, The silencing complex SAS-I links histone acetylation to the assembly of repressed chromatin by CAF-I and Asf1 in Saccharomyces cerevisiae. Genes Dev, 2001. **15**(23): p. 3169-82.

171. Enomoto, S. and J. Berman, Chromatin assembly factor I contributes to the maintenance, but not the re-establishment, of silencing at the yeast silent mating loci. Genes Dev, 1998. **12**(2): p. 219-32.

172. Enomoto, S., et al., RLF2, a subunit of yeast chromatin assembly factor-I, is required for telomeric chromatin function in vivo. Genes Dev, 1997. **11**(3): p. 358-70.

173. Jones, D.T., Protein secondary structure prediction based on position-specific scoring matrices. J. Mol. Biol. , 1999. **292**: p. 195-202.

174. McGuffin, L.J., K. Bryson, and D.T. Jones, The PSIPRED protein structure prediction server. Bioinformatics, 2000. **16**: p. 404-405.

175. Ward, J.J., et al., Prediction and functional analysis of native disorder in proteins from the three kingdoms of life. . 2004.